ULTRAWEAK PHOTON EMISSION IN CELLS: COUPLING TO MOLECULAR PATHWAYS, APPLIED MAGNETIC FIELDS, AND POTENTIAL NON-LOCALITY

by

Blake T. Dotta

A thesis submitted in partial fulfillment of the requirements
for the degree of
Doctor of Philosophy (PhD) in Biomolecular Sciences

The School of Graduate Studies
Laurentian University
Sudbury, Ontario

THESIS DEFENCE COMMITTEE/COMITÉ DE SOUTENANCE DE THÈSE

Laurentian Université/Université Laurentienne
School of Graduate Studies/École des études supérieures

Title of Thesis Titre de la thèse	ULTRAWEAK PHOTON EMISSIONS IN CELLS: COUPLING TO FIELDS, MOLECULAR PATHWAYS, APPLIED MAGNETIC AND POTENTIAL NON-LOCALITY
Name of Candidate Nom du candidat	Dotta, Blake T.
Degree Diplôme	Doctor of Philosophy

Department/Program Département/Programme	Biomolecular Sciences	Date of Defence Date de la soutenance	November 29, 2013

APPROVED/APPROUVÉ

Thesis Examiners/Examinateurs de thèse:

Dr. Michael Persinger
(Supervisor/Directeur de thèse)

Dr. Robert Lafrenie
(Committee member/Membre du comité)

Dr. Abdel Omri
(Committee member/Membre du comité)

Dr. Michal Cifra
(External Examiner/Examinateur externe)

Dr. Tammy Eger
(Internal Examiner/Examinatrice interne)

Approved for the School of Graduate Studies
Approuvé pour l'École des études supérieures
Dr. David Lesbarrères
M. David Lesbarrères
Director, School of Graduate Studies
Directeur, École des études supérieures

ACCESSIBILITY CLAUSE AND PERMISSION TO USE

I, **Blake T. Dotta**, hereby grant to Laurentian University and/or its agents the non-exclusive license to archive and make accessible my thesis, dissertation, or project report in whole or in part in all forms of media, now or for the duration of my copyright ownership. I retain all other ownership rights to the copyright of the thesis, dissertation or project report. I also reserve the right to use in future works (such as articles or books) all or part of this thesis, dissertation, or project report. I further agree that permission for copying of this thesis in any manner, in whole or in part, for scholarly purposes may be granted by the professor or professors who supervised my thesis work or, in their absence, by the Head of the Department in which my thesis work was done. It is understood that any copying or publication or use of this thesis or parts thereof for financial gain shall not be allowed without my written permission. It is also understood that this copy is being made available in this form by the authority of the copyright owner solely for the purpose of private study and research and may not be copied or reproduced except as permitted by the copyright laws without written authority from the copyright owner.

ABSTRACT

The possibilities and implications of photons within the infrared, visible, and ultraviolet behaving as sources of intracellular and intercellular communication and information were investigated experimentally for melanoma cells during the 24 hrs following removal from incubation. Specific wavelengths during different intervals were associated with specific classes of biomolecules that were predicted based on the physical properties associated with their amino acid sequences. Application of a specific intensity and physiologically patterned magnetic field predicted from a model that applied the concept of magnetic moment to the whole cell resulted in photon emissions. They were detected at distances sufficient to allow intercellular communication. The occurrence of macroscopic entanglement or non-locality was shown between two loci of where simple chemically-based photons emissions were generated. Within all three experiments there was marked quantitative congruence between the energies associated with the power density of the photon emissions and the physicochemical variables involved with their reduction. These results indicate that photon emissions coupled with classic biomolecular pathways and processes may behave as intra- and inter-cellular sources of information that could control the complex dynamics of cells. The effect may not depend upon locality but exhibit non-local characteristics.

ACKNOWLEGMENTS

I would like to thank my thesis supervisor Dr. Michael A. Persinger. His continued support, guidance, and wisdom have allowed me achieve goals that were seemingly unattainable. I would also like to thank my committee members Dr. Rob Lafrenie, Dr. Abdel Omri and my examiners Dr. Michal Cifra and Dr. Tammy Eger. Their helpful comments and suggestions greatly increased the clarity of this thesis.

Thank you to my funding sources Dr. Ed Bosarge and Ontario Graduate Scholarships for allowing me the opportunity to complete these projects.

And a personal thank you LSD, PLC, ADJ, LSP, NRG, SAA, SLTD, ALTD, SXA, PXD, DMAA, HMAA, MMMA, and MAP. This could not have been done without all of you.

Table of Contents

List of Tables

CHAPTER TWO:

List of Figures

CHAPTER TWO:

CHAPTER THREE:

1 Introduction

Communication within and between cells is essential for the development, maintenance, and proliferation of biological systems. This fundamental component of life allows for interaction with nearby cells and also for a cell system to interact with its environment. There is a surplus of mechanisms by which biological systems can communicate, and these interactions can occur at multiple levels. For example, when an individual learns a basic task neighbouring cells within the brain (neurons) undergo conformational changes, or synaptic plasticity, to ensure the long-term storage of this information. This process of long lasting changes at the cellular level is known as long-term potentiation (LTP). The synaptic plasticity that is associated with learning can be influenced by multiple factors including electrical stimulation, cell signalling such as CREB (cAMP-response element binding protein) levels, cholinergic activity, and actin filaments [Malenka and Bear, 2004]. It can be inferred from the above example that the majority of known cellular communication mechanisms are either electrical or chemical based. This inference is accurate as very little is known of any communication between cells that is non-electrical and non-chemical.

Potential mechanisms for the types of physical interaction between cells that is neither chemical nor electrical include electromagnetic fields, biophotons, and even the idea of non-

locality [Popp, 1979a, 1979b; Cifra, 2011; Bohr, 1958; Schrodinger, 1944]. Our understanding of these processes could contribute to an alternate form of cellular communication is nascent. However the idea of a non-chemical non-electrical communication system between cells is not a novel concept. Work in the early 1900's by Alexander Gurwitsch demonstrated findings that onion roots would undergo division faster if other cells undergoing division were present in the same area [Gurwitsch, 1923]. This was originally termed "mitogenic radiation" by Gurwitsch and in the last few decades work studying this phenomena has begun to reappear in the scientific literature [Quickenden, 1974; Popp et al, 1988]. Gurwitsch originally proposed that ultraviolet light (UV) was the source of this effect. When the two dishes were separated by glass (UV resistant) the effect disappeared. If the cells were separated by quartz glass (UV permeable) the effect returned [Gurwitsch, 1923]. This led to the hypothesis that ultraweak photon emission (UPE) was responsible for the increased cellular division and the term biophoton was created.

Since that time, work by numerous groups has shown the effects biophotons have on biological systems. Work by Popp [1979a], Kobayashi [1999], and van Wijk [2005] have repeatedly demonstrated that living organisms emit biophotons. The intensity of emission ranges from 100 - 1000 photons$\cdot$cm^{-2} of tissue [Popp, 1979a]. Biophotons are generally between the UV and IR division of the electromagnetic spectrum. However, any form of energy emitted

or absorbed by charged particles that has wave like behavior is considered electromagnetic radiation. In fact, the visible range only accounts for a small portion of the electromagnetic spectrum, Radiofrequencies (~1 Hz to 1 THz) account for the majority of the spectrum. Electromagnetic radiation can consist of, but not be limited to, radiowaves, microwaves, UV radiation, visible light, IR radiation, x-rays and gamma rays.

In addition to measuring emitted electromagnetic energy from biological systems, studies have demonstrated the effects of applying electromagnetic energy to biological systems. Work by our lab [Dotta et al., 2011b] has shown multiple effects of applied electromagnetic fields. Multiple levels of discourse have been affected ranging from the cell to the whole organism. Effects include decelerated cell growth, suppression of tumour growth, and behavioural effects of increased analgesia in the whole animal [Buckner, 2011; Buckner et al, 2013; Wu & Persinger, 2011; Martin & Persinger, 2004]. The multitude of effects demonstrated by our lab and others reflect the powerful effects that electromagnetic fields can have on biological systems and their molecular substrates. This thesis will examine how biological systems, and their subcomponents, are affected by applied magnetic fields. It will also explore how applied magnetic fields affect the system's ultraweak photon emission. But first we will begin with a discussion of the qualities of electromagnetic fields and their role in biological systems.

1.1 Electromagnetic Fields

Fields of force can be static or dynamic. The former types of fields display minimal (if any) discernible alteration in strength within the area of application per second. The latter manifestations display temporal variations in intensity and direction that range from a few changes ("cycles") per second (Hz) to potentially ~10^{43} Hz that is the inverse of Planck's time or the "jitter" of the intrinsic structure of the smallest space (Planck's distance, ~10^{-35} m). The nature of these temporal variations can be more or less symmetrical, such as sine-waves or square waves, or remarkably complex, such as those generated by cells. The most typical examples of the latter would be the action potential of the neuron or the intricately structured dynamics of the cerebral cortical field as inferred by quantitative electroencephalography.

The major fields of force relevant to this dissertation are magnetism and electricity. For a static field the flux lines of magnetic fields and electric fields do not alter over time or by convention at more than once a second. To obtain changes within the object, such as a cell, within these static fields there must be motion of either the constituents of the cell or the cell itself across the flux lines. The third force that might be relevant but would be implied only theoretically is gravitational force. Although this force between two masses, such as potassium ions separated by the typical distance (~10 nm) that constitute the resting plasma membrane potential is miniscule when applied the

distance of the universe (10^{26} m) the energy is ~10^{-20} J, the essential quantum of the action potential and the resting membrane potential [Persinger, 2010]. Such minute energies and extraordinary distances are important elements to concepts of entanglement and non-locality.

A time-varying magnetic field is associated with an electric field and a time-varying electric field is associated with a magnetic field. Time-varying fields are reflected in two major classes: non-propagating and propagating. An example of a non-propagating magnetic field would be a horse-magnetic rotating along its major axis. The flux lines rotate through space but they do not propagate through space. A propagating magnetic field could theoretically move though space for substantial distances. Although the information within the field pattern would not attenuate the measure of magnitude would diminish according to some function of distance. The classic example is the electromagnetic field generated by antennae for radio communication.

Biological systems, from the molecules within the cells, to the cell as an integrate entity, to aggregates of cells that compose organs and organisms, are immersed in a complex mixture of static and time-varying magnetic fields. The most prominent magnetic field originates from the earth. On average the steady-state intensity is about 50,000 nT. However much like the ratio between the steady-state fields electric field of the brain compared to its time-varying (electroencephalographic) components,

there are time-varying changes whose amplitudes around approximately one-thousand times smaller than the steady-state value.

There is a large literature showing that these changes in geomagnetic intensity, which are in the order of tens of nanoTesla to a about 200 to 500 nT, affect biological and biochemical systems. Most of the contributions to these perturbations originate from the sun and its mediating medium the interplanetary magnetic field (solar wind). However there are smaller magnitude changes due to lunar orbit and secondary and tertiary effects from inductions of currents within the upper ionosphere. Some of these smaller fluctuations show marked local and diurnal variations.

The earth itself generates unique electromagnetic fields that have been present since abiogenesis. Between the earth and the ionosphere a fundamental frequency (7 to 8 Hz) and its harmonics are generated continuously primarily by discharges of lightening [Persinger, 2012]. The shapes of these fields are remarkably similar to all of the primary forms of electroencephalographic activity as well as those obtained from single cell recordings. The amplitudes of these propagating fields, whose attenuation is minimal over megameters of distance, are in the order of picoTesla and tens of millvolts per m. This is the same order of magnitude as the electric and magnetic fields generated by the cerebral cortices of mammals.

Within the last century the natural electromagnetic environment has been complimented with multiple sources of manufactured electromagnetic fields. Their intensities and temporal patterns, through the phenomena of beats (with the subtraction of frequencies the difference emerges as a "virtual" frequency), have the potential to generate patterns that are so identical to molecular and cell systems that resonant interactions could occur. There are now plausible models that DNA itself behaves as a type of electromagnetic antennae that could discern, differentiate and transform electromagnetic energies to differences in base-pair sequences. The intensities of the manufactured electromagnetic fields can cross several orders of magnitude.

Because of the potential for synergism [Whissell and Persinger, 2007], the effect of magnetic fields on the health of cells and organisms has become a central topic for science and medicine. It is important to ascertain whether or not EMFs can interact with cells and biological systems, and to determine the potential effects and implications. First a discussion on how cells can generate and detect magnetic fields will be discussed.

1.1.1 EMF Generation from Cells

There is an abundance of hypotheses of how a cell can generate and detect electromagnetic fields. As stated earlier, the production of a magnetic field can be produced by a charged

particle in motion. Living cells do have a gradient of charge across the plasma cell membrane. These voltage gradients across the cell membrane can be altered by many factors including environmental or physiological stressors, growth and development, or injury. But more simply these voltage gradients are the mechanisms by which a cell will depolarize and therefore become activated. This moving charge through a voltage gradient would be associated with an EMF, albeit at a weak intensity. However, in a system like the brain at any given moment there may be a million cells (10^6) firing coherently to produce a certain behaviour. This cohesive neuronal firing of $1O^6$ cells would produce a substantially larger EMF than a single cell alone.

In addition to the cellular membrane other cellular elements like microtubules are thought to play a part in EMF generation by the cell [Havelka & Cifra, 2009; Cifra, 2011]. Microtubules are highly polar (electrically) structures that allow for the production of EMF. Metabolically, the citric acid cycle also produces IR and visible radiation as a function of energy dissipation [Hideg et al, 1991]. This UPE is a result of the citric acid cycle's 40% efficacy in ATP production. These various cell functions would be associated with the generation of an EMF. The potential candidates discussed as EMF generators potentially describe the cell as being associated withh alternating and static magnetic fields.

1.1.2 EMF Detection from Cells

A cell as a detector of EMFs is much less characterized than EMF production from a cell. Despite this however there is still research discussing cells as EMF "sensors" [Berzhanskaya et al, 1995a; Berzhanskaya et al, 1995b]. These initial studies point to bacteria as organism particularly responsive to geomagnetic disturbances. They found that luminous bacteria displayed increased ultraweak photon emission at least 24 hours prior to a geomagnetic storm. Furthermore, Berzhanskaya's group [1995a] found that artificially induced applied magnetic fields had an effect on the luminous bacteria's photon emission as well. They found that only specific frequencies (36 to 55 GHz), adjacent to fundamental water absorption bands, were successful in altering the bacteria's photon emission.

It is important to note that only specific frequencies affected the bacteria. If all frequencies or applied fields induced changes in the bacteria's photon emission than one could argue that there is a potential induction effect of energy by the field itself. Because only select frequencies were successful in varying photon emissions, it implies that there must be a frequency modulated pattern that is able to successfully affect the cells. In other words, a sophisticated "lock and key" system may be the best analogy to describe EMF detection of cells.

Furthermore, the fact that luminous bacteria reliably and consistently responded to geomagnetic disturbances 24 hours prior

to the incident suggests that they are responding to a non-chemical non-electrical form of stimuli that was produced before the geomagnetic event took place. Responding to an event before it occurs is not uncommon in the scientific literature. For example, we found that 2 weeks prior to a magnitude 9 earthquake there were perturbations in the local background photon emissions from Sudbury Ontario [Persinger et al, 2012].

These perturbations were noted on 2 separate occasions and produced persistent (~10 day) elevations in background photon emissions. The peak elevations occurred within 24 hours of the seismic event. Following the large event there was a consistent drop in background photon emissions that took roughly 10 days to return to normal levels. This example simply illustrates that there was an energy (photon) increase in a non-local space before an event took place at a spatially separated location. If a seemingly unrelated process of measuring background photon emissions can predict magnitude >8 earthquakes ~9,000 km away, then a biological system (bacteria) that is sensitive to weak electromagnetic perturbations could respond to early EM perturbations of much lesser intensity at potentially comparable distances.

Other cell systems, like mammalian cells, may be susceptible to EMF detection. For example, the depolarization of a neuron produces a massive influx of Calcium (Ca^{2+}) as well as potassium and sodium ion across the membrane. This depolarization and flow of calcium will produce a low intensity magnetic field. This magnetic

field could be mimicked to potentially produce the depolarization of the cells as if the cell had naturally fired [Pall, 2013; Grassi et al, 2004]. If a properly patterned and intensity modulated EMF was applied to the membrane with the exact resonant frequency of Calcium 2++ gated channels, then this EMF application could in theory activate or stimulate the cell.

1.2 Ultraweak Photon Emission (UPE)

A photon is a discrete packet of energy that can be considered a particle-wave. Its energy is directly related to its wavelength and can be calculated with the following equation:

$$E=hc/\lambda \quad (1)$$

Where "E" is energy, "*h*" is Planck's constant, "*c*" is the speed of light, and "λ" is wavelength. Photons in the UV to IR range (~200 nm to 1500 nm) have energies ranging from $2 \cdot 10^{-19}$ J to $6 \cdot 10^{-19}$ J. The UV portion of the spectrum has more energy per photon than the IR spectrum. The energies associated with higher energy photons can potentially affect surrounding tissues [Popp, 1979a]. The interaction of photons and surrounding tissues could occur as the photons behaves as a quantum particle that interacts via electromagnetic forces with other quantum particles in matter [Gabrielli, et al, 2006].

Several papers and experiments have shown spontaneous photon emission from virtually all living systems tested [Popp, 1979a; van Wijk, 2005]. The amount of photon emission has been quantified by Popp to be anywhere from 10^6 - 10^7 photons$\cdot s^{-1} \cdot m^{-2}$ of tissue. In the literature this spontaneous photon emission has been termed many things including biophotons, bioluminescence, and ultraweak photon emission (UPE). Generally, these are all referring to the property of small amounts of light emitted from a biological system. These biological systems emit photons as a component of multiple chemical processes from (very likely) many sources and mechanisms.

Typically, UPE is a product of the chemical reactions of oxygen, specifically reactive oxygen species. However it should be noted that reactions of oxygen are not the only source of UPE from cells. With any metabolic reaction there will be the subsequent release of a photon. The ensuing photon release can be a marker for activity. However, more recently it has been discussed as a possible "purposeful product" of cell functioning [Sun et al, 2010; Choi et al, 2012]. The production, role, and theoretical possibilities associated with UPE have significant implications for biomolecular mechanisms.

1.2.1 UPE from Metabolic Reactions

As mentioned earlier the most likely candidate for UPE during metabolic processes are reactive oxygen species (ROS) [Popp, 1979a; Rastogi and Pospisil, 2011]. For example, the classic

physical chemical process: H_20_2 + NaClO → H_2O + NaCl + O_2 or more precisely HOOH + OCl^-→ $^1O_2$ [Kahn & Kasha, 1994], produces photon emission with its source attributed to the excited singlet oxygen $^1O_2$. More generally, any reaction involving a ROS will produce the release of a photon. Further evidence implicating oxygen as a primary source of UPE has been demonstrated in the last few decades. Through experimentation, UPE intensity was shown to be highly dependent upon oxygen levels within the system [Tilbury & Quickenden, 1988; Hideg et al, 1991]. In fact under anaerobic conditions there is virtually no UPE from traditional generators.

1.2.2 UPE from Biological Systems

Biophoton emissions have been recorded from cell cultures [Dotta et al, 2011a], human subjects [van Wijk & van Wijk, 2004; van Wijk, 2008], brain slices [Kobayashi et al, 1999a], and bacteria [Tilbury & Quickenden, 1988]. Tilbury and Quickenden [1988] measured photon emissions specifically from *Escherichia coli* (*E. Coli*) during different stages of the growth cycle. In addition to describing regular photon emission from *E. Coli* during growth phases, they found different frequencies of photons associated with different phases of the growth cycle. The UV (210 – 310 nm) spectrum contributed most significantly, along with portions of the visible spectrum (450 - 620 nm), during the exponential growth phase of the bacteria. During the second component of the growth phase (stationary) only the visible region contributed to this UPE.

These time and spectral composition depend results imply a serial order of biophoton emission during division or cellular process. These results also lend support to Cosic's Resonant Recognition Model for Macromolecules [Cosic, 1994]. This model states that specific macromolecules are associated with an optimal spectrum. If specific cellular processes are associated with specific frequency emission, as found by Tilbury and Quickenden [1988], it may be a product of protein turnover within the cell and demonstrate the Cosic model.

Work by our group has identified cultured B16-BL6 as a critical source of UPE [Dotta et al, 2011a]. During this experiment we removed cell cultures from the incubator and placed them at room temperature. We found stable and reliable photon emission from ~10^6 cultured B16-BL6 cells over the course of 12-24 hours. Over this 24 hour testing period the energy associated with cellular photon emission was $26 \cdot 10^{-10}$ J. With 10^6 cells this energy value corresponds to 10^{-20} $J \cdot s^{-1} \cdot cell^{-1}$. Using various cellular inhibitors and activators revealed that the amount of energy (photon emissions) associated with a cell culture was quantitatively limited and discrete. Results using acridine orange and ethidium bromide indicated that the membranes were still intact with no indication of (trypan blue) cell necrosis at greater than 18 hours post removal. Furthermore, treatments with activators, such as epithelial growth factor and Ionomycin produced rapid early (first 3 hr) increases in energy emission while glutamine-free, Na-azide and

Wortmanin-treated cells showed a general diminishment 3 to 9 hours later. These results paired together strongly suggested the origin of the photon emission was primarily the plasma cell membrane.

Other groups [Scott et al, 1991] have also discussed the plasma membrane as a significant source of UPE. Scott's group considers photon emission intensity to be associated with lipid peroxidation within the membrane. Through careful experimental manipulation it was possible to monitor membrane phase transition through UPE intensity only. The experiments demonstrated that lipid peroxidation is susceptible to membrane lipid conformation. These results link the kinetics of the membrane with lipid peroxidation (and subsequent photon emission). The results described illustrate, whether purposeful or not, the plasma membrane is a viable source of UPE from the cell.

Another structure within the cell known to produce UPE is the mitochondria [Kobayashi et al, 1999; Hideg, 1991]. The mitochondria play a major role in cell functions associated with energy production, growth, ageing, and even communication. Work by Hideg and colleagues showed copious amounts of UPE from mitochondria of a spinach leaf. They found that this UPE was highly dependent upon respiration. Mitochondria induced photon emission was abolished with the administration of inhibitors like antimycin-A and increased by the drug 1,4-diazabicyclo[2,2,2]-octane (DABCO). Given the effectiveness of these drugs it was deduced that singlet

oxygen species play an important role in UPE production from mitochondria.

1.2.3 UPE as a Purposeful Product of Cell Functioning

Photon emissions from biological systems as a purposeful product of cell functioning is still argued within the scientific community. Original articles by Popp [1979a], van Wijk [van Wijk et al, 1993], and Kobayashi [1999] have postulated that light emission from cells may perform specific communication functions. For example light emission can induce activation of neighboring cells. van Wijk [1993] demonstrated that a variety of mammalian cells (rat, dog, mouse, human, etc.) can be induced to produce UPE following the application of light.

In addition to this, work by Wu and Persinger [2011] have shown that irradiation with IR (880 nm) light can increase cell mobility and stem cell proliferation rate in planaria. These two studies illustrate that applied light has reproducible effects on cell systems and whole organisms. Each study demonstrates measurable responses to induced light application. Mammalian cells produce increased photon emissions following light application, and planaria exposed to IR irradiation exhibit cellular and behavioral effects. These responses illustrate that cells can respond to external light.

In addition to studies showing biophoton effects in cell cultures and planaria, mammalian brains have also exhibited

reliable UPE. Exciting studies by Kobayashi [1999a; 1999b] and Isojima [1995] have demonstrated reliable biophoton emission from a rat's brain in vivo. Rat hippocampal slices were stimulated electrically and photon emissions were measured. This research showed that the amount of UPE from a rat's brain was proportional to the amount of theta stimulation (4-7 Hz). Theta activity within the brain in humans is related to sleep, meditation and a myriad of other behaviours. Specifically, theta activity within the hippocampus (brain structure responsible for memory) is heavily tied to the ability to consolidate memory. Consolidation of memory occurs through conformational changes within the brain (neurite growth).

Studies by Choi and colleagues [2012] found that conformational changes in mammalian cells could be induced with visible light (710 nm) irradiation. Choi's results indicated an increase in MAP-Kinase (MAPK) activity and subsequent neurite outgrowth in rat cortical neurons following an ischemic insult if there was irradiation of 710 nm light. They found that this increase in activity was best achieved with 1 to 2 stimulations of 710 nm light per day. Synaptogenesis was completely increased from light stimulation. If Choi, Isojima, and Kobayashi's results are combined there is a potential for light induced learning within the brain through neurite outgrowth from theta activity-induced photon emissions.

It is also interesting to note that after head injuries, both those that produce loss of consciousness and no loss of consciousness, there is an overall increase in low frequency global power in the brain. If theta power is strongly correlated with UPE from the brain and head injuries are analogous to an ischemic insult, then we can deduce that more cells are protected from this insult through the theta activation. In other words, the increased theta activity following head injuries may be a protective mechanism to protect cells from death.

In summary these experiments have shown that not only can mammalian brain cells produce UPE these same brain cells can be affected by light irradiation. Taken together, a stimulus and response relationship between two different cells can be elicited through biophoton production. As one cell becomes excited and produces UPE, a proximal cell may interact and respond to this emission. This process might be considered analogous to paracrine relationships between similar cells.

Recent work by Dai's group [2010] may have validated this hypothesis. Dai's group has qualitatively demonstrated that neural communication can occur through biophotons within the nervous system [2010]. Dai found that specific light stimulation at one end of a spinal nerve produced significant increases in biophoton activity at the other. This again was strongly related to the spectral characteristics of the light that was applied. As expected

this UPE could be inhibited by adding metabolic inhibitors and enhanced with activators.

All of the above work on UPE from cells and metabolic reactions demonstrate how common biophoton emissions are within and between living systems. Within and outside the cell there may be a consistent bath of photon radiation distributed across infrared, visible, and ultraviolet wavelengths that interact with neighbouring cells. Other cells can respond to these emissions. One important question involves the extent, that is, the ultimate distance, over which photons from one cell can influence the photons and hence the associated biomolecular responses in another cell.

1.3 Excess Correlations and Quantum effects (Non-locality)

A implicit assumption if not axiom of the space-time contingencies upon which biomolecular processes within cells and organisms occur is locality. Locality indicates that for one molecule to affect another molecule or for one cell to affect another cell, there must be a causal, directly linked connection, within the level of space and time. For molecules the parameters would involve picometer space and picosecond time. For cells the space would involve nanometers to micrometers and comparable temporal increments.

Non-locality, defined as action at a distance which involves interactions between two objects, such as cells, separated by space

when there is no intermediate mechanism or agency such as a force or charge. Non-locality has been considered to be a feature of gravity. Within quantum approaches, non-locality has been considered the "anomalous" action at a distance resulting in excess temporal correlations between two spatial loci. This means that when a pattern of events occur in one of the loci there is a correlation above random variation (chance) with the pattern of events occurring in the other locus. Theoretically there is no spatial limit to non-locality. If it occurs, a pattern of events occurring in one location could display excess correlation with patterns of events in the second locus located at the other side of the universe.

One of the features of non-locality involves entanglement. If two particles share an original space-time property or occupy condition, such as a particular pattern of electromagnetic fields with specific geometry and changing rates of angular velocity, alteration in one space produces an equal change or alteration in the other [Stapp, 2009; Persinger & Koren, 2007]. They can be considered equivalent to parity over distance. A change in the parity of one unit of the pair results in the change in parity in the opposite direction in the other. One can consider this a variant of Newton's third law, for every force there is an equal and opposite force, applied to non-locality.

Photons are intricately coupled to the idea of non-locality as a feature of their quantum properties. Aczel [2002] has stated

that any quantum system that contains more than one particle would be influenced by the superposition principle. This principle states that in a system with multiple units any response of two or more stimuli is equivalent to the sum of responses as if each of the stimuli had been applied individually. This idea gives rise to the phenomena of entanglement.

Previous research [Dotta et al, 2011b] has shown an "excess" correlation of the irradiance or power density of photon emissions with pairs of cell cultures or pairs of human brains when they are separated by non-traditional distance but both sharing the same, very specific type of circularly rotating magnetic field. When magnetic fields exhibiting differences between phase and group velocities around the circle of solenoids were generated at the same time application of photon fields to one of the pair resulted in the quantitative emission of photons from the other member of the pair even though it was maintained in complete darkness. This excess correlation or entanglement required photomultiplier tubes (PMT) but was also evident with quantitative electroencephalography [Dotta et al, 2009; Dotta et al, 2011b].

These excess correlations, that is, the increase in photon emission from one locus when light was applied to the other locus only occurred when the shared rotating magnetic field was applied synchronously to the two separate sites. This excess correlation was not obvious when light was applied to one locus and photons were recorded from the other locus if the specific magnetic field

configurations were not present. Non-specific magnetic fields, particularly those that showed no changing angular velocity or second derivative (a rate of rate of change) did not reveal the effect.

The important component of these results is the potential for a novel form of communication between similar systems. If a weak applied magnetic field could produce this information transfer, is there anything similar in biological systems that could produce such conditions? We hypothesized that the plasma membrane could be a suitable target for this type of communication due to its circular shape, distribution of charges, liquid crystal states and the polar groups of proteins composing ion channels. We designed experiments to quantitatively test this "excess" correlation hypothesis.

1.4 Organization of Experiments and Dissertation

The major theme of this dissertation is to discern the conditions that could be considered a proof of principle for a primary role of photons as the primary carriers of information associated with specific molecular pathways and signalling. If photons exhibit this role, specific wavelengths, intrinsic to quanta of energies, could be associated with specific classes of biomolecular substances. These wavelengths should be derived from a rational model that incorporates the physical charge or electromagnetic characteristics of the amino acids that constitute

proteins and in large part determine their intermolecular functions.

In order to encourage specific information, a model of cell heterostasis was selected. Unlike more traditional methods of measuring cells within a stable environment, the heterostatic approach removes cells from the incubator and measures the physical changes that occur as they habituate to the novel and potentially non-viable environment. This environment often leads to the type of "degradation" chemistry and an activation of cell dynamics that promotes "enhanced communication" within and between cells. Degradation photons which are emitted at high rates during these periods of instability and habituation to the new demands can be easily measured and meet the criteria for medium of intercellular communication. The first chapter demonstrates this concept in principle.

Previous research by this experimenter [Dotta et al, 2011a] showed that the cell plasma membrane was the most likely candidate associated with the photons emitted from melanoma cells once they were removed from the incubator and measured over the subsequent 24 hr. The reliable release of these photons as measured by a photomultiplier tube allowed the direct test of an important model by which applied electromagnetic fields could interact with the cell to encourage photon emission.

The originators of quantum physics and quantum chemistry assumed that the dynamic relationships that created fundamental

forces would be reiterated, like the current concept of the fractal, within larger spaces and more complex organizations. The most fundamental source of the magnetic field is an electron moving in a closed path around a proton. Bohr's magneton showed that when the moment of inertia, charge and mass were accommodated appropriately with dimensional analyses a magnetic moment emerged. The units for magnetic moment are Joules per Tesla. Hence application of a known intensity of a magnetic field would produce a discrete amount of energy.

The cell membrane can be viewed as a three dimensional (surface) boundary that is analogous to the shell of an electron orbit around a nucleus. Lateral diffusion of proteins and lipids around through this shell would allow charge movements that would potentially interact with the appropriately patterned and intensity magnetic field. Because magnetic fields penetrate tissue with minimum attenuation, unlike most drugs that require vasculature for delivery to specific membrane interfaces, direct contact with cell chemistry occurs. The coupling between moving constituents of the plasma membrane and the applied magnetic field had the potential to release photons. They would be direct consequences and if they were patterned appropriately could be considered experimentally-inducible means of generating intra and inter-cell communication. The second chapter demonstrates this principle.

Finally the release of photons from molecular interactions within the cell indicates that the information associated with

packets of cell-relevant information-containing, photons could affect cells at substantial distances. This would include non-local effects. It may not be spurious that the time required for an electron to complete one orbit of an electron (10^{-16} s) is in the same order of magnitude as the time for a light quantum to traverse a 10 nm plasma cell membrane. In other words the information contained within the traversal would have to the potential to be recorded as one bit within a single complete rotation.

In the third experiment the fact that photons from the simplest of chemical reactions can be entangled over distance was explored. In previous research non-local effects were shown between pairs of dishes of cells or pairs of brains as long as they shared the appropriate magnetic field configuration. Technically the non-local effects, or the excess correlation, could have been confounded by some aspect of the complexity of either the brains or the cells. By demonstrating that the excess correlations of photon emissions in two non-traditional spaces simultaneously could be produced by a simple chemical reaction the importance of light, per se, would be demonstrated.

The existence of such non-local effects would suggest alternative processes by which photons could behave as initiators of signalling pathways or alterations in membrane dynamics. Proximal adjacency, charge proximity or even chemotaxic gradients would not be the only mechanisms by which cells could be affected. The non-locality would suggest that photon patterns that might

stimulate aberrant changes in other cells could occur over distances far beyond the source cell and even to cells in other organisms. The existence of these phenomena would have significant implications for perspective for alternative explanations for both “metastases” as well as “contagion”.

1.5 References

Aczel A. D. (2002) Entanglement: the greatest mystery in physics. Vancouver: Raincoast Books.

Adey, W.R. (1981) Tissue interactions with non-ionizing electromagnetic fields. Physiol. Rev, 61: 435-513.

Berzhanskaya, L. Y., Beloplotova, O. Y., Berzhansky, V. N. (1995) Electromagnetic field effect on luminiescent bacteria. IEEE Transactions on Magnetics, 31: 4274-4275.

Berzhanskaya, L. Y., Berzhanskii, V. N., Beloplotova, O. Y., Pil'Nikova, T. G., Metlyayev, T. N. (1996) Bacterial luminescent activity as a pointer to geomagnetic disturbances. Biophys, 40: 761-764.

Bohr, N. (1958) Atomic physics and human knowledge. N.Y.: John Wiley & Sons.

Buckner, C.A. (2011) Effects of electromagnetic fields on biological processes are spatial and temporal-dependent. Laurentian University: Ph.D. Dissertation, Biomolecular Sciences Program.

Buckner, C.A., Buckner, A.L., Koren, S.A., Persinger, M.A., Lafrenie, R.M. (2013) Exposure to a specific time-varying electromagnetic field inhibits cancer cell growth by affecting calcium influx (in submission).

Cifra, M., Fields, J.Z., Farhadi, A. (2011) Electromagnetic cellular interactions. Prog. Biophys. Mol. Biol. 105, 223-246.

Choi, D-H., Lee, K-H, Kim, J-H, Moon Young, K., Lim, J-H. (2012) Effect of 710 nm visible light irradiation on neurite outgrowth in primary rat cortical neurons following ischemic insult. Biochem. Biophys. Res. Commun. 422, 272-279.

Cosic, I. (1994) Macromolecular bioactivity: is it resonant interaction between macromolecules? Theory and application, IEEE Trans. BioMed. Engineer. 41, 1101-1114.

Dotta, B. T., Mulligan, B. P., Hunter, M. D. and Persinger, M. A. (2009) Evidence of macroscopic quantum entanglement during double quantitative electroencephalographic (QEEG) measurements of friends vs strangers. *NeuroQuantology*, 7, 548-551.

Dotta, B. T., Buckner, C. A., Cameron, D., Lafrenie, R. M., Persinger, M. A. (2011a) Biophoton emissions from cell cultures: biochemical evidence for the plasma membrane as the primary source, Gen. Physiol. Biophys. 30, 301-309.

Dotta, B. T., Buckner, C. A., Lafrenie, R. M., Persinger, M. A. (2011b) Photon emissions from human brain and cell culture exposed to distally rotating magnetic fields shared by separate light-stimulated brains and cells. Brain Res. 388, 77-88.

Gabrielli, E., Huitu, K., Roy, S. (2006) Photon propagation in magnetic and electric fields with scalar/pseudoscaler couplings: A new look. Physical Review D. 74, 1-21.

Grassi, C., D'Ascenzo, M., Torsello, A., Martinotti, G., Wolf, F., Azzena, G. B. (2004) Effects of 50 Hz electromagnetic fields on voltage-gated Ca2+ channels and their role in modulation of neuroendocrine cell proliferation and death. Cell Calcium, 35(4), 307-315.

Gurwitch, A. G. (1923) Das problem der zellteilung physiologisch betrachtet, In A. G. Gurwitsch et al, (eds). Monographien aus dem Gesamtgebiet der Physiologie der Pflanzen und der Tiere. 473-475.

Havelka, D., Cifra, M. (2009) Calculation of the electromagnetic field around a mitochondria. Acta Polytechnia; 49, 58-63.

Hideg, E., Kobayashi, M., Inaba, H. (1991) Spontaneous ultraweak light emission from respiring spinach leaf mitochondria. Biochemica et Biophysica Acta (BBA)-Bioenergetics, 1098(1), 27-31.

Isojima,Y., Isoshima, T., Nagai, K., Kikuchi, K., Nakagawa, H. (1995) Ultraweak biochemiluminesence detected from rat hippocampal slices. NeuroReports, 6, 658-660.

Kahn, A. U. and Kasha, M. (1994) Singlet molecular oxygen evolution upon simple acidification of aqueous hypochlorite: application to studies on the deleterious health effects of chlorinated drinking

water. *Proceedings of the National Academy of Sciences*, **91**, 12362-12364.

Kobayashi, M., Takeda, M., Ito, K.-I., Kato, H., Inaba, H. (1999a) Two dimensional photon counting imaging and spatiotemporal characterization of ultraweak photon emission from a rat's brain in vivo.J. Neurosci. Met. 93, 163-168.

Kobayashi, M., Takeda, M., Sato, T., Yamazaki, Y., Kaneko, K., Ito, K. I., Kato, H., Inaba, H. (1999b) In vivo imaging of spontaneous ultraweak photon emission from a rat's brain correlated with cerebral energy metabolism and oxidative stress. Neurosci. Res. 34, 103-113.

Mach, Q.H., Persinger, M.A. (2009) Behavioural changes with brief exposures to weak magnetic fields patterned to stimulate long term potentiation. Brain Res., 1261, 45-53.

Malenka, R. C., Bear, M. F. (2004) LTP and LTD: An Embarrassment of Riches. Neuron. 44, 5-21

Martin, L.J., Koren, S.A., Persinger, M.A. (2004) Thermal analgesic effects from weak, complex magnetic fields and pharmacological interactions. Pharm. Biochem. Behav. 78, 217-227.

Pall, M. L. (2013) Electromagnetic fields act via activation of voltage-gated calcium channels to produce beneficial or adverse effects. J Cell Mol Med. doi: 10.1111/jcmm.12088.

Persinger, M. A. and Koren, S. A. (2007) A theory of neurophysics and quantum neuroscience: implications for brain function and the limits of consciousness. *International Journal of Neuroscience*, 117, 157-175.

Persinger, M.A. (2010) 10^{-20} Joules as a neuromolecular quantum in medicinal chemistry: an alternative approach to myriad molecular pathways. Cur. Med. Chem. 17, 3094-3098.

Persinger, M. A., Lafreniere, G. F., Dotta, B. T. (2012) Marked increases in background photon emissions in Sudbury Ontario more than one week before the magnitude > 8.0 earthquakes in Japan and Chili. International Journal of Geosciences. 3(3), 10.4236/ijg.2012.33062

Popp, F.-A. (1979a) Photon storage in biological systems, In F. A. Popp, G. Becker, H. L. Konig, W. Pescha (eds), Electromagnetic bioinformation. Munich: Urban and Schwarzenberg: 123-149.

Popp, F.-A. (1979b) Electromagnetic bioinformation. New York: Urban and Schwarzberg. pp. 123-149.

Popp, F-A. (1988) Biophoton emission, Experientia 44 543-630.

Popp, F.-A., Li, K.H., Mei, W.P., Gale, M., Neurohr, R. (1988) Physical aspects of biophotons. Experientia 44, 576-585.

Potenza, L., Ubaldi, L., De Sanctis, R., De Bellis, R., Cucchiarini, L., Dacha, M. (2004) Effects of a static magnetic

field on cell growth and gene expression in *Escherichia coli*. Mutation Research; 561, 53-62.

Scott, R. Q., Roschger, P., Devarj, B., Inaba, H. (1991) Monitoring a mammalian nuclear membrane phase transition by intrinsic ultraweak light emission. FEBS; 285, 97-98.

Stapp, H. (2009) Nonlocality. In D. Greenberger, K. Hentschel, & F. Weinert (Eds). *Compendium of Quantum Physics.* Springer: N.Y., pp. 404-410.

Quickenden, T.I. (1974) Weak luminescence from yeast saccharomyces cerevisiae and the existence of mitogenetic radiation. Biochem. Biophys. Res. Comm. 60, 764-770.

Rastogi, A., Pospisil, P. (2011) Spontaneous ultraweak photon emission imaging of oxidative metabolic processes in human skin: effect of molecular oxygen and antioxidant defense system. J. Biomed Opt.; 16(9), doi:10.1117/1.3616135

Schrodinger, E. (1944) What is life? Cambridge: Cambridge Univer. Press,.

Sun, Y., Wang, C., Dai, J. (2010) Biophotons as neural communication signals demonstrated in situ biophoton autography. Photochem. Photobiol. Sci. DOI: 10.1039/b9pp00125e.

Tilbury, R. N., Quickenden, T. I. (1988) Spectral and time dependence studies of the ultraweak bioluminescence emitted by the bacterium *Escherichia coli*, 47, 145-150.

van Wijk, R., van Wijk, E. P. A. (2005) An introduction to human biophoton emission. Forsch Komplemntarmed Naturheilkd. 12, 77-83.

van Wijk, E. P. A., van Wijk, R., Bajpai, R. P. (2008) Quantum squeezed state analysis of spontaneous ultra weak light photon emission of practitioners of meditation and control subject. Indian J Exp Biol. 46, 345 – 352.

van Wijk, R., van Aken, H., Mei, W., Popp, F-A. (1993) Light induced photon emission by mammillian cells. J Photochem Photobiol B. 18(1), 75-79.

Whissell, P. D., Persinger, M. A. (2007) Emerging synergisms between drugs and physiologically-patterned weak magnetic fields: implications for Neuropharmacology and the human population in the twenty-first century. Curr Neuropharmacol. 5(4), 278-288.

Wu, H-P., Persinger, M.A. (2011) Increased mobility and stem-cell proliferation rate in Dugesia tigrina induced by 880nm light emitting diode. J Photochem. Photobiol. B., 102(2), 156-160.

Chapter 2: Shifting Wavelengths of Ultraweak Photon Emissions From Dying Melanoma Cells: Their Chemical Enhancement and Blocking Are Predicted by Cosic's Theory of Resonant Recognition Model for Macromolecules

Published in Naturwissenschaften

Abstract

During the first 24 hr after removal from incubation melanoma cells in culture displayed reliable increases in emissions of photons of specific wavelengths during discrete portions of this interval. Applications of specific filters revealed marked and protracted increases in infrared (950 nm) photons about 7 hrs after removal followed 3 hr later by marked and protracted increases in near ultraviolet (370 nm) photon emissions. Specific wavelengths within the visible (400 to 800 nm) peaked 12 to 24 hr later. Specific activators or inhibitors for specific wavelengths based upon Cosic's Resonant Recognition Model elicited either enhancement or diminishment of photons at the specific wavelength as predicted. Inhibitors or activators predicted for other wavelengths, even within 10 nm, were less or not effective. There is now evidence for quantitative coupling between the wavelength of photon

emissions and intrinsic cellular chemistry. The results are consistent with initial activation of signaling molecules associated with IR followed about three hours later by growth and protein-structural factors associated with UV. The greater than exhibited photon counts compared to raw measures through the various filters, which also function as reflective material to other photons, suggest that photons of different wavelengths might be self-stimulatory and could play a significant role in cell-to-cell communication.

2.1 Background

Ultraweak photon emissions (UPE) have been measured from cells, organs and organisms [Chang and Popp 1998] but the precise coupling between molecular pathways and specific wavelengths of these pervasive electromagnetic phenomena have not been completely established. Popp [1988] has argued that *all* living tissue display very weak photon emissions. Several decades ago Gurwitsch [1923] suggested that "mitogenetic radiation" or photons within biological tissue could trigger and regulate cell growth. Biophotons have recently been demonstrated by *in situ* biophoton autography to behave as neural communication signals [Sun et al. 2010]. The numbers of photons emitted are in the order of a few to a few hundred per second per cm^2 and require measurement by photomultiplier tubes.

The quanta of energies associated with the photons vary depending upon the state of the cells and can range from the ultraviolet through the visible range into the infrared. Cohen and Popp [1997] indicate the emissions continuously cover the spectral range from at least 200 to 800 nm. Tilbury and Quickenden [1988], employing cultures of *Escherichia coli*, found that the UV (210-300 nm) and visible (450-620 nm) regions were associated with the exponential phase of growth while a second period or stationary

phase of growth produced photons only in the visible region. The magnitude of these emissions was in the order of 10^3 counts s^{-1}.

That applied light of specific frequencies affect cell growth has received recent attention. Wu and Persinger [2011] reported increased stem cell proliferation in sectioned planarian following exposure to 880 nm light emitting diodes (LED) compared to incandescent red or white light or darkness and ambient light; a similar effect with 685 nm laser radiation was found by de Souza et al. [2005]. Treatment of primary rat cortical neurons, following ischemia, by 710 nm light promoted synaptogenesis through MAPK activation [Choi et al. 2012]. Photobiomodulation, depending upon wavelength, can stimulate or inhibit biological functions without producing irreducible damage [Liu et al. 2009]. In fact shrinkage of tumors occurs after exposure to near-infrared light in target cells that express the receptor for epidermal growth factor [Mitsunaga et al. 2011].

Although original research utilized paradigms where luminescence was measured in cells following irradiation of light with varying wavelength, the occurrence of "degradation radiation" [Popp 1979] from dying cells has been considered a means by which one could study the nature of the cellular states. Dotta et al. [2011a] measured photon flux density from 8 different cell lines for 24 hr after removal from incubation. One of the types, B16-BL6 (mouse melanoma) cells, demonstrated a conspicuous emission

profile. Exposure of ~10^6 of these cells to compounds related to signaling pathways and synchronized M- and S-phase measures strongly suggested the plasma cell membrane was the source of the UPE and that the rates were in the order of 10^{-20} J per second per cell [Dotta et al. 2011a]. The photon flux density was ~10^{-11} $W \cdot m^{-2}$ for ~1 million cells which was comparable to levels found in other tissue from other studies [Isojima et al. 1995].

In the present experiments we decided to discern if the wavelengths of the photon emissions changed over the first 24 hr after the cells had been removed from incubation. Pilot studies had indicated powerful and reliable emissions at specific wavelengths. In order to couple the specific wavelengths with the molecular activity within the cell, we required a rational mechanism by which specific molecular compounds could be selected. In 1994 Irena Cosic [1994] published a new physicomathematical approach, the Resonant Recognition Model (RRM). It was based upon the representation of the protein primary structure as a numerical series. This was accomplished by assigning each amino acid a physical value (specifically the energy of delocalized electrons for each amino acid) that was relevant to the protein's biological activity. She obtained characteristic RRM frequencies for different functional groups of proteins and DNA regulatory sequences.

Cosic had developed this model to explain the unexpected but significant resemblances between functionally dissimilar proteins

and the nonsignificant similarities between functionally related peptides. Previously we Wu & Persinger, 2011] found that the wavelength predicted from Cosic's procedure for cyctochrome C and cytochrome oxidase II (proteins most likely involved with regenerating planarian blastema) was within error range of our effective infrared treatment. Here we present evidence that photons with different wavelengths display different peak activities as melanoma cells respond to the change from incubators to ambient temperature and that these specific emissions can be blocked or facilitated by promoters or inhibitors predicted by the Cosic model.

2.2 Methods

Over several months a total of 60 experiments were completed on separate days. For each experiment approximately 1 million B16 cells approaching 100% confluence were used for measurement. Cells were maintained in 150 x 20 mm tissue culture plates (Sarstedt, Laval, Qc) in Dulbecco's Modified Essential Medium (DMEM, Hyclone, Logan, UT) supplemented with 10% fetal bovine serum, 100 ug/m streptomycin, and 100 U/ml penicillin (Invitrogen, Burlington, ON). Cells were incubated at 37°C in 5% CO_2 and subcultured 1:5 about every 4 days. The cell monolayers were washed with PBS, pH 7.4 and harvested by incubation in 0.25% trypsin-EDTA and then collected by centrifugation at 1000 g for 10 min. All treatments were added to

cell culture plates ~30-60 min prior to photon emission measurement. After removal from the incubator the single plate of ~10^6 cells were transported to the biophysics area within 30-60 min and placed over the 3 cm^2 aperture of a SENS-TECH LTD. Model DM0090C digital photomultiplier tube (PMT). The rationale for removing the cells from physiological temperature was based on past research indicating that stressed cells produced consistent robust emission levels at ambient temperature [Dotta et al. 2011a]. According to specifications, the range of sensitivity for photons was 280 nm to 850 nm. Typical dark counts of this PMT were in the range of 15-16 counts/sec. Measurements were recorded by the system software every 2.5 s for 22.5 hr (the maximum rate and duration determined by the software). Compared to dark counts a plate of 10^6 cells generated about 40 to 55 counts s^{-1} above noise during the beginning of the experiment and about 5 to 10 counts s^{-1} above noise by the end of the experiment. In addition, controls were performed with a single plate with only medium and with no plate whatsoever. Both of these control conditions produced null results. While typical averaged absolute counts in the first hours averaged 35-40 counts s^{-1}, the first few minutes (5-15 min) consistently produced absolute values in the 80 - 120 counts s^{-1} range.

Assuming $5 \cdot 10^{-19}$ J per photon for mid-range light, an average 55 photons s^{-1} and a cross section area of the aperture of ~$3 \cdot 10^{-4}$ m^2, the irradiance flux density would have been about $1.1 \cdot 10^{-13}$ $W \cdot m^{-}$

^{2}. However because the ~0.5 million cells were confluent over the 28 cm^2 of the dish but the aperture was only 3 cm^2 across, the UPE would have been measured from 0.11 of the total dish area (about 10^5 cells). The light generated in 3-D space by the single layer of cells in one direction to the aperture (πr^2) relative to the area of the sphere from the plane of the cells to PMT ($4\pi r^2$) about 1 cm in distance indicates that only about one-fourth of the UPE would be recorded. Consequently the effective flux density was ~$0.4 \cdot 10^{-11}$ $W \cdot m^{-2}$ which is within the range of our previous measurements using a separate PMT model (Model 15 Photometer from Pacific Photometric Instruments with photomultiplier tube housing for a RCA electron tube (BCA IP21)) [Dotta et al 2011a].

All experimental conditions were completed in triplicate on different days. To discern the differential emissions from different wavelengths, the following bandpass filters (Chroma Technologies) were interposed between the PMT aperture and the bottom of the cell container: 370 nm, 420 nm, 490 nm, 500 nm, 620 nm, 790 nm, 950 nm, and 995 nm. According to the manufacturer each filter selected the peak wavelength ± 5 nm. These filters are typically designed for normal incidence of the photon beam; however light emission from cells will be emitted at all angles. Because of this it is possible that light approaching the filters at varying angles (i.e. 20 degrees) can have their wavelength shifted. Because of this, cell dishes were placed directly over the filter

(dish depth 1 mm) and each condition had multiple replicates to ensure the most accurate results.

These filters were selected based upon our theoretical approach [Cosic 1994] and to ensure coverage of the ultraviolet, visible, and infrared wavelength. In addition we selected the 500 nm and 490 nm filters to investigate the functional "band width" of the effective light emissions for the biological functions. There was no response, i.e., a flat line activity of 15 photons s^{-1} for the 995 nm filter while the 950 nm showed marked cell-related activity. Given the various Quantum Efficiency (QE) values for each wavelength (~0.1% for 995 nm and ~20% for 420 nm) absolute photon counts for individual wavelengths may be higher than measured. Because of this we have chosen to focus on alteration of temporal profile (enhancement/diminishment of peaks) rather than overall intensity.

Once the temporal profile for the peak photon emissions for the different wavelengths (the filters) were obtained, specific activators and inhibitors were selected based upon Cosic's calculation from:

$$\lambda = K/f_{rrm} \quad (1),$$

where λ is the wavelength of the light irradiation in nm, K is the RRM frequency space calculated by Cosic [1994], and f_{rrm} is the numerical frequency obtained by the RRM. K value used was 201 with standard deviation of 15%. Here λ was the wavelength of interest and K was Cosic's constant. After obtaining the f value we consulted Cosic's tables for the protein family that optimally matched her f value [Cosic 1994].

Table 1. List of individual wavelengths calculated F, potential protein target, and potential protein target's theoretical F. Target protein's theoretical F is within ~0.15 of calculated F. These proteins were the specific targets of our inhibitors/activators.

Wavelength (nm)	Calculated F (f=K/λ ; K=201 SD 15%)	Protein	Theoretical F
370	0.543	Insulin-like Growth Factors / Fibroblast Growth Factors	0.500 / 0.502
420	0.478	SOS operators, Actin / Myosin	0.468, 0.488 / 0.340
490	0.410	Kinase –PI3K	0.429
500	0.402	Kinase - PKC	0.429
620	0.032	Lysosomes / Glucagon	0.328 / 0.320
790	0.254	Growth Factors / Restriction Enzymes	0.292 / 0.291
950	0.211	Signal Proteins	0.214

For example Cosic's value for 370 nm was 0.543 and because growth proteins (IGF) had been calculated with a value of 0.50, this class of proteins was used. For 5 different filters we selected compounds from Cosic's table that were specific activators or inhibitors for the wavelength and those that were not specific activators or inhibitors, that is they were specific to another wavelength. We then obtained those compounds from what was available in our repertoire.

The list of compounds and the specific filter were: 370 nm, inhibitor: Wortmannin; 420 nm, inhibitor: Genistein, activator: PMA [phorbol 12-myristate 13-acetate]; 490 nm, inhibitor: SC79 [2-Amino-6-chloro-α-cyano-3-(ethoxycarbonyl)-4H-1-benzopyran-4-acetic acid ethyl ester], activator: SQ22536; 500 nm, inhibitor: BIS (Bisindolylmaleimide), and 950 nm, inhibitor: PD (PD8059), activator: forskolin. These compounds were considered specific inhibitors or specific activators for that wavelength. The use of term non-specific inhibitor or activator indicates the compound contained with the media for those cells whose UPE were measured was optimal for another filter. All chemicals were obtained from Sigma and from EMD Calbiochem. SQ22536 and Forskolin were prepared in DH_2O, all other were prepared in DMSO.

Given the range of above wavelengths and the temporal differences in the appropriate directional responses to these compounds we directly tested responses for the two most adjacent

filters: 490 and 500 nm. When the 490 nm filter was employed we tested the activator for 490 nm (SC79), the specific inhibitor for 490 (SQ) and the specific inhibitor for 500 nm (BIS), i.e., a non-specific inhibitor. For 500 nm we applied BIS (the specific inhibitor), SQ (the one most optimal for 490 nm, non-specific inhibitor) and SC79 (the one most optimal for 490 nm as a specific activator).

The dilution was 1:1000 and 2.5 uL of drug was added per 2.5 mL of media. All compounds were prepared at 10 µM concentrations except for BIS and SQ79 which were prepared at 5 µM concentrations. These concentrations were chosen based upon past research that elicited reliable increases in photon emissions from B16-BL6 mouse melanoma cells [Dotta et al. 2011a]. The means of the absolute numbers of photons per sec for each treatment for each filter from the triplicates were analyzed as results. The baseline levels of photon counts s^{-1} for raw (no filters) when cells were not present were not significantly different from photon counts when cells were present with the 995 nm filter, suggesting that photon emissions from cells were <995 nm or that this threshold reflected the limits of the PMT. Where relevant, z-scores were calculated in order to compare UPE through different filters.

2.3 Results

The most conspicuous source of photon emissions from the melanoma cells during the first 24 hrs following removing from standard incubation was the marked increase in the numbers of UPE through the 370 nm and 950 nm filters. The results are shown in Figure 1 and reflect the mean of three triplicates for each filter.

About 6 hr after the removal from the incubators and after photon measurements began there was a sudden increase in infrared (invisible) photons (950 nm) that were maintained for the remainder of the measurements. About 3.5 hrs after this increase there was a second sudden increase in the ultraviolet (invisible) range (370 nm) that was also maintained for the remainder of the experimenter. Lagging of the two curves by 3.5 hrs resulted in a correlation (Pearson r) of ~0.85.

The second conspicuous effect is shown in Figure 2 that includes the results for all of the filters including those within the visible wavelengths. In order to accommodate differences in the absolute values for the numbers of photons per second z-scores were obtained.

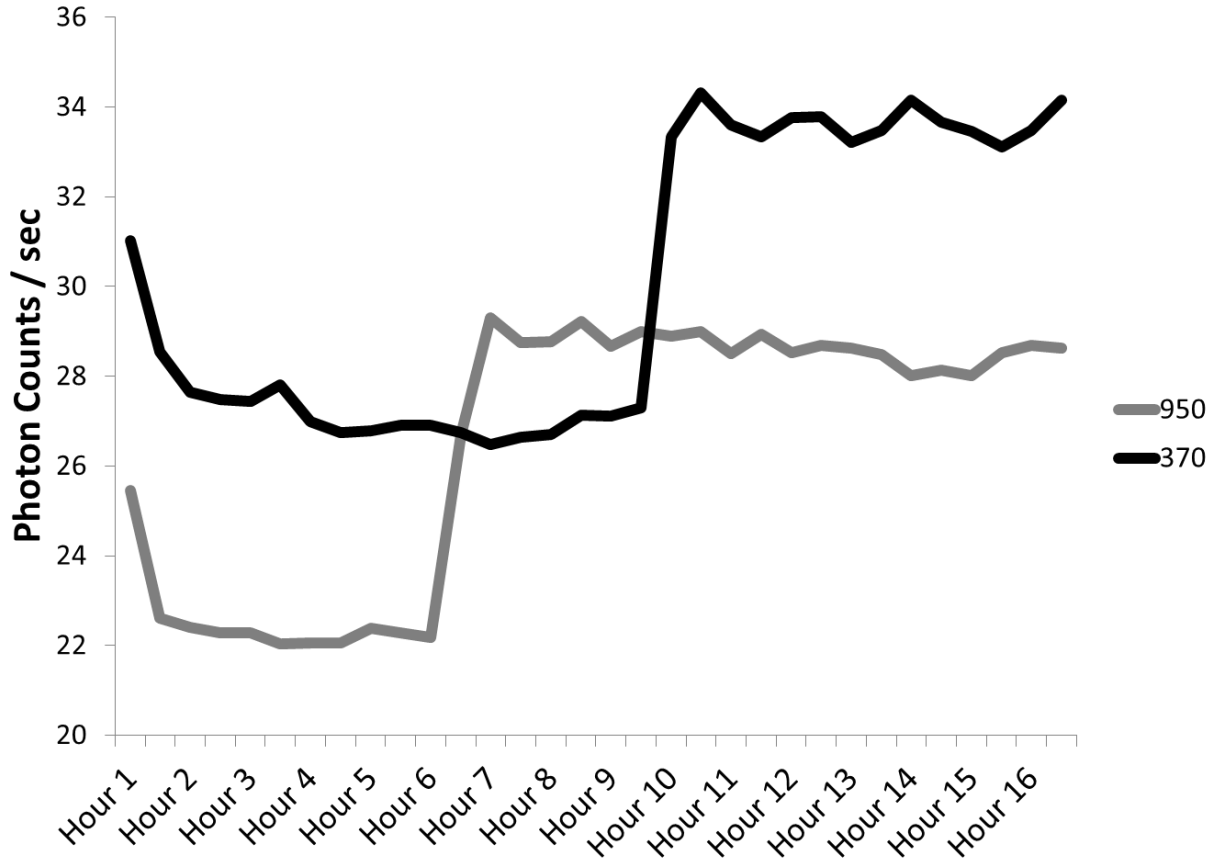

Figure 1. Absolute photon counts (sec) of 2 different filters (370 nm and 950 nm) as a function of time for untreated cell cultures (10^6 cells) removed from an incubator and placed at room temperature. Black line corresponds to 370 nm filter, while grey line corresponds to 950 nm filter.

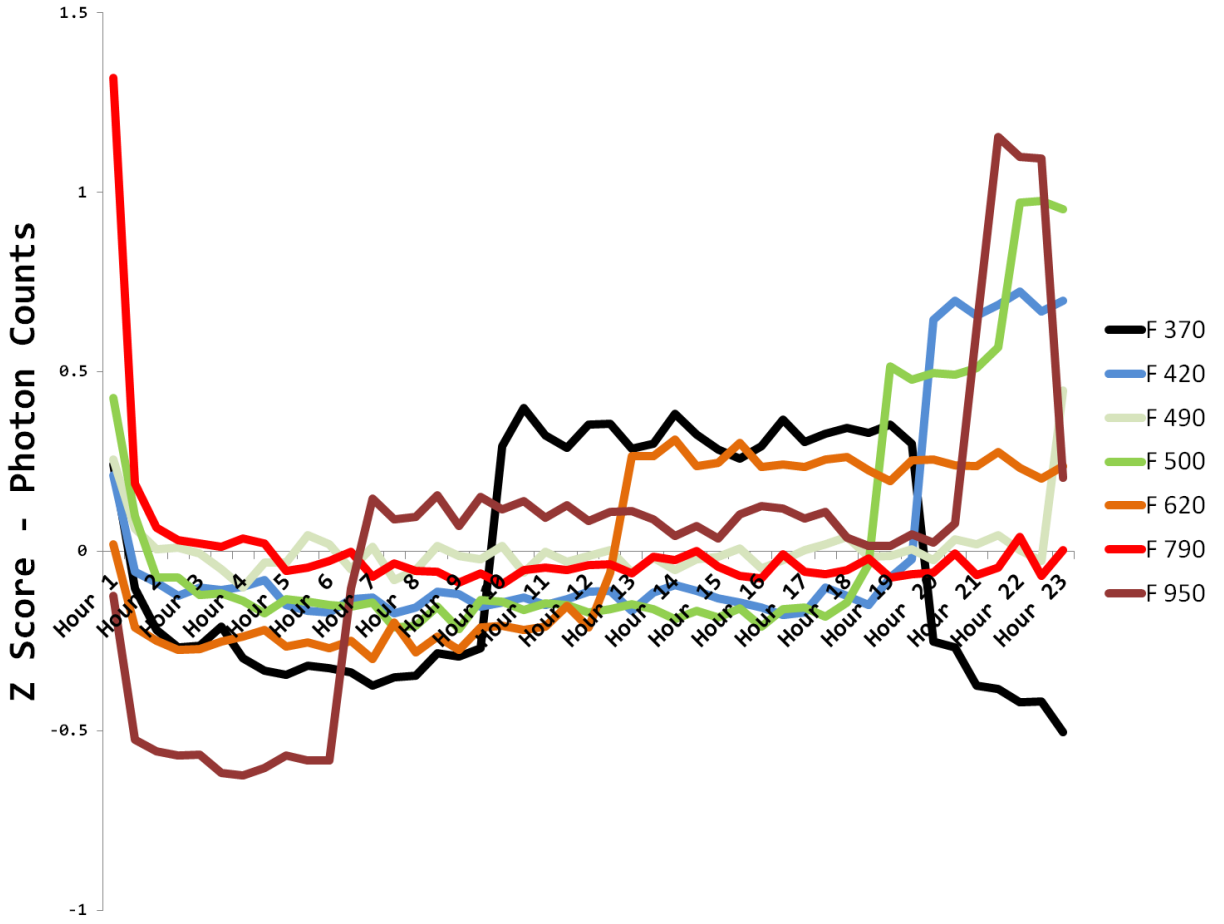

Figure 2. Z-Scored photon counts (sec) for untreated cell cultures (10^6) removed from an incubator and placed at room temperature as a function of time. Each filter condition is in triplicate. The ranges of average absolute counts s^{-1} are: 370 nm (26 – 35 counts s^{-1}), 420 nm (22 – 30 counts s^{-1}), 490 nm (24 – 28 counts s^{-1}), 500 nm (23 – 35 counts s^{-1}), 620 nm (21 – 27 counts s^{-1}), 790 nm (22 – 30 counts s^{-1}), and 950 nm (22 – 37 counts s^{-1}).

The interface between visible and infrared (790 nm) displayed a dramatic diminishment within an hour (~30 min) of removal from incubation. The major increases in photon emissions within the remainder of the visible range began after the 12^{th} hour for the 620 nm, 500 nm, and 420 nm. The 490 nm wavelength displayed a relative increase only at the end of the measurement period, at about 22 hr. After the increase in photon emissions within the visible range, photons within the 950 nm range displayed a second peak emission. In comparison the numbers of photons (about 10 per s) through the 995 filter remained constant (flat line) across the entire experiment.

A clear relationship between wavelengths of photons associated with a particular filter and the class of compounds predicted by Cosic's equation was verified. As shown in Figure 3, the photon counts through the 490 nm filter showed that specific activator (SQ22536) increased the photon counts while the specific inhibitor (SC79) diminished the photon counts by comparable numbers [$F(3,31)=201.1$, $p=<0.001$, $eta^2=.95$].

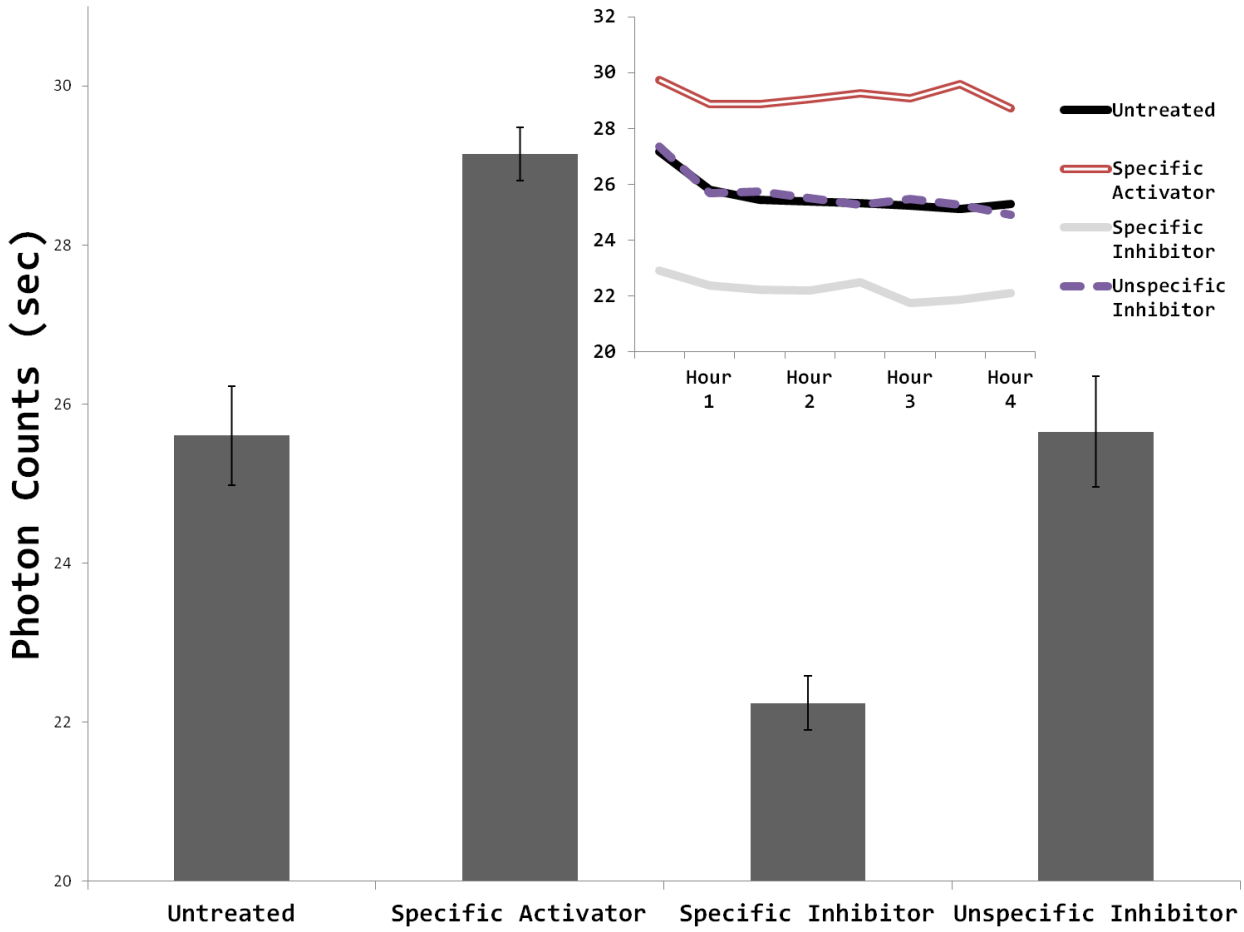

Figure 3. Means and standard deviations of absolute photon counts per second for 4 separate treatment conditions of filter 490 during the first 4 hours of testing. Untreated corresponds to the no drug 490 nm condition, specific activator refers to SC79, specific inhibitor refers to SQ, and unspecific inhibitor refers to BIS. Raw data of each condition throughout the first 4 hours can be seen in the upper right quadrant.

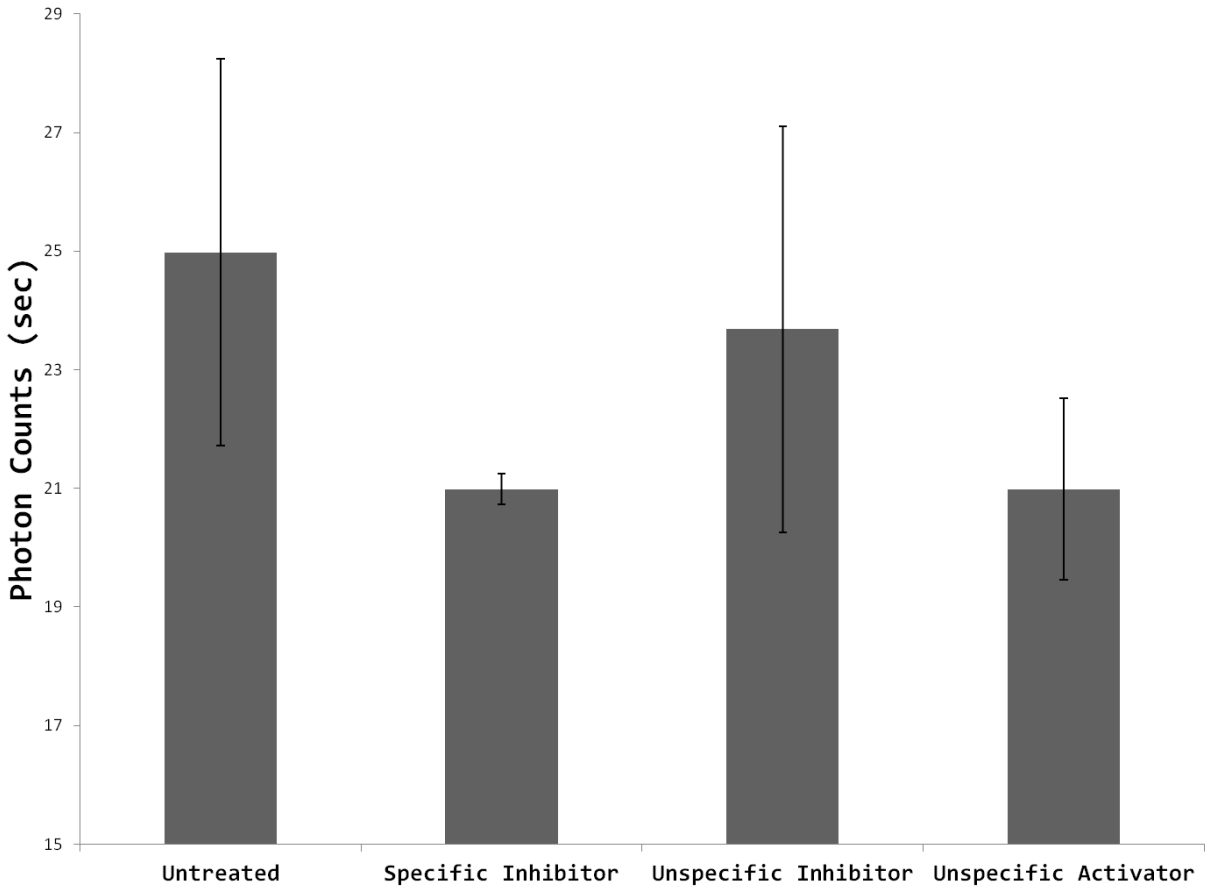

Figure 4. Means and standard deviations of absolute photon counts per second for 4 separate treatment conditions of filter 500 during the entire testing sample (22.5 hrs). Untreated corresponds to the no drug 500 nm condition, specific inhibitor refers to BIS, unspecific inhibitor refers to SQ, and unspecific activator refers to SC79.

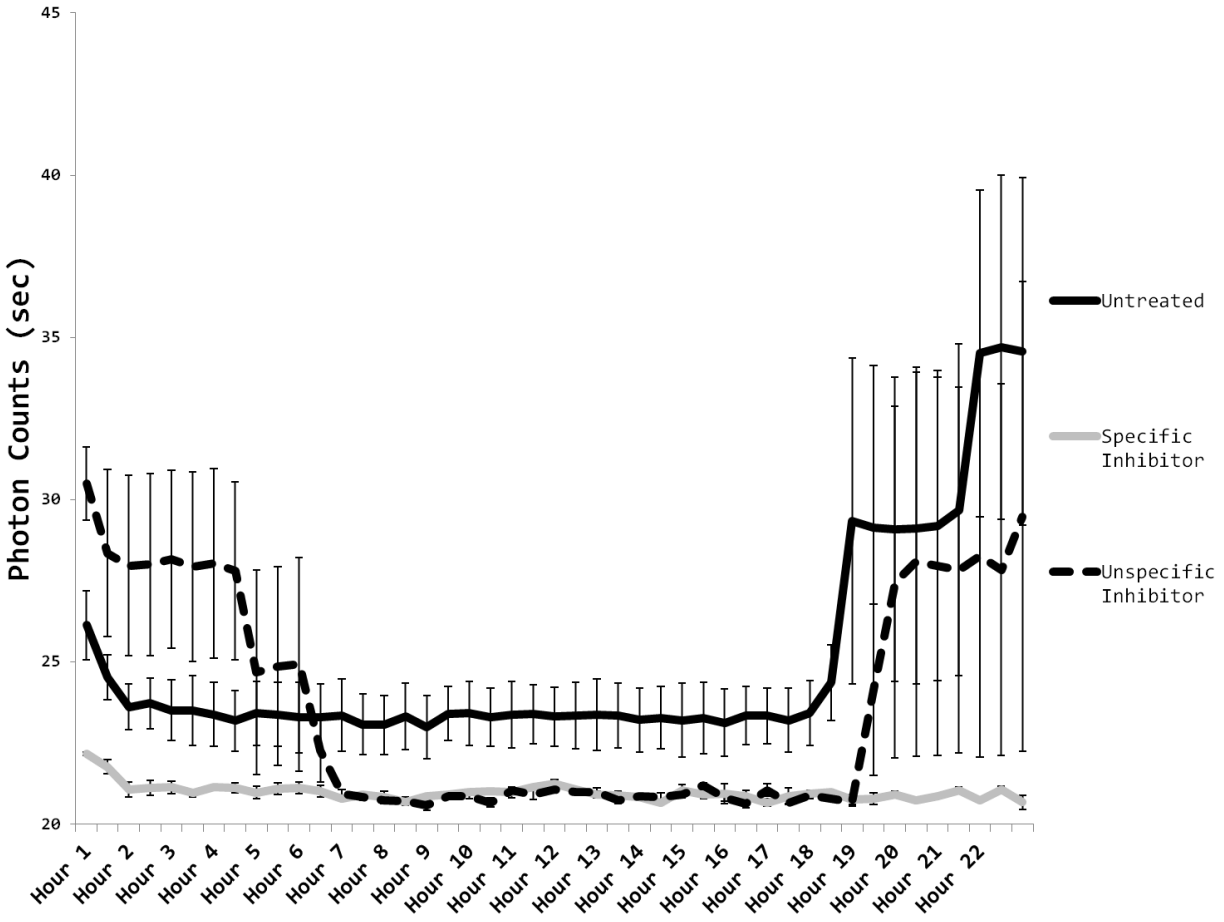

Figure 5. Means and standard errors of absolute photon counts per second for 3 separate treatment conditions of filter 500 during the entire testing sample (22.5 hrs). Untreated corresponds to the no drug 500 nm condition, specific inhibitor refers to BIS, and unspecific inhibitor refers to SQ.

Photon emissions after a non-specific inhibitor (BIS) had been added to the cells did not differ from the values for untreated cells. The effects across the three triplicates completed on different days were consistent.

On the other hand, Figure 4 demonstrates that when the two drugs that were selected specifically for the 490 nm Cosic solution were applied to cells where 500 nm photons were measured; there was no evidence of either persistent facilitation or inhibition of raw numbers of photon emissions. Only the specific inhibitor for the 500 nm filter photons produced significant inhibition of counts as demonstrated by ONEWAY analysis of variance [$F(3,179)=28.5$, $p=<0.001$, $eta^2=.32$]. What did occur was the shift in when the maximum numbers of photons were emitted during the experiment. The specific inhibitor selected by Cosic criteria for the 500 nm wavelength (BIS) suppressed the photon emissions in this band throughout the experiment whereas the non-specific inhibitor (SC79) diminished the emissions only between the 7^{th} and 19^{th} hours (Figure 5). During the first few hours it actually enhanced UPE.

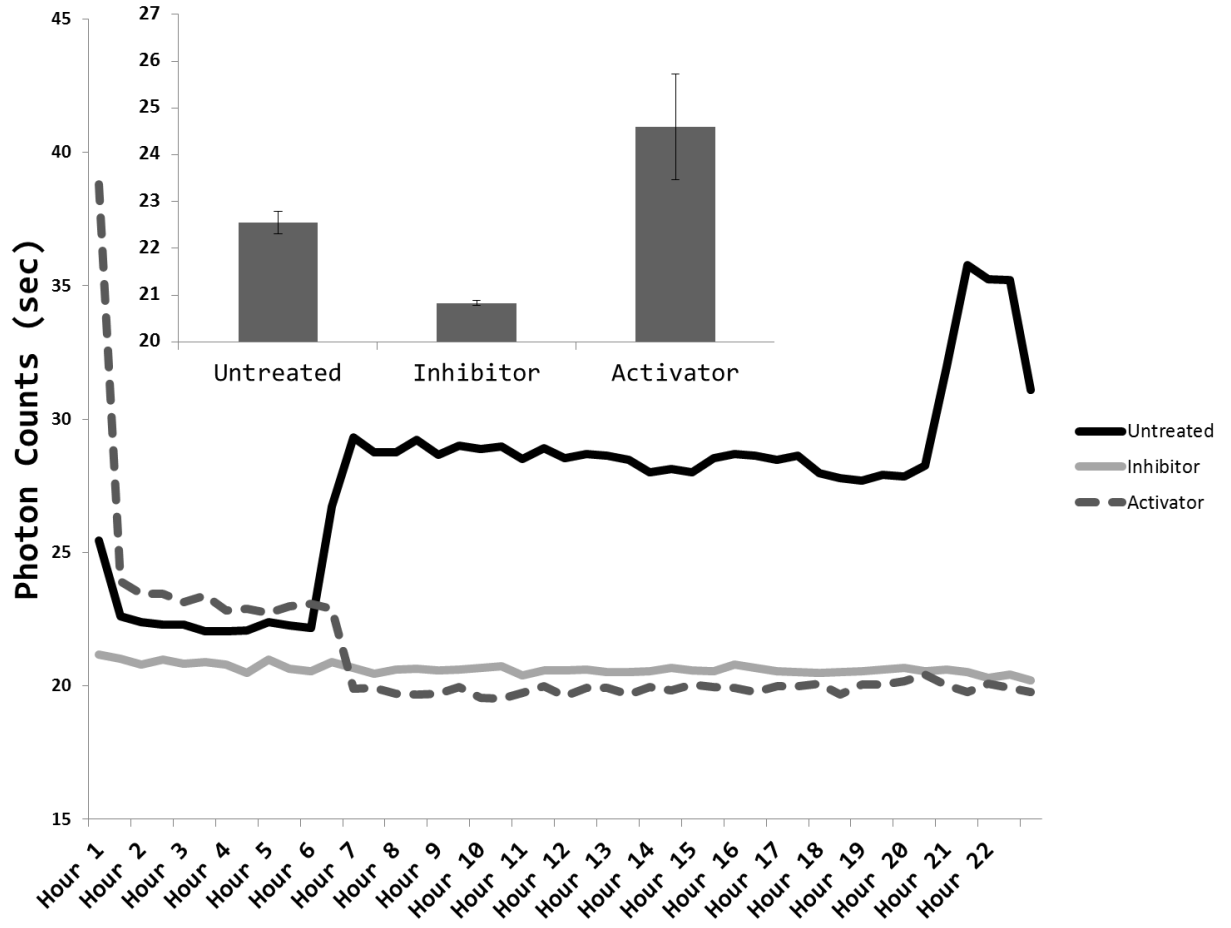

Figure 6. Means of absolute Photon counts (sec) of Filter 950 with 3 separate treatment conditions as a function of time. Untreated refers to the no drug 950 nm condition, inhibitor refers to PD, and activator refers to Forskolin. Means and standard error values for photon counts per second for the first 6 hours of testing can be seen in the upper left quadrant.

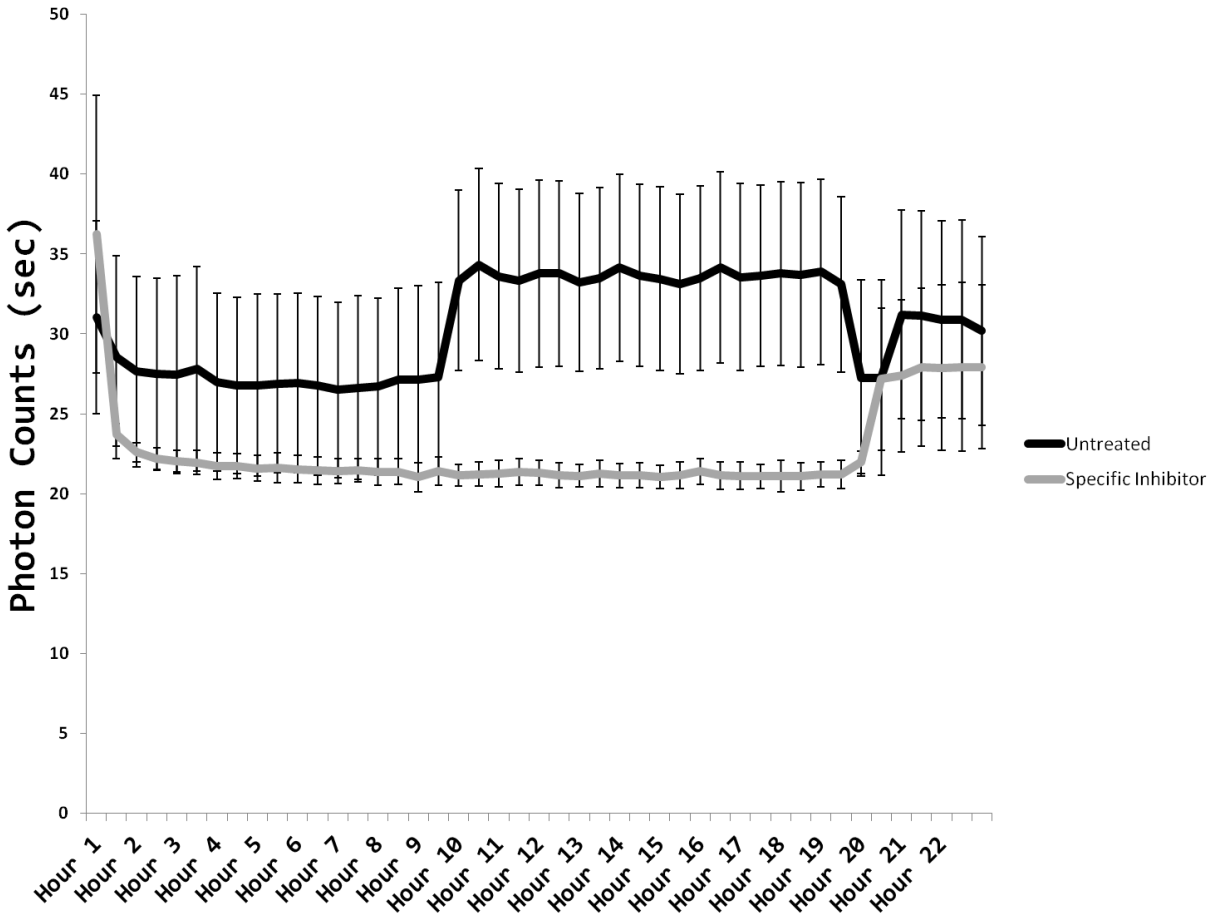

Figure 7. Means and standard errors of absolute photon counts per second for 2 separate treatment conditions of filter 370 during the entire testing sample (22.5 hrs). Untreated corresponds to the no drug 370 nm condition, inhibitor refers to Wortmannin.

Even the wavelengths associated with the largest numbers of photon emissions were inhibited by the appropriate Cosic-predicted molecules. As can be seen in Figure 6, the inhibitor (PD8059) for 950 nm suppressed the powerful and protracted emission of photons from 6 hrs to the end of the experiment [$F(2,32)=5.065$, $p=0.01$, $eta^2=.25$]. The activator (forskolin) transiently increased emissions for the first 6 hours. Following this transient elevation there was a decrease in photons counts to baseline levels.

At the other end of the spectrum, 370 nm, the inhibitor (Wortmannin) based on this wavelength suppressed the increase in photon emissions during the period of 9 to 16 hours but was no longer effective when enhancement began to drop after about 19 hrs. This can be seen in Figure 7 [$F(1,89)=151.2$, $p=>0.001$, $eta^2=.63$]. These results are very interesting as Wortmannin has a very short half-life (~10 min). So by hour 9 there would be less than 1 molecule per ml. While this effect was reliable, the short half-life of the compound makes it difficult to deduce when this effect of inhibition of UPE is taking place.

For the 500 nm filter the specific inhibitor (BIS) flattened the UPE emission while the non-specific inhibitor (SQ) and non-specific activator (SC79) produced transient activation and inhibition of UPE.

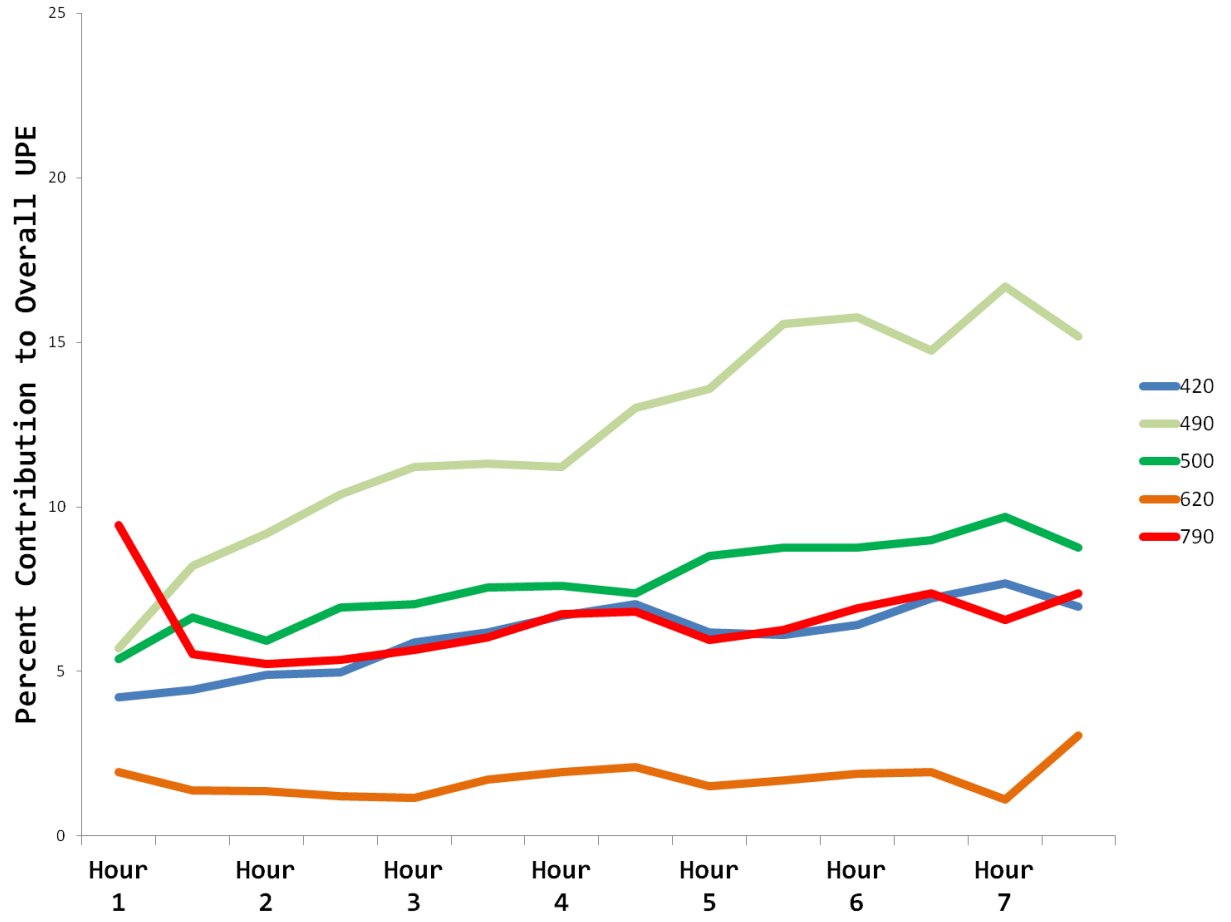

Figure 8. Percent contribution of each of the visible wavelengths tested (420 nm, 490 nm, 500 nm, 620 nm, 790 nm) to overall UPE as a function of time. Overall contribution was calculated by subtracting noise (dark counts) from the raw scores for each wavelength measured and dividing each wavelength's UPE by overall UPE (raw minus noise) from untreated cells with no filter. During the first 90 minutes the combination for all 7 responsive filters (sum=70 nm) contributed to 30% to 40% of the total photon output.

In order to discern if the quantity of photons measured from specific filters for a given wavelength (± 5 nm) were congruent with total numbers of photons measured from these cells without filters, the percentages from each wavelength contributing to the overall photon counts were calculated. These results are shown in Figure 8. The composition from the two non-visible (370 nm and 950 nm) filters were equal to the combined output of the five visible wavelength filters. During the first 90 minutes the combination for all 7 (995 nm remained as a flat line) responsive filters (sum=60 nm) contributed to 30 to 40% of the total photon output. The increasing trend noted in Figure 8 continued until the end of the experiment.

2.4 Conclusion

The results of these experiments demonstrated reliable and conspicuous shifts in specific bands of wavelengths of photon emissions from melanoma cells during the first 24 hours following removal from incubation. By far the most obvious protracted effects were the relative increase in UPE through the infrared 950 nm filter after about 7 hours followed about three hours later by the marked enhancement of 370 nm photons. According to Cosic's theory to predict macromolecular bioactivity, the 950 nm band is associated with molecules involved with signaling activities within the cell as well as cell proliferation. The 370 nm band is more

related to macromolecules involved with cell growth and structure. The discrepancy of about three hours is very similar to the latency between cell signaling and the transcriptions of proteins [Gossen et al. 1994; Bensaude 2011; Bondos and Tan 2011].

The hypothesis that there are specific relationships between the numbers of photons emitted during Popp's "degradation radiation" within a specific wavelength and the corresponding molecular machinery was supported. When a specific activator predicted by Cosic' theory had been added to the media containing the cells during measurement of photons when the 490 nm filter was applied, the photon counts increased for several hours. When the specific inhibitor was added there was a comparable magnitude of decrease in photon counts for several hours. The photon counts after a non-specific inhibitor, that was considered more optimal for 500 nm wavelengths, had been added did not differ significantly from untreated controls.

On the other hand when the inhibitor most optimal for the 500 nm was added to the media and photon counts were obtained through the 500 nm filter there was persistent diminishment of emission. The non-specific inhibitor (the optimal one for 490 nm) actually produced increased photons during the first 5 hrs, the opposite than what would be expected for an inhibitor, before diminishment was occurred. For narrow-band specificity, such as the molecular structure most optimally matched for sequestering to receptors,

very small changes in morphology in a ligand can produce effects opposite to that of the traditional agonist.

The most consistent quantitative changes associated with effective facilitation of photon emission by molecular activators or diminishment by molecular inhibitors was the shift of ± ~5 photon counts s^{-1} with respect to untreated baseline levels (~25 photon counts s^{-1}) for all treatments. The relatively fixed quantity of increased or decreased photon counts with activators and inhibitors, respectively suggests a boundary condition. Whether this was related to the fixed concentration of the compounds, the fixed numbers of receptor molecules that mediate their effects on the cells' plasma membranes, or to the restraints of intrinsic kinetics for these biomolecular reactions is not clear at this time.

The functional emission, when the directionality of the photons and the cross-sectional area are accommodated (a multiplication factor of about 40) is there was either an enhancement of 400 photons s^{-1} or diminishment of this amount within the population of ~$0.5 \cdot 10^6$ cells. Assuming each photon is associated with an interaction with a structure within the plasma membrane this would suggest that the activators and inhibitors were producing about 400 reactions per s for several hours of measurement.

The dosages of compounds contained within the cell media were $(2.5 \cdot 10^{-6}$ L·dish$^{-1}) \cdot (5 \cdot 10^{-6}$ M·L$^{-1}) \cdot (6.023 \cdot 10^{23}$ molecules M$^{-1})$ or ~$7.5 \cdot 10^{12}$ molecules of agent. Within 2.5 cc ($2.5 \cdot 10^{-6}$ m^3) of media containing the cells this would be $0.3 \cdot 10^{-18}$ m^3 per molecule or an effective length of 0.6 nm. Such density would be sufficient to occupy ion channels or to influence the distribution of the layer of charge that contributes to resting membrane potential [Persinger 2010]. Our [Dotta et al. 2011a; Dotta et al. 2011b] previous experiments have implicated the equilibrium chemistry associated with the plasma membrane as the primary source of UPE in these cells.

One of the interesting quantitative anomalies was the discrepancy between the percentages of photons for all of the 7 filters that contributed. Assuming equal distribution across the 580 nm band to which the PMT responded (370 to 950 nm), the summed increment of 70 nm should have contributed ~10%. We measured about three to four times the numbers. We suggest one explanation that could also accommodate this discrepancy as well as the slow rise in photon emissions over time. The actual filter mechanism is based upon a series of mirror-like processes which results in the reflection of the non-filter band photons back to the source. If photons are the primary stimuli that initiate the major changes in cell activity, including the metabolic and signaling processes associated with photon emissions, then this enhancement would be

expected. This pattern could be interpreted as addition support for the quintessential role of very small quantities of photons within the visible and near infrared and ultraviolet bands as the initiators of myriad molecular processes involved with cell proliferation, repair, and adaptation.

2.5 General Significance

The concept of duality of matter and energy within biological systems has had a long history. Whereas the manifestations of matter are presented as spatial patterns (molecular structures) the manifestations of electromagnetic energy is presented as temporal patterns (frequency). The quantitative transformation or equivalence between matter and energy, although both contribute to cellular function, have been considered by some as spurious or even incomprehensible The observation that cells adapting to a shift from normal to abnormal conditions exhibit a time-dependent shift in the wavelengths of the photons that are emitted is consistent with the coupled relationship between molecular states of cell function and specific quantum of electromagnetic energies within the ultraviolet to near infrared range. Cosic's rational molecular structures based upon a model that predicts optimal wavelengths of light from a representation of the distribution of free electron energy along a protein, that is delocalized electrons of each amino acid that constitutes the protein, may contain the "Rosetta Stone"

or code by which complex molecular structure and electromagnetic frequency can be equated. The experimental results that compounds that are activators or inhibitors based upon these predictions actually enhanced or diminished photon emissions strongly supports the theory's validity.

2.6 References

Bensaude O (2011) Inhibiting eukaryotic transcription. Transcription 2; 103-108

Bondos SE, Tan XX (2011) Combinatorial transcriptional regulation: the interaction of transcription factors and cell signaling molecules with homeodomain proteins in Drosophila development. Crit Rev Eukaryote Gene Expr 11; 145-171

Chang JJ, Popp FA (1998) Biological organization: possible mechanism based on coherence of "biophotons". In: Chang JJ et al (ed) Biophotons. Kluwer Pub. The Boston, pp 217-222

Choi DH, Lee KH, Moon JJ, Kim Y, Lim JH, Lee J (2012) Effect of 710 nm visible light irradiation on neurite outgrowth in primary rat cortical neurons following ischemic insult. Biochem Biophys Res Com 422; 274-279

Cohen S, Popp FA (1997) Biophoton emission of the human body. J Photochem Photobiol B Biol 40; 187-189

Cosic I (1994) Macromolecular bioactivity: is it resonant interaction between macromolecules? Theory and application. IEEE Trans BioMed Engineer 41; 1101-1114

de Souza SC, Munin E, Alves LP, Castillo Salgado MA, Pacheo MTT (2005) Low power laser radiation at 685 nm stimulates stem-cell proliferation rate in *Dugesia tigrina* during regeneration. J Photochem Photobiol B Biol 80; 203-207

Dotta BT, Buckner CA, Cameron D, Lafrenie RM, Persinger MA (2011a) Biophoton emissions from cell cultures: biochemical evidence for the plasma membrane as the primary source. Gen Physiol Biophys 30; 301-309

Dotta BT, Buckner CA, Lafrenie RM, Persinger MA (2011b) Photon emissions from human brain and cell culture exposed to distally rotating magnetic fields shared by separate light-stimulated brains and cells. Brain Res 388; 77-88

Gossen M, Binin AL, Freundlieb S, Bujard H (1994) Inducible gene expression systems for higher eukaryotic cells. Curr Opin Biotecnol 5; 516-520

Gurwitch AG (1923) Das problem der zellteilung physiologisch betrachtet. In: Gurwitsch AG et al. (eds) Monographien aus dem Gesamtgebiet der Physiologie der Pflanzen und der Tiere, pp 473-475

Isojima Y, Isoshima T, Nagai K, Kikuchi K, Nakagawa H (1995) Ultraweak biochemiluminescence detected from hippocampal slices. NeuroReport 6; 658-660

Liu TC, Liu R, Zhu L, Yuan J, Hu M, Liu S (2009) Homeostatic photobiomodulation. Front Optoeletron China 2; 1-8

Mitsunaga M, Ogawa M, Kosaka N, Rosenblum L, Choyke P, Kobayashi H (2011) Cancer cell-selective in vivo near infrared photoimmunotherapy targeting specific membrane molecules. Nature Medicine 17; 1685-1691

Persinger MA (2010) 10^{-20} Joules as a neuromolecular quantum in medicinal chemistry: an alternative approach to myriad molecular pathways? Cur Med Chem 17; 3094-3098

Popp FA (1979) Photon storage in biological systems. In: Popp FA, Becker G, Konig HL, Pescha W (eds) Electromagnetic bioinformation. Urban and Schwarzenberg, Munich, pp 123-149

Popp FA (1988) Biophoton emission. Experientia 44; 543-630

Sun Y, Wang C, Dai J (2010) Biophotons as neural communication signals demonstrated by in situ biophoton autography. Photochem Photobiol Sci 9; 315-322

Tilbury RN, Quickenden TI (1988) Spectral and time dependence studies of the ultraweak bioluminescence emitted by the bacterium *Escherichia coli*. Photochemistry and Photobiology 47; 145-150

Wu HP, Persinger MA (2011) Increased mobility and stem-cell proliferation rate in *Dugesia tigrina* induced by 880 nm light emitting diode. J Photochem Photobiol B Biol 102; 156-160

Chapter 3: Photon Emission From Melanoma Cells During Brief Stimulation by Patterned Magnetic Fields: Is the Source Coupled to Rotational Diffusion Within the Membrane?

Published in General Physiology and Biophysics

Abstract

If parameters for lateral diffusion of lipids within membranes are macroscopic metaphors of the angular magnetic moment of the Bohr magneton then the energy emission should be within the visible wavelength for applied ~1 μT magnetic fields. Single or paired digital photomultiplier tubes (PMTs) were placed near dishes of ~ 1 million B16 mouse melanoma cells that had been removed from incubation. In very dark conditions (10^{-11} $W \cdot m^{-2}$) different averaged (RMS) intensities between 5 nT and 3.5 μT were applied randomly in 4 min increments. Numbers of photons were recorded directly over or beside the cell dishes by PMTs placed in pairs within various planes. Spectral analyses were completed for photon power density. The peak photon emissions occurred around 1 μT as predicted by the equation. Spectra analyses showed reliable discrete peaks between 0.9 and 1.8 μT but not for lesser or greater intensities; these peak frequencies corresponded to the energy difference of the

orbital-spin magnetic moment of the electron within the applied range of magnetic field intensities and the standard solution for Rydberg atoms. Numbers of photons from cooling cells can be modified by applying specific intensities of temporally patterned magnetic fields. There may be a type of “cellular” magnetic moment that, when stimulated by intensity-tuned magnetic fields, results in photon emissions whose peak frequencies reflect predicted energies for fundamental orbital/spin properties of the electron and atomic aggregates with large principal quantum numbers.

3.1 Background

The interactions between applied weak intensity magnetic fields and plasma cell membranes have been explored by multiple models that emphasize direct forces such as Lorenz effects [Engstrom and Fitzsimmons 1999; Adey 1981; Weaver et al 1999], resonance processes [Ludwig 1968; Liboff 1992; Lednev 1991; Mulligan et al. 2012], or challenges to the kT boundary [Cifra et al. 2011; Bini and Rubin 2007]. The components of the membrane that have been most frequently emphasized have been the distribution of charges, alterations in the capacity of the polar groups of proteins composing ion channels, and the liquid crystal states of the lipid components [Lenaz 1987]. In the pursuit of the mechanism by which photons are emitted during slow depolarization from cancer and normal cells after removal from incubation, we examined the potential validity of a model and mechanism that involves the release of photon energy from the interaction between components of the membrane that could display circumferential movements and the application of specific, weak rotating magnetic fields. Here we present data to support this possibility.

Within the last two decades there has been a re-examination of the role of "mitogenic" radiation that was enthusiastically pursued during the 1930s [Quickenden 1974; Popp et al. 1988]. There are several reviews of ultraweak photon emissions that are coupled to the cell's function [Isojima et al. 1995] and intercellular

communication [Sun et al. 2010]. We [Dotta et al. 2011a; Dotta et al. 2011b] recently completed a series of experiments showing that cells from many normal and aberrant cell lines, removed from incubation, emit photons during the subsequent approximately 10 hours. The estimated numbers of photons measured by photomultiplier tubes indicated that the losses occur in increments of energy in the order 10^{-20} J [Dotta et al. 2011a] as the cell membrane slowly depolarizes. This "quantum" of energy is the same order of magnitude as that associated with action potentials in axons, the separation of potassium ions that maintain the resting plasma membrane potential, forces applied over distances occupied by covalent and hydrogen bonds, and the sequestering of ligands to receptors [Persinger 2010].

Movement in a closed path, such as a circle or even certain fractal configurations, has potential properties to interact with applied magnetic fields. Technically velocity within a circle is accelerating. Circumferential movements, as manifested by the lateral diffusion of lipids within the plasma cell membrane, have been inferred by a variety of methods [Lenaz 1987; Furtula et al. 1990]. The diffusion coefficients (D) of selected lipids, such as the mobile lipophilic quinones involved with electron transfer, range from 10^{-6} $cm^2 \cdot s^{-1}$ [Lenaz 1987] to $3 \cdot 10^{-9}$ $cm^2 \cdot s^{-1}$ [Furtula et al. 1990]. The equivalent diffusion length $(4Dt)^{1/2}$, where t is time, in one second would be between $2 \cdot 10^{-5}$ $m \cdot s^{-1}$ to $5.5 \cdot 10^{-7}$ $m \cdot s^{-1}$. Lenaz

[1987] suggested the slower diffusions occur over longer linear distances because the lipids are obstructed by the proteins dispersed within the phospholipid matrices. Asymmetrical soma geometry would also affect the coefficients for this "smooth" rotation.

This continuous movement over a bound surface could be considered a condition analogous to the magnetic moment ($A \cdot m^2$) of the orbit of an electron around an atom. In traditional expression:

$$\mu = ep(2m)^{-1} \quad (1),$$

where μ=the magnetic moment, e and m indicate the unit charge and mass of the electron and p is the angular momentum. The orbital magnetic moment of the electron for the Bohr magneton is in the order of 10^{-24} $A \cdot m^2$.

When applied to the cell the "magnetic moment" would be the product of angular velocity $(m \cdot s^{-1}) \cdot m^{-1}$ divided by the cell radius, moment of inertia ($kg \cdot m^2$) and the unit charge ($A \cdot s$) divided by mass (kg). For estimates for the "rotating components with charge" for the cell membrane we assumed the slowest diffusion rates, between 10^{-7} $m \cdot s^{-1}$ to 10^{-8} $m \cdot s^{-1}$ [Lenaz 1987; Persinger 2010], which were divided by cell radius. Assuming a radius of between 7.5 μm and 12.5 μm to accommodate the range for most melanoma cells [Ochalek

et al. 1988] and the density of water, the mass of each cell would range from 1.8 to 8.2 $\cdot 10^{-12}$ kg.

The resulting cellular "magnetic moments" would be between 10^{-23} and 10^{-24} $kg \cdot m^2 \cdot s^{-1}$. We assumed there would be a central tendency, given the expected heterogeneity of velocities of lateral diffusion, within more or less normally distributed dispersions. When multiplied by the unit charge ($1.6 \cdot 10^{-19}$ $A \cdot s$) and divided by the mass of an electron $9.11 \cdot 10^{-31}$ kg, the median "cellular" magnetic moment is within the 10^{-23} $A \cdot m^2$ or $J \cdot T^{-1}$. If a magnetic field with the appropriate cell-coupled frequency were applied with an intensity of ~1 μT (10^{-6} T), the resulting energy would be within the range of 10^{-19} J.

This domain of quanta of energy is within visible wavelength that could be detected by photomultiplier tubes. The intensity also results in a peak frequency of ~16 to 18 Hz when applied to the discrepancy between an electron's orbital and spin magnetic moments. This frequency is remarkably congruent with solutions for Rydberg atoms. These excited atoms display at least one electron with very high principal quantum numbers and exhibit amplified responses to applied electric and magnetic fields. Here we present data to support these possibilities.

3.2 Materials and Methods

3.2.1 Preparation of Cells

B16-BL6 mouse melanoma cell cultures were maintained in 150 x 20 mm tissue culture plates (Sarstedt, Laval, Qc) in Dulbecco's Modified Essential Medium (DMEM, Hyclone, Logan, UT) accompanied with 10% fetal bovine serum, 100 µg/ml of streptomycin and 100 U penicillin/ml (Invitrogen, Burington, ONT). Cells were incubated at 37°C in 5% CO_2. The cell monolayers were harvested by incubation in 0.25% trypsin-EDTA, collected by centrifugation, and seeded onto 6.0 cm by 1.5 cm tissue plates to a final count (~10^6 cells/plate). The cells were then removed from the incubator and transported to the biophysics laboratory.

3.2.2 Magnetic Field Equipment and Exposure

We [Persinger 2003] have developed a technology for computer-generating patterned magnetic fields with basic temporal parameters that simulate many cellular processes. Depending upon programming, one can generate any theoretical or simulated physiological pattern. The magnetic fields in this study were generated by converting a row of numbers between 1 and 256 to incremental voltages between -5 and +5 V employing complex software, where 127=0, that we have described previously. The series of numbers generated a specific pattern that was frequency-modulated and has

been shown to increase analgesia in rodents [Martin et al. 2004] and invertebrates [Thomas et al. 1997]. The same pattern modifies biomolecular pathways [Buckner 2011] and alters T-type calcium channel conduction in cancer cells but not normal cells [Buckner et al. 2013]. The shape of this frequency- modulated sequence is shown in Figure 1. This pattern was also instrumental as the second stage for the establishment of a brief (~8 min) entanglement between distant loci of experimentally-induced bursts of photons from the simultaneous injection of hydrogen peroxide into plates containing small volumes of sodium hypochlorite [Dotta and Persinger 2012].

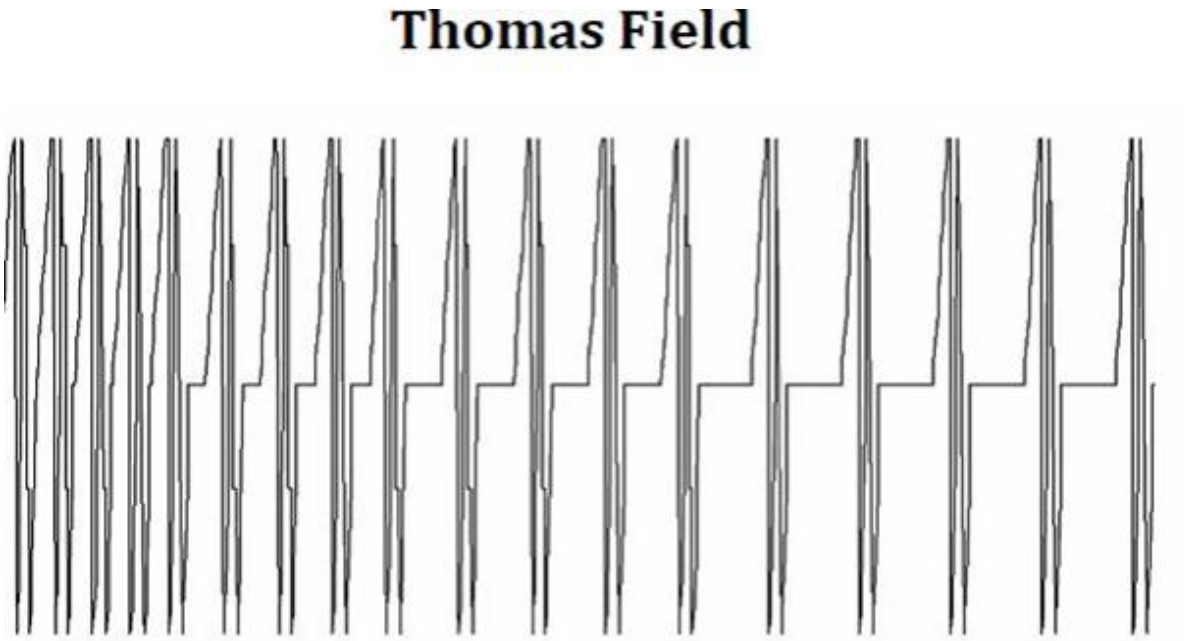

Figure 1. Pattern of the frequency-modulated field primarily employed in the experiments. Vertical axis refers to amplitude (1 to 256 or -5 to +5 V) and the horizontal axis refers to serial order of the voltage. The duration of each value (point) was 3 msec.

The DOS-based computer software was programmable and allowed the specification of numbers of cycles (repetitions of the pattern), the duration of each number or voltage (point duration), the time between cycles (interpattern interval), and the amplitude (intensity) of the output. The optimal computer is a 286 Zenith because of its stability of internal timing, although any computer can be functional if the variable processing speeds from WINDOWS and intrinsic circuitry are stabilized by a small software program. In this study the duration of each point, that is the time a given voltage was presented for each point (n=849) that composed the patterned magnetic field application, was 3 msec. This discrete voltage for this duration was presented to a pair of the application solenoids. This value was selected because previous research had shown its efficiency for slowing cancer cell growth [Karbowski et al. 2012] and affecting physiological responses coupled to overt behaviour [Whissell and Persinger 2007]. This precision is important. Point durations that are less (1 ms, 2 ms) or greater (4 ms, 5 ms, 10 ms) produce less analgesic effect in rodents [Martin et al. 2004], do not delay the growth of several types of cancer cells [Buckner 2011], and do not facilitate the influx of Ca^{++} through T-type channels [Buckner et al 2013].

The discrete voltage values were converted from the range of numbers by a custom constructed digital-to-analogue converter. It delivered the discrete value to one of four pairs of solenoids

contained within the boxes. Consequently a magnetic field was generated at any given time between the two opposing solenoids. They were reed relays (Radioshack Compact 5VDC/1A SPST Reed relays; Model 275-232, 260 Ω,~50 m copper wire). The four solenoids were arranged in a "circle" within each of the two 5 cm by 8.5 cm boxes. The circumference of the "circle" of solenoids was about 15 cm. A built-in commutator successively activated a pair of solenoids every 0.5 s. Consequently the time required for all four pairs of solenoids to be activated before the circular "rotation" was complete was 2 s. The plane of the rotation was perpendicular to the plane upon which the tissue plates were placed. The layer of cells at the bottom of the dishes was also normal to the rotational plane.

The two boxes were separated by 10 to 11 cm. Direct measurements by power meters with input to laptop computers and verification of the pattern through commercial, calibrated telephone hookup solenoids coupled to audioamplifiers indicated that the programmable range of mean intensities of the applied field in the space occupied by the cells varied from an average RMS of 5 nT to 3.5 μT. We selected this range because it included and extended below and above the intensities of the field that were predicted by the ("membrane magnetic moment") model to enhance photon emissions.

Two standard plastic dishes (5 cm wide, 1 cm deep) each containing ~1 million melanoma cells in 5 cc of fluid were stacked between the two boxes. The superimposed (2) plates of cells were employed because direct measurements indicated more spontaneous photon emissions. The distance between the ~0.2 cc fluid containing the layer of cells in one plate and the one below (or above) was 1.4 cm. The cells and the exposure equipment were housed within an industrial acoustic chamber that was also a Faraday cage. The computers that controlled the generation of the magnetic field and measured the PMTs were housed outside of the room. Magnetometers (FVM-400 Vector, MacIntyre Electric Design Associates) indicated that the resultant geomagnetic field intensity within the chamber where the cell dishes were placed was ~26,000 nT compared to the typical 45,000 nT outside of the chamber.

3.2.3 Exposure Procedure and PMT Measurements

During our pilot studies with digital photon units (Sens Tech LTD DM0090C; spectral response range 280nm to 850 nm, peak sensitivity around 370 nm) involving about 60 different samples and 10 different days over several weeks to establish appropriate parameters we found that the photon emissions were most reliable when the ambient background photon levels were above ~400 counts per 20 ms. Assuming 10^{-19} J per photon, $2 \cdot 10^{4}$ photons s^{-1} and the

aperture of the photomultplier tube (2.1 cm), this threshold was calculated to be about 10^{-11} $W \cdot m^{-2}$.

When the chamber was darkened extensively by black terry cloth over the windows and complete removal of ambient external light (counts < 100 photons per 20 ms; background measures in the chamber during the maximum darkness were between 4000 and 5000 photons/s) the phenomena described in this study were not observed. We could also produce the phenomena by adding light from a rectified (green) LED in the chamber that elevated the background to above 400 counts per 20 ms. All measurements were recorded by Lenovo laptops (Windows 7) that were maintained outside the chamber. The text edited by Chang et al [Chang et al. 1998] on the measurement and nature of biophotons was particularly instructive to avoid artifact problems.

During the first part of the experiment that involved about 20 different plates of cells the two apposed plates of cells were placed over the aperture of a single digital photomultiplier tube. The range of delay from the time the cells were removed from the incubator to the time they were exposed and measured ranged between 1.5 and 2 hours. Our previous work, employing analogue PMTs, indicate that biophoton emissions were still copious during this period [Dotta et al. 2011a]. After accommodating for numbers of cells and aperture area, the output from each cell per sec was in the order of 2 to $4 \cdot 10^{-20}$ $J \cdot s^{-1}$ according to both digital and

analogue instrumentation. This is within the range both measured and theoretically derived from a variety of approaches [Dotta et al 2011a; Persinger 2010].

For each experiment a set of plates containing melanoma cells was exposed for ~4 min to each of the 10 different intensities of the frequency-modulated field and to the no field condition. There were a total of 6 replicates per intensity and for the no field condition (66 samples). Pilot studies indicated that there was an enhancement of the effect if there was a pre-exposure for 2 to 4 min to a complex sequenced magnetic field with an average intensity of ~3 μT.

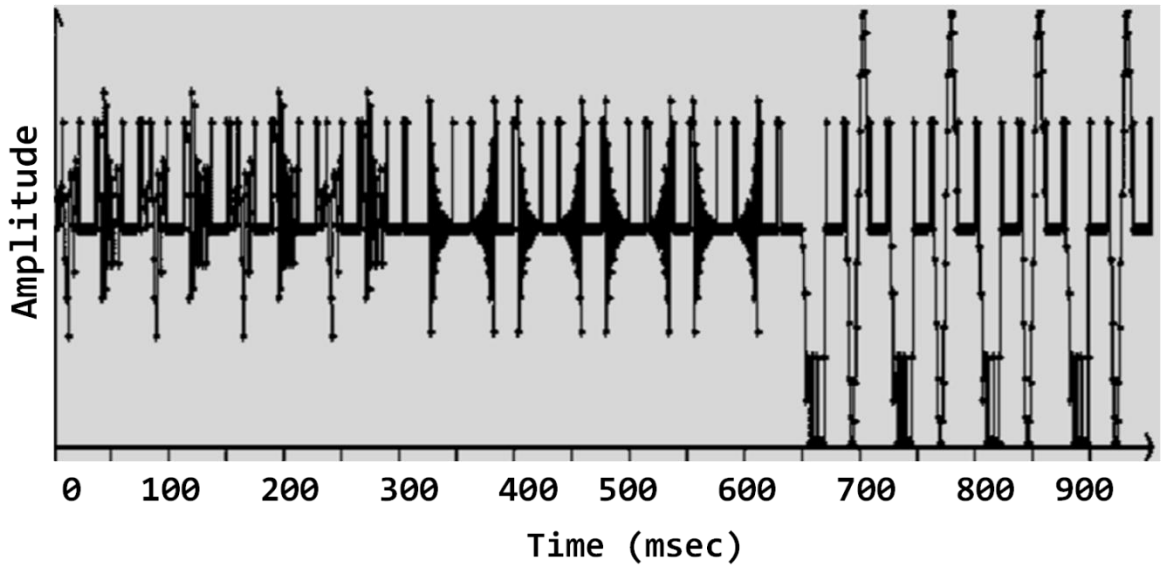

Figure 2. Pattern of the complex sequenced pre-exposure field employed in the experiments. Vertical axis refers to amplitude (0 to 256 or -5 to +5 V) and the horizontal axis refers to serial order of the voltage.

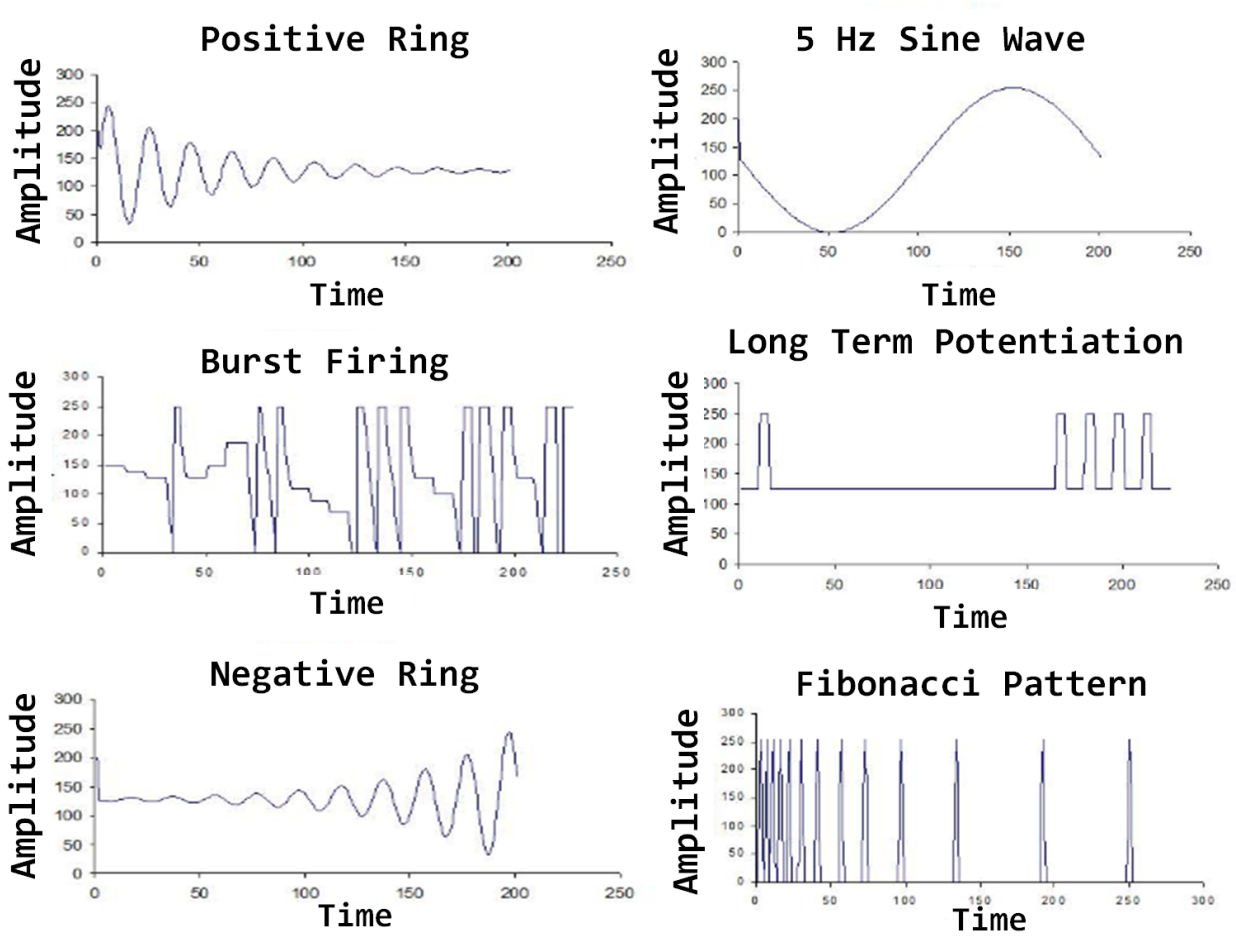

Figure 3. The six shapes of the fundamental patterns whose various combinations produced the complex sequenced pre-exposure field. Each point duration (voltage) was 1 msec.

This specific complex sequenced magnetic field has been shown to affect cellular differentiation [St-Pierre et al, 2003; Persinger et al, 2001] and repair [Lado and Persinger, 2012]. The pattern is composed of 10,000 points (discrete voltages between 0 and 256), each presented for 1 ms. The gestalt shape is shown in Figure 2. The individual patterns that composed the complex sequenced field, each presented for 200 ms, are shown in Figure 3. The order was: Burst, LTP, FM, LTP, repeated 4 times, followed by a neutral field, then P-ring, LTP, N-ring, LTP presented 4 times, followed by a neutral field, and, then Fibonacci, LTP, 5 Hz, LTP presented four times.

Because of these results all experiments began with this procedure before baseline which was followed by the subsequent counterbalanced order of presentation of the 10 intensities. The numbers of photons per 20 ms were recorded by specialized software by the external laptop for 2 complete minutes for each of the intensities. The 20 ms sample time was selected to maximum data collection without obtaining excessive numbers of data points for subsequent spectra analyses.

During the second part of the experiment after the clear display of the non-linear intensity magnetic field effect upon photon emission was replicated multiple times over several months, a paired PMT procedure was instituted. For some experiments two identical digital PMTs each with their own laptops external to the

chamber were placed over the top and under the bottom of the plates, perpendicular to this position and the placement of the solenoid boxes, or, asymmetrically such that one was under the cells and the other was perpendicular to the plane of the plates and the solenoid boxes. A diagram of the various orientations is shown in Figure 4. The two PMTs were altered in the different paired positions to minimize instrumental artifact. The same procedure of field exposure was employed. However the data were sampled in 50 ms increments (20 samples per s) in order to visualize the changes more effectively in real time from the laptop because of the nature of the software.

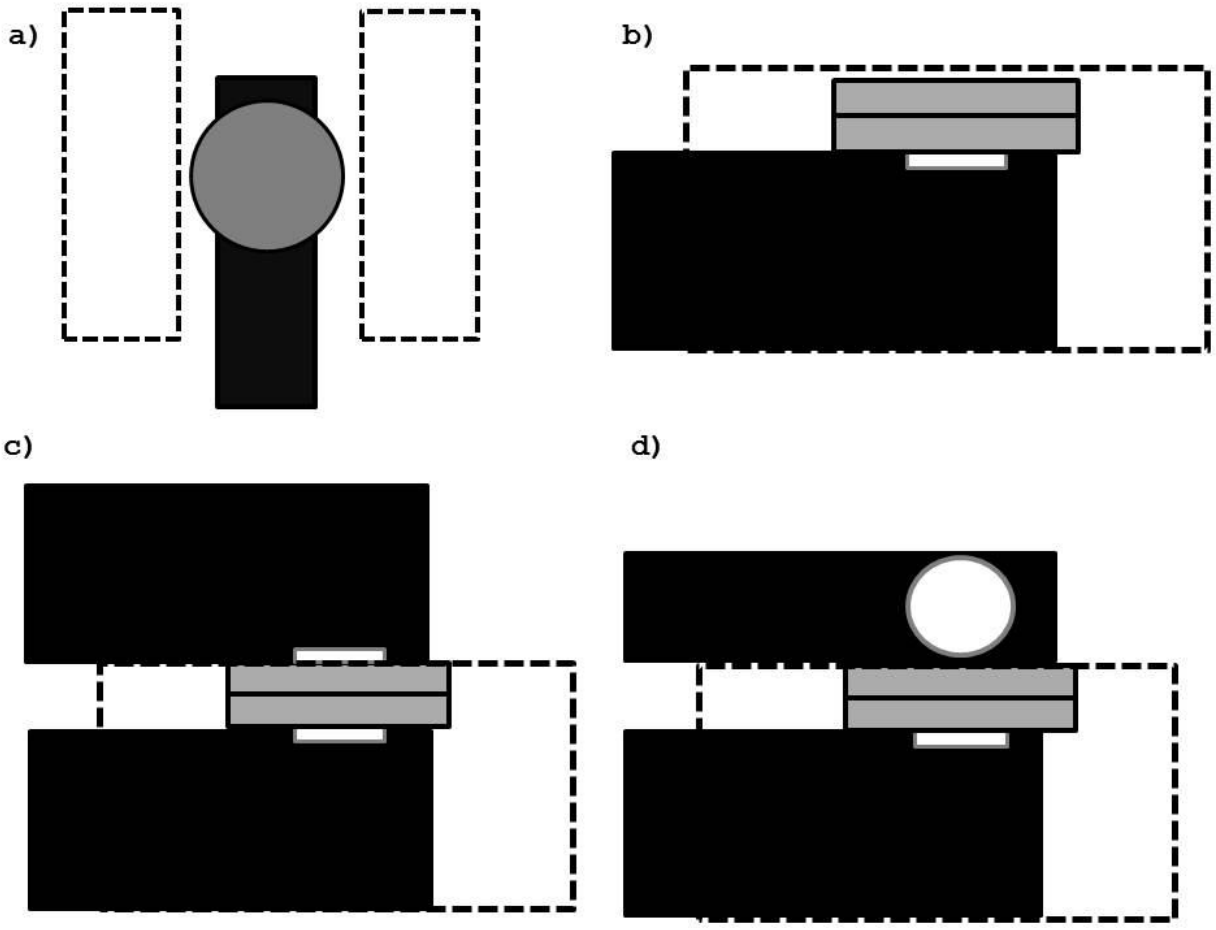

Figure 4. Block diagrams of variations in orientations of the PMTs with respect to the double dishes of melanoma cells. Boxes with dotted lines (not to scale) refer to the boxes containing the solenoids, grey figures are the cell dishes, black boxes containing white circles are PMTs with white circles corresponding to the PMT aperture. A) Single PMT with double plates sitting on aperture (B). C) Double PMT with one PMT aperture on top and the other PMT aperture on the bottom of the two plates. D) Double PMT with one PMT beneath and the other PMT perpendicular to the plane of the cells.

3.2.4 Data Analyses

In part 1 of the experiment, the total numbers of photons per 20 ms increment above the mean background for the 2 min sample period for each of the 10 increments of the applied field intensities as well as the no field condition were calculated from the raw data. The means and standard deviations were computed for each of the 6 different experiments for each intensity. The means and standard deviations for the deviations from the baseline as a function of the intensity of the applied frequency-modulated field were plotted.

Triplicate samples from each of the 2 min PMT samples for each of the different intensities were randomly selected from the data. Spectra analyses were completed by SPSS-PC version 16. These analyses were completed because we had predicted specific peaks in power within the optimal intensity band that would reflect solutions for the Rydberg frequency and the differential energy between the spin and orbital magnetic moments for electrons for the specific range of the applied magnetic fields.

For the second part of the experiment involving the twin (coupled) PMTs, the time-coupled correlations between the total numbers of photon counts per unit time for the two measurements were completed for no field and various intensities of the field conditions. The photon counts for the serial 4,400 samples for one PMT were plotted against the 4,400 values for the second PMT.

Although the sampling rate for each independent PMT was 20 per s (50 ms increments) direct measurements indicated the discrepancy between the two instruments was not more than one temporal increment. Because there was a conspicuous shift in the shape and dispersion of photon numbers when the optimal field strengths were present vs not present, additional analyses were completed for the numbers of photons that exceeded 4.0 standard deviations from the central cluster.

3.3 Results

3.3.1 Optimal Intensity for Photon Emissions Matches Predicted Value

Figure 5 shows the discrepancy in photon counts from background during the first 2 min durations of the different intensities of the magnetic field pattern (Samples from the last 2 min of a field exposure produced comparable effects). The maximum photon emissions from the plates of cells occurred when the field strengths were between 0.9 and 1.8 μT. Above 1.8 μT and below 0.9 μT the photon emissions were either inconsistent or minimal and approached that of baseline conditions. The mean peak of 80 photon counts per gate time of measurement would correspond to a radiant flux density of roughly $1.4 \cdot 10^{-11}$ $W \cdot m^{-2}$. This value was obtained by multiplying the numbers of photons per gate ($8 \cdot 10^{1}$ photons$\cdot \Delta t^{-1}$) by:

1) the number of gates per second ($5 \cdot 10^{1}$ Δt s^{-1}), 2) the average energy value of a single photon at 630 nm ($3.6 \cdot 10^{-19}$ $J \cdot photon^{-1}$) and 3)the width of the active diameter of the PMT's photocathode (10^{4} $cm^{2} \cdot m^{-2}$). In this instance the conventional symbol Δt corresponds to the sampling window, or the gate time of measurement. The wavelength 630 nm was selected as an average because it is the median spectral response range of the PMT. This increase of $1.4 \cdot 10^{-11}$ $W \cdot m^{-2}$ was superimposed upon the background baseline (BL) of ~400 photons per gate. This background level of ~400 photons per gate has a corresponding flux density of $\sim 7 \cdot 10^{-11}$ $W \cdot m^{-2}$ (assuming the energy of a photon at 630 nm), which was the approximate limen to produce the effect.

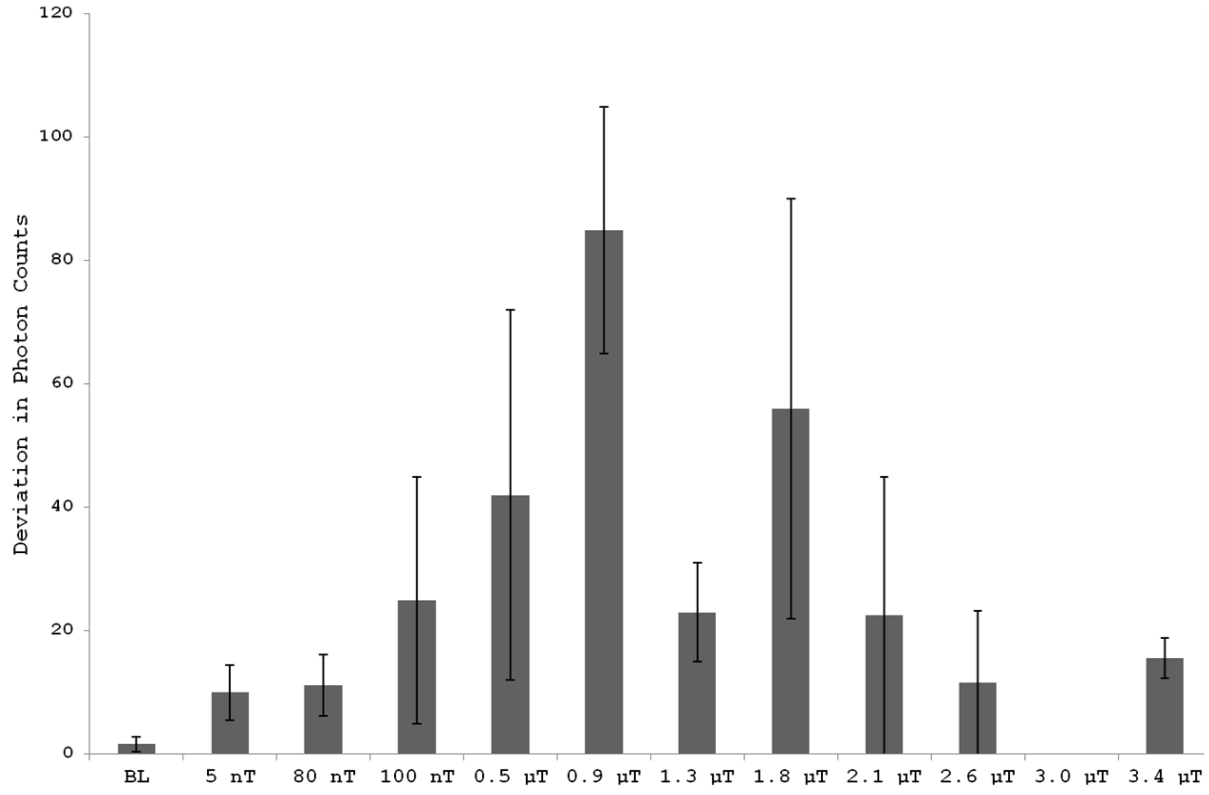

Figure 5. Deviation from baseline of numbers of photons per 20 ms increment from the cells exposed to the various intensities (RMS) in nanoTesla to microTesla of the patterned magnetic field shown in Figure 1. Vertical bars indicated standard deviations.

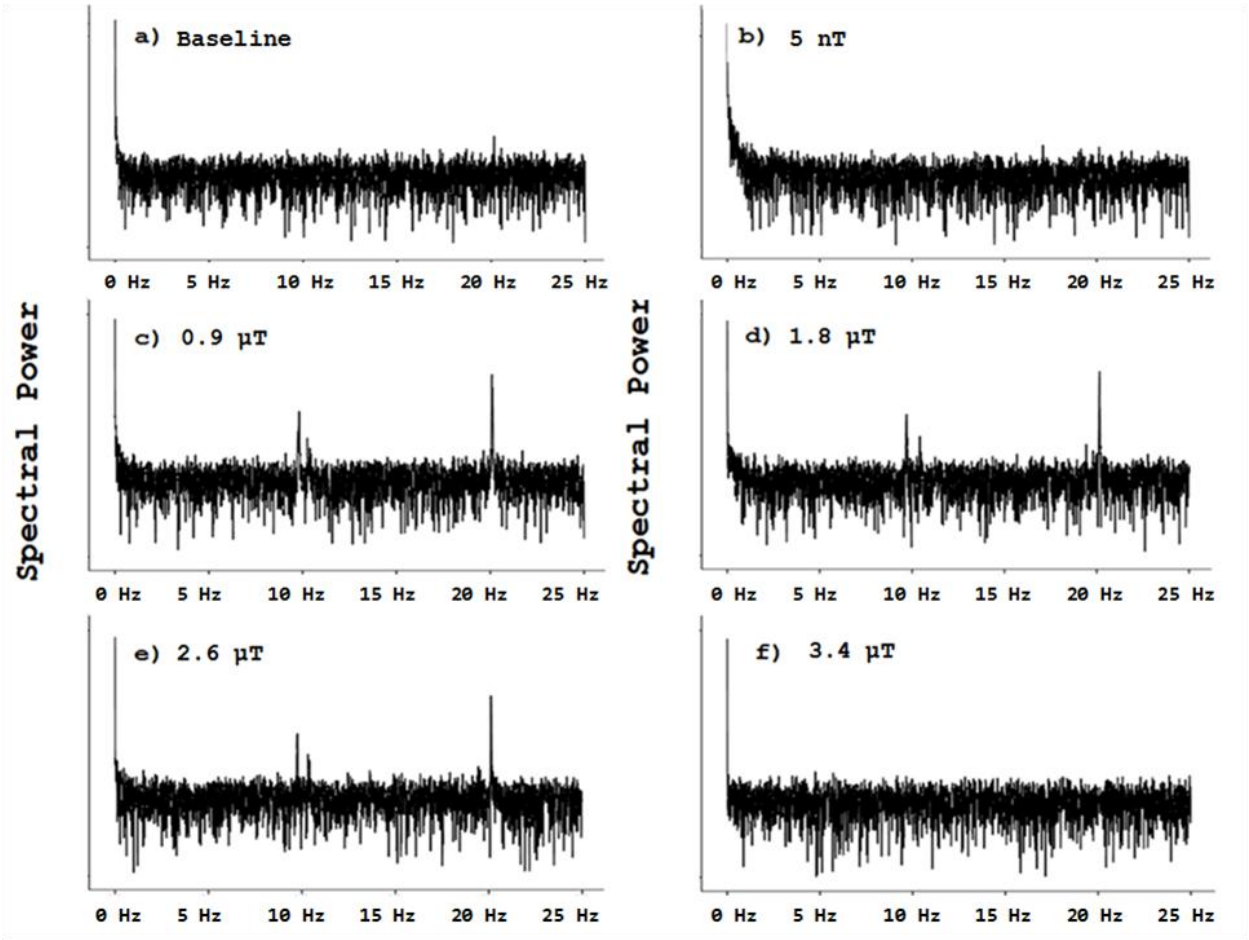

Figure 6. Spectral analyses (Fourier transform) of raw photon counts per 20 ms increment for 120 s from samples of cells that had been exposed to the various intensities of the applied frequency-modulated magnetic fields. Vertical axes indicate relative power while the horizontal axis indicated intrinsic frequency based upon the unit (20 ms). The emergence of the large sharp peak around 20 Hz and the two small peaks around 10 to 12 Hz only emerged with the intensities calculated by the model.

3.3.2 Spectral Analyses

Representative results of the spectra analyses (Fourier transform) of each trial for sample intensities are shown in Figure 6. For all triplicates for the three samples from each intensity there were reliable peaks of power within the photon spectra within the equivalent of ~20 Hz (tallest peak on the right in Figure 6) and two smaller peaks at 9.65 Hz and 10.37 Hz frequency for the 0.9 μT to 1.8 μT intensity fields only. These frequencies were never present when the applied intensity of the field was below 0.9 μT or 3.0 μT or above. We included the 2.6 μT in the figure because it displayed this pattern once.

The intrinsic structure of the primary spectral peak (20 Hz) is shown in Figure 7a for two of the intensities within the range of optimal intensities. The increased power displayed a normal-like distribution with a slow rise starting around 19.95 Hz, a peak between 20.05 Hz and 20.15 Hz and a slow decline until about 20.25 Hz. In comparison the dark thick horizontal line at the base represents the values for this band for cells exposed to lesser or greater intensities. The secondary double peaks around 10 Hz also displayed a narrow band (Figure 7b).

3.3.3 Double PMT Simultaneous Correlational Patterns

Figure 8 shows the correlational configurations (scatterplots) between the two PMTs placed at different orientations when the optimal strength magnetic field was either absent or present. The vertical and horizontal axes represent standardized values. Figure 8a is representative of the relationship between photons generated from the two plates of cells when the PMTs were above the top dish and below the bottom dish (Figure 4c). The shape on the left is when no field is present. The shape on the right is when an optimal field strength was applied (0.9 – 1.8 μT). It is important to note that magnetic fields alone had no discernable effect upon these PMTs. In addition, the same experiments performed with a plate of cell culture media only produced no effects. Only when cells were present were these effects produced.

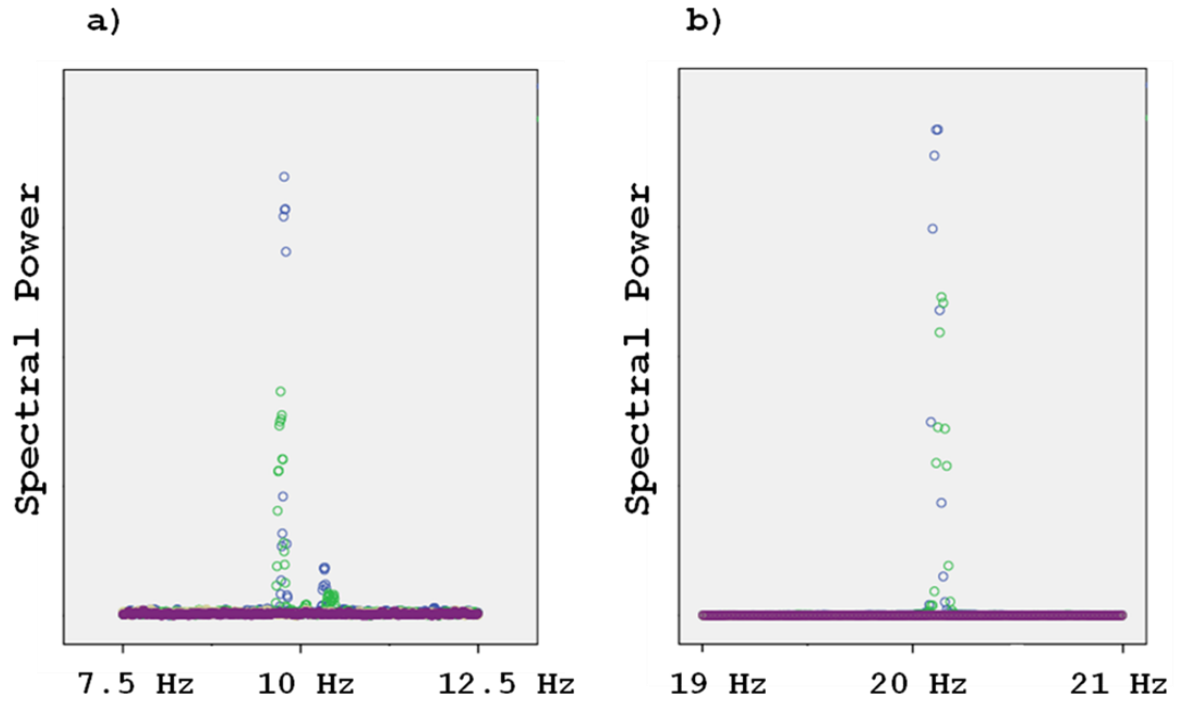

Figure 7. A) Relative power peaks for the secondary double spikes (9-10 Hz) in photon emission frequency for cells exposed to the 0.9 or 1.8 µT fields. There was no response from the same cells exposed to lower strengths or to those above 2.8 uT. These measures are contained with the thick zero line. B) Relative power peaks for the primary spike around 20 Hz for cells exposed to the 0.9 µT or 1.8 µT field.

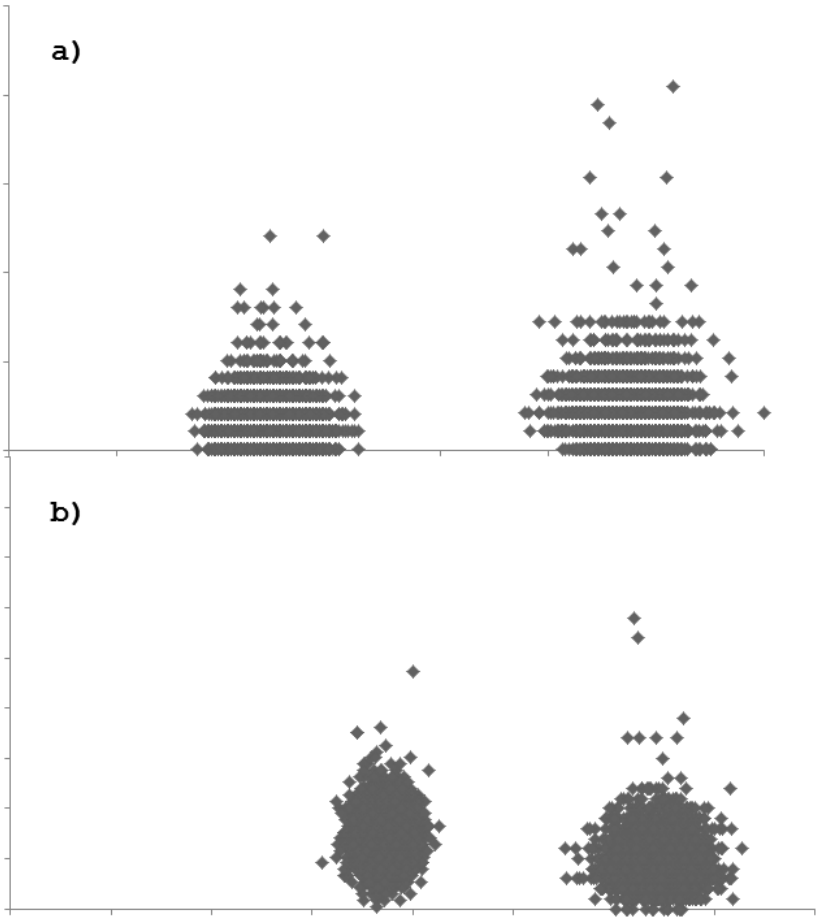

Figure 8. A) Real-time (50 ms increments) correlations (scatterplots) of photon emissions between the two apposing PMTs between which the cells were placed. Vertical and horizontal axes correspond to raw photon counts (per 50 msec) for PMT1 and PMT2. The plot on the left is the no field condition; plot of the right with the dorsal scatter occurred when the optimal intensity field was applied. B) Real time correlations between photon emissions when the optimal fields were present when the two PMTs were perpendicular to each other (left) or apposing (parallel) to each other.

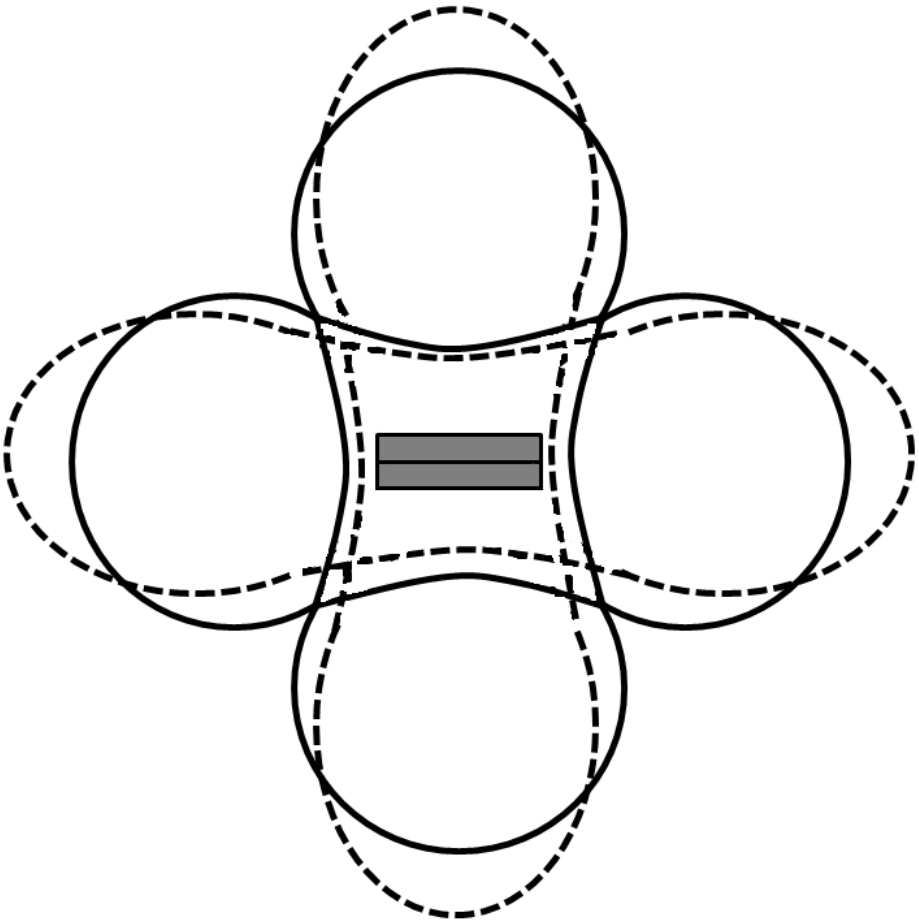

Figure 9. Artistic depiction of inferences from the quantitative photon emission data collected by the different angles and orientations of the two PMTs around the double plates of cells. Closed lines indicate shape of "photon field" normally (no field). Dotted lines indicate the "constriction and elongation" of form when the appropriate field intensity was applied.

Figure 8b shows the relationship in numbers of photons between the two PMTs when the optimal field was being applied to the cell dishes. The more vertically distorted shape on the left reflects the association between two PMTs orthogonal to each other (Figure 4d) while the one of the right shows the temporal association between photon outputs when the two PMTS are parallel (one top, one bottom) to each other (Figure 4c). Switching the two PMTs to the different positions did not alter this effect.

The median range of increased peaks (spikes) in photons per 50 ms was between 6 and 8 per 2 min interval when the optimal field strength was present. This was equivalent to about 1 spike every 15 to 20 s. On the other hand when there was no field present the typical numbers of spikes were between 0 and 2 per 2 min interval.

On the bases of the shapes of the scattergrams and quantitative values for numbers of photons for the different orientations we inferred that the presence of the optimal intensity field elongated and constricted the shape of the "photon fields" being emitted from the double layer of cells. A picture, not to scale, of how this might appear with optimal measurement is shown in Figure 9. The two horizontal grey boxes represent the cell dishes, the solid lines depict the no-field condition and the dotted lines indicate the alteration in the shape of the "photon field" when the magnetic field was applied parallel to the surface of the plates (and cell layer) while the generated field rotated

through the perpendicular plane. This elongation and constriction was not present in control conditions.

3.4 Discussion and Conclusion

One approach to Life, as cogently articulated by both Bohr [1958] and Schrödinger [1944], is that living systems reflect at the macroscopic level the fundamental processes of quantum phenomena. Cells emit photons as a component of multiple chemical processes from (very likely) many sources and mechanisms. In previous experiments [Dotta et al. 2011a] we found that one major source in cancer and normal cells in culture was the plasma cell membrane when the cells were removed from stable incubation and maintained at room temperatures. The temperature of these cells could potentially affect their viscosity at higher and lower temperatures, but at such temperatures the cells would no longer be viable. The numbers of photons emitted per unit time per cell was equivalent to about 10^{-20} $J \cdot s^{-1}$. This "quantum" is within the order of magnitude and convergent with the coefficients for the energy over distance for the forces between K+ charges that maintain the plasma membrane potential [Persinger 2010] and the energy associated with the sequestering of many agonists to receptors.

The movements of components of the cell membrane, particularly classes of lipids and proteins, through this three-dimensional

shell indicated that this expansive torus might display properties analogous to moving charge-currents. They might be considered a field of point current charges. The physical properties would be similar to (but reflective of the more complex macroscopic level) an electron moving around a proton in the hydrogen atom. The resulting "*membrane magnetic moment*" when exposed to the appropriate intensity from an applied magnetic field would be associated with an energy that might be discerned by measurement of photons. In this experiment the ratio of the applied magnetic field compared to background was ~1:10 (applied field strength of ~2 μT with a background of 26 μT). The ratio of applied to background field intensities may be important and should be investigated.

The results of our experiments strongly suggest that there is moderately strong quantitative accuracy for the model. We assumed the standard range of cell circumferences reported for melanoma cells and the estimated lateral diffusion rates (particularly when accommodating their deviation for symmetrical spheroids). We found a peak in photon emissions within two minutes after application of the predicted intensity of magnetic fields by this model. We are assuming at present that the wide range of the distribution of effective intensities between about 0.5 and occasionally 2.1 μT could represent either different populations of intramembrane components representing the charge or the different geometries of cell shape within different "splits" of cells. The shapes of these

melanoma cells were irregular; however this irregularity is common among all the cells within the dish. These calculations were based upon an average. We suggest that the field intensity range of the responses reflected the different arrays of the shapes of the cells as well.

The non-linearity of the effect also reduces the possibility that the increased photon emissions were artifacts of some anomalous microcurrent induction within the PMTs. The intensity-dependent increase in photon emissions only required about 4 min of exposure, about the same duration as a single cycle of NAD(P)H oscillations (~4.2 to 5.5 mHz). Rosenspire et al (2001) showed that pulsed d.c. electric fields could couple to the natural NAD(P)H oscillations in fibrosarcoma cells.

We considered that the functional atomic aggregates associated with the photon emissions from circumferential diffusion of lipids through the membrane might be analogous to or display properties like an excited atom with relatively high principal quantum numbers. Such Rydberg atoms [Dudin and Kuzmich 2012] are known for their amplified response to applied magnetic and electric fields, electron wave functions that approximate classic orbits (including the Bohr magneton) and relatively protracted decay periods. The attenuation of the influence from nuclear protons by the more proximal electrons allows the outer electrons to behave and display

properties of the Bohr magneton upon which our model is largely based.

According to the classic Rydberg relation, $e^2 \cdot [4\pi e_o r^2]^{-1} = mv^2 r^{-1}$. The solution for $f(s^{-1})$ is $e^2 [4\pi e_o r^2 mv]^{-1}$. Assuming a cell radius of 7.5 μm and a lateral diffusion rate of 10^{-6} $m \cdot s^{-1}$ the standing frequency would be ~18 Hz. This value is remarkably congruent with the highly reliable spectral peak measured from the photon emission amplitudes (sampled 50 times per sec) from the melanoma cells measured in our experiments.

Our assumptions had been that lateral diffusion of an optimal population of lipids whose functional groups display Rydberg atomic properties are macrocosmic analogues, but not equivalents, of the two magnetic moments of the electron. The minute but significant difference between the spin moment of $9.28476 \cdot 10^{-24}$ $J \cdot T^{-1}$ and the orbital moment of $9.27408 \cdot 10^{-24}$ $J \cdot T^{-1}$ for a model electron is $1.068 \cdot 10^{-26}$ $J \cdot T^{-1}$. If 1 μT fields are applied to this difference, the resulting energy of $1.068 \cdot 10^{-32}$ J, when divided by Planck's constant ($6.624 \cdot 10^{-34}$ $J \cdot s$), results in a frequency of 16 Hz. If the effective field strength was ~1.3 μT (well within the range of standard deviation of the variable field intensities for our RMS value of 0.9 μT), the solution would be 20 Hz. Interestingly, several authors have reported enhancement of either tumor growth or weight when magnetic field frequencies between 12 Hz (Bellossi et al,

1988; 1991) and 20 Hz (Babincova et al, 2000; 2004) have been applied to animals.

We approached the interactions between the circumferential component within the cell membrane and the facilitated photon emission by the applied magnetic field as if they were classical electromagnetic processes. This assumes a dipole characteristic of the electromagnetic radiation. However the cells show a marked departure from spherical symmetry. If the source of the photon emissions could be described as a quadrupole within this non-symmetrical context then energies more typical of gravitational phenomena could be involved. As aptly stated by Puthoff [1989], gravitational potentials share many of the characteristics of van der Waals and Casimir forces more than fundamental Coulomb forces. The Casimir effect is the interaction between a pair of neutral, parallel conducting planes because of the quantum effects relate to disturbances in the vacuum of the electromagnetic field or the zero-point energy of a quantized field. Recent calculations [Persinger 2012] indicate that specific solutions for electromagnetic and "gravitational" phenomena may converge within the band of the visible wavelength.

Van der Waals forces are prominently present in surface-surface interactions of cells. This may be relevant to our observations because application of the Casimir equation:

$$F=(\pi^2/240)\cdot(\hbar c\cdot a^{-4})\cdot S \quad (2)$$

where F is the Casimir force, "S" is the area of the surface (of the plate or area of the cell culture), "a" is the separation between the two layers (1.4 cm), ħ= the modified Planck's constant, and c is the velocity of light, results in a force of $\sim 5\cdot 10^{-23}$ N. Applied across the 1.4 cm the force results in an energy of $9.317\cdot 10^{-25}$ J. When divided by Planck's constant the equivalent frequency is about 1.41 GHz, or within measurement error of interstellar neutral hydrogen (the 21 cm hydrogen line).

The 21 cm wavelength is congruent with the small differences in energy when the angular momentum and energy of the proton-electron rotations shift from parallel to antiparallel configurations. As noted earlier the difference in energy between the spin and orbital electron magnetic moments when applied to strengths of optimal fields employed in this study would be equivalent to the peak in spectral power noted in the photon emissions. Whether or not this is spurious or contributory to what we have observed must still be established.

Although from some perspectives the application of a Casimir potential may be considered to be unlikely, even a remote probability has potential significance. According to Bordag et al [2001] material boundaries from concentrated external

electromagnetic fields polarize the vacuum resulting in creations of real particles from virtual particles (vacuum oscillations) by the transfer of energy. Such “particle creation” occurs only if the boundary condition is a function of time. In the present study the boundary condition of the applied field was changing.

The shift in the spatial distribution of the scattergram during the double PMT measurements reinforces the validity of the effect. As noted in Figure 9, the most parsimonious interpretation of the data patterns we measured would be the presence of a “quadrupole”-like display of photons with the direction of emissions above and below and to each side of the pairs of plates. The application of the rotating field with flux lines along the same plane as the surface of the cells resulted in “constriction” of the field such that more photons protruded outside the boundaries (the solid line in Figure 9). These were detected as the photon spikes that occurred on average every 15 to 20 s when the optimal intensity of fields was present. Given the differences in resting membrane potentials between cancer cells and non-cancer cells it would be interesting to discern if there would be a shift in frequency in visible light that could potentially differentiate cancer cells from non-cancer cells.

3.5 References

Adey, W.R. (1981) Tissue interactions with non-ionizing electromagnetic fields. Physiol. Rev. **61**, 435-513.

Babincová, M., Sourivong, P., Leszczynska, D., Babinec, P. Influence of alternating magnetic fields on two-dimensional tumor growth. (2000). Electromagnetic Biology and Medicine. 19(3):351-355.

Babincová, M., Sourivong, P., Leszczynska, D., Babinec, P. (2004). Effects of GSM microwaves, pulsed magnetic field, and temperature on fractal dimension of brain tumors. Chaos, Solitons and Fractals;20(5):1041-1045.

Bellossi, A., Desplaces, A. (1991). Effect of a 9 mT pulsed magnetic field on C3H/Bi female mice with mammary carcinoma. A comparison between the 12 hz and the 460 hz frequencies. In Vivo;5(1):39-40.

Bellossi, A., Desplaces, A., Morin, R. (1988). Effect of a pulsed magnetic field on tumoral C3H/Bi female mice. Cancer Biochem Biophys;10(1):59-66.

Bini, V., Rubin, A. (2007) Magnetobiology: the kT paradox and possible solutions. Electromag. Biol. Med. **26**, 45-62.

Bohr, N. (1958) Atomic physics and human knowledge. N.Y.: John Wiley & Sons,.

Bordag, M., Mohideen, U., Mostepanenko, V.M. (2001). New Developments in the Casimir effect. Physics Reports. 353, 1-205.

Buckner, C.A. (2011) Effects of electromagnetic fields on biological processes are spatial and temporal-dependent. Laurentian University: Ph.D. Dissertation, Biomolecular Sciences Program,.

Buckner, C.A., Buckner, A.L., Koren, S.A., Persinger, M.A., Lafrenie, R.M. (2013) Exposure to a specific time-varying electromagnetic field inhibits cancer cell growth by affecting calcium influx (in submission).

Chang, J.-J., Fisch, J., Popp F.-A. (1998) (eds), Biophotons, Kluwer Academic Pub: Dordrecth,.

Cifra, M., Fields, J.Z., Farhadi, A. (2011) Electromagnetic cellular interactions. Prog. Biophys. Mol. Biol. **105**, 223-246.

Dotta, B.T., Buckner, C.A., Cameron, D., Lafrenie, R.M., Persinger, M.A. (2011a) Biophoton emissions from cell cultures: biochemical evidence for the plasma membrane as the primary source. Gen. Physiol. Biophys. **30**, 301-309.

Dotta, B.T., Buckner, C.A., Lafrenie, R.M., Persinger, M.A. (2011b) Photon emissions from human brain and cell culture exposed to distally rotating magnetic fields shared by separate light-stimulated brains and cells. Brain Res. **388**, 77-88.

Dotta, B.T., Persinger, M.A. (2012) "Doubling" of local photon emissions when two simultaneous, spatially separated, chemiluminescent reactions share the same magnetic field configurations. J. Biophys. Chem. **3**, 72-80.

Dudin, Y.O., Kuzmich, A. (2012) Strongly interacting Rydberg excitations of a cold atomic gas. Science **336**, 887-889.

Engstrom, S., Fitzsimmons, R. (1999) Five hypotheses to examine the nature of magnetic field transduction in biological systems. Bioelectromag. **30**, 423-440.

Furtula, V., Kahn, I.A., Nothnagel, E.A. (1990) Selective osmotic effect on diffusion of plasma membrane lipids in maize protoplasts. Proc. Nat. Acad. Sci. **87**, 6532-6536.

Isojima, Y., Isoshima, T., Nagai, K., Kikuchi, K., Nakagawa, H. (1995) Ultraweak biochemiluminescence detected from rat hippocampal slices. NeuroReport **6**, 658-660.

Karbowski, L.M., Harribance, S.L., Buckner, C.A., Mulligan, B.P., Koren, S.A., Lafrenie, R.M., Persinger, M.A. (2012) Digitized quantitative electroencephalographic patterns applied as magnetic fields inhibit melanoma cell proliferation in culture. Neurosci. Lett. **523**, 131-134.

Lado, W. E. and Persinger, M. A. (2012) Spatial memory deficits and their correlations with clusters of shrunken neuronal soma in the

cortices and limbic system following a “mild” mechanical impact to the dorsal skull in female rats. J. Behav. Brain Sci. **2,** 333-342.

Lednev, V.V. (1991) Possible mechanisms for the influence of weak magnetic fields on biological systems. Bioelectromag. **12,** 71-75.

Lenaz, G. (1987) Lipid fluidity and membrane protein dynamics. Biosci. Rep. **7,** 823-837.

Liboff, A.R. (1992) Cyclotron resonance in membrane transport. In B. Norden and C. Ramel, Eds. Interaction mechanisms of low level electromagnetic fields and systems. Oxford Press, Oxford, pp. 130-147.

Ludwig, H.W. (1968) A hypothesis concerning the absorption mechanisms of atmospherics in the nervous system. Int. J. Biometeor. **12,** 93-98.

Martin, L.J., Koren, S.A., Persinger, M.A. (2004) Thermal analgesic effects from weak, complex magnetic fields and pharmacological interactions. Pharm. Biochem. Behav. **78,** 217-227.

Mulligan, B.P., Gang, N., Parker, G.H., Persinger, M.A. (2012) Magnetic field intensity/melatonin-molarity interactions: experimental support with planarian (Dugesia sp.) activity for a resonance-like process. Open J. Biophys. **2,** 137-143 .

Ochalek, T., Nordt, F.J., Tullberg, K., Burger, M.M. (1988) Correlation between cell deformability and metastatic potential in B16-F1 melanoma cell variants. Cancer Res. **48,** 5124-5128.

Persinger, M.A. (2003) Neurobehavioral effects of brief exposures to weak intensity, complex magnetic fields within experimental and clinical settings. In M. J. McLean, S. Engstrom, R. R. Holocomb (eds) Magnetotherapy: potential therapeutic benefits and adverse effects. N.Y.: TFG Press, pp. 89-118.

Persinger, M.A. (2010) 10^{-20} Joules as a neuromolecular quantum in medicinal chemistry: an alternative approach to myriad molecular pathways. Cur. Med. Chem. **17,** 3094-3098.

Persinger, M.A. (2012) Potential origins of a quantitative equivalence between gravity and light. Open Astron. J. **4,** 19-25.

Persinger, M. A., St-Pierre, L. S., Koren, S. A. (2001) Geophysical variables and behavior: XCI. Ambulatory behavior in rats following prenatal exposures to complex magnetic field designed to interact with genetic expression. Percep. Mot. Skil. **92,** 183-192.

Popp, F.-A., Li, K.H., Mei, W.P., Gale, M., Neurohr, R. (1988) Physical aspects of biophotons. Experientia **44,** 576-585.

Puthoff, H.E. (1989) Gravity as zero-point-fluctuation force? Phys. Rev. **39,** 2333-2342.

Quickenden, T.I. (1974) Weak luminescence from yeast saccharomyces cerevisiae and the existence of mitogenetic radiation. Biochem. Biophys. Res. Comm. **60**, 764-770.

Rosenspier, A.J., Kindzelskii, A.L., Petty H.R. (2001) Pulsed DC electric fields couple to natural NAD(P)H oscillations in HT-1080 fibrosarcoma cells .Journal of Cell Science Vol 114, page 1515-1520.

St-Pierre, L. S. and Persinger, M. A. (2003) Conspicuous histomorphological anomalies in the hippocampal formation of rats exposed prentally to a complex sequenced magnetic field within the nanoTesla range. Percep. Mot. Skil. **97**, 1307-1314.

Schrodinger, E. (1944) What is life? Cambridge: Cambridge Univer. Press,.

Sun, Y., Wang, C., Dai, J. (2010) Biophotons as neural communication signals demonstrated by in situ biophoton autography. Photochem. Photobiol. Sci. **9**, 315-322.

Thomas, A.W., Kavaliers, M., Prato, F.S, Ossenkopp, F.-A. (1997) Antinociceptive effects of pulsed magnetic fields in the land snail, Cepaea nemoralis. Neurosci. Lett. **222**, 107-110.

Weaver, J.C., Vaughn, T.E., Martin, G.T. (1999) Biological effects due to weak electric and magnetic fields: the temperature variation hypothesis. Biophys J. **76**, 3026-3030.

Whissell, P.D., Persinger, M.A. (2007) Emerging synergisms between drugs and physiologically patterned weak magnetic fields: implications for neuropharmacology and the human population in the twenty-first century. Curr. Neuropharm. **5,** 278-288.

Chapter 4: "Doubling" of Local Photon Emissions When two Simultaneous, Spatially Separated, Chemiluminescent Reactions Share the Same Magnetic Field Configurations

Published in Journal of Biophysical Chemistry

Abstract

The aim of the present experiments was to discern if the "entanglement"-like photon emissions from pairs of cell cultures or human brains separated by significant distances but sharing the same circling magnetic field could be demonstrated with a classic chemiluminescent reaction produced by hydrogen peroxide and hypochlorite. Simultaneous injection of the same amount of peroxide into a local dish (above a photomultiplier tube) and a dish 10 m away in a closed chamber produced a "doubling" of the durations of the photon spikes only when the two reactions were placed in the center of separate spaces around each of which magnetic fields were generated as accelerating group velocities containing decreasing phase modulations followed by decelerating group velocities embedded with increasing phase modulations. The duration of this "entanglement" was about 8 min. These results suggest that separate distances behave as if they were "the same space" if they are

exposed to the same precise temporal configuration of magnetic fields with specific angular velocities.

4.1 Background

The concept of locality (local causes) requires each physical event or change in event to have a physical cause which occupies the immediate space-time of the effect [Stapp, 2009; Persinger & Lavallee, 2010; Persinger & Koren, 2007]. We have been developing a procedure to study experimentally the characteristics of non-locality [Dotta et al, 2009; Dotta et al, 2011]. When particular temporal configurations of changing angular velocities of weak magnetic fields are generated at the same time within two separate rings of solenoids separated by 10 m simultaneous phenomena that are congruent with the theoretical expectations for "excess correlations" or "entanglements" are observed [Arnesen et al, 2001]. Measurements in two separate loci that should have been randomly associated were excessively correlated if they shared the same unique magnetic space. We interpreted the effect as a transposition of space-time coordinates for the two distant loci such that they behave as the "same space" without involvement of classically propagating electromagnetic fields.

We found that the most robust "excess correlations" that implied non-locality required accelerating or decelerating rates of change in angular velocity as determined by the duration of the magnetic field at each solenoid within a circular array as they were serially activated. For example, when two human subjects

separated by 10 m shared the same circumcerebrally rotating magnetic fields the changes in power within specific electroencephalographic frequencies of the person sitting in the dark reflected the light flash frequency presented to the other person who was sitting in a closed acoustic chamber in another room [Persinger et al, 2010].

To pursue this phenomenon with more precision, and fewer organismic complexities subsequent experiments measured photon emission by a photomultiplier tube (PMT) from cells in one space within the ring of solenoids while light flashes were delivered to cells within another ring of solenoids. Dotta et al [2011] found reliable and statistically significant increases (~ 2x) in photon emissions (background levels of ~ 5 x 10^{-11} W/m^2) from plates of approximately one million melanoma cells housed in darkness if the other plate of melanoma cells in the closed chamber was stimulated with light. The cells housed in the dark and in the other room shared the same configurations of magnetic fields rotating around the plates. The effect was not evident if the light was flashed without the presence of the shared magnetic fields with changing angular velocities.

However this excess correlation required two stages of magnetic field exposure that involved first an accelerating rotational field for about 5 min followed by a decelerating magnetic field for a comparable period; the "shared photon" effect was evident only

during the latter sequence. Additional research [Dotta et al, 2011] indicated that the likely source of the photon emissions from melanoma cells was the plasma cell membrane as it slowly depolarized following removal from incubation. There are multiple hypothesized processes that could mediate this effect through relatively complex biochemical sequences including lipid peroxidation, excited triplet state carbonyls Tilbury & Quickenden, [1988] and interactions with oxygen radicals [Vogel & Suessmuth, 1988].

In order to discern if this nonlocal photon coupling could be reproduced with a more direct photon reaction, we selected a classic physical chemical process: H_20_2 + NaClO → H_2O + NaCl + O_2 or more precisely HOOH + OCl^-→ $^1O_2$ for generating photons [Kahn & Kasha, 1994]. The source of the photon has been attributed to the excited singlet oxygen $^1O_2$. When repeated quantities of 0.1 cc hydrogen peroxide were injected at fixed intervals (every 1 min) into the same 6 cc of sodium hypochlorite plates placed over the aperture of the PMT, discrete reliable spikes with fixed durations (~ 2 s) in photon emissions between 10^{-8} W/m^2 and 10^{-9} W/m^2 (or when the aperture of 1.26 x 10^{-3} m^2 is accommodated, quantum amounts of between ~10^{-11} and 10^{-12} J) were observed.

However if both this plate and the plate 10 m away in an acoustic chamber (and Faraday cage) were exposed to the same magnetic field protocol as the one that produced the "double photon" effect in the

melanoma cells [Dotta et al, 2011] and 0.1 cc of hydrogen peroxide was injected into both plates simultaneously, there was a conspicuous widening of the duration of the photon emission that occurred reliably for about 6 to 8 min during a specific type of change in angular acceleration. An example of the spikes of photon emissions during serial single local injections and the local+nonlocal paired injections are shown in Figure 1.

The duration that nonlocal+local injections produced the effect was much longer than the 0.5 msec maintenance of entangled spin states reported by Julsgaard et al [2001] for paired volumes of about 10^{12} molecules of caesium gas. The effect from local+nonlocal paired injections compared to single local injections was so qualitatively conspicuous we designed a series of experiments to isolate the important components of the physical conditions that promoted the phenomenon. Unlike the "double photon" effect seen with the coupled plates of melanoma cells, which continually generate photons (especially after they are removed from the incubator), we found that the injections of the reactant to produce the enhanced photon emission during the local+nonlocal paired injections required *simultaneous* injections of 0.1 cc into both plates of sodium hypochlorite. Here we present the results of our experiments that show the temporal duration and magnetic field configurations required to generate the "photon doubling".

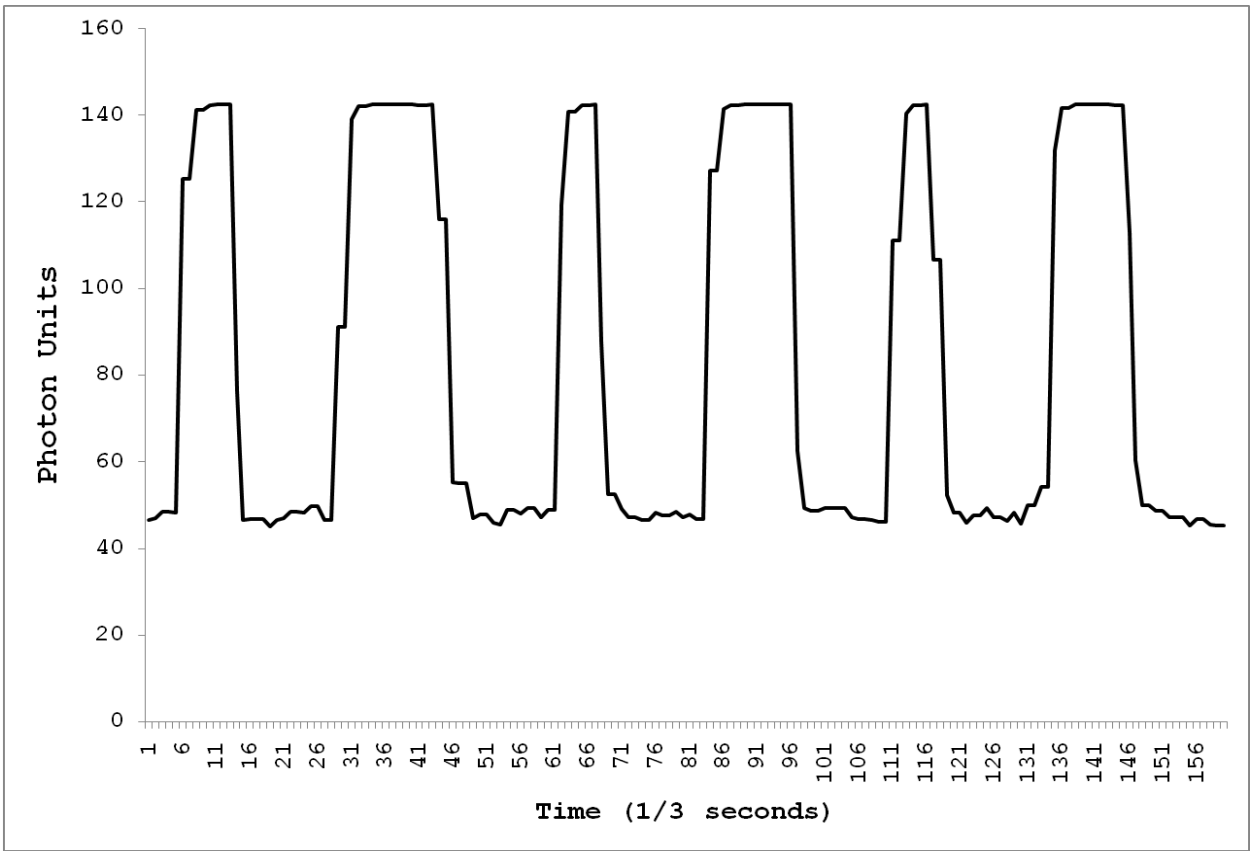

Figure 1. Photon emissions (1 unit ~5 x 10^{-11} W/m^2) as a function of time (in increments of 0.3 s) from injections of H_2O_2 into NaClO. The narrow spikes occurred during single local injections while the conspicuously wider spikes occurred during the simultaneous nonlocal+local injections.

4.2 Materials and Methods

4.2.1 Photon Emission Procedures and Measurements

The equipment and rooms used for these experiments were identical to those employed for the tissue culture [Dotta et al, 2009; Dotta et al, 2011] and human brain [Persinger et al, 2010] studies. There was only one experiment per day which was conducted between 18 and 21 hr local time. A total of 6 cc of refrigerated reagent grade ≥ 4% Cl) of NaHClO (Sigma-Aldrich) was placed into each of two tissue culture dishes (Sarstedt, 60 x 14 mm) that were then covered. They were transported to the experimental room.

One plate (cover removed) was placed over the aperture of the PMT sensor that was housed in a dark room. The Model 15 Photometer from SRI instruments (Pacific Photometric Instruments) and the PMT housing (BCA IP21) for a RCA electron tube had been employed in other experiments [Dotta et al, 2009; Dotta et al, 2011]. It was connected to the meter (scaled 1 to 100) whose voltages were recorded by an IBM laptop computer with a sampling rate of 3 times per sec. Two methods of calibration indicated that an increase of 1 unit was equivalent to ~5 x 10^{-11} W/m^2. At this setting the typical background range for the meter over days was between 45 and 55 units. Within a single hour the range of variation around the central tendency was between 5 and 6 units.

The PMT sensor was surrounded by an array of 8 solenoids as described previously. A 1 cc plastic syringe with a 23 gauge needle was inserted into a 0.6 m length of intramedic tubing. The distal 2 cm of the tubing was attached to the wooden (cotton removed) center of a Q-tip to add weight and stability to the end of the tubing. After 2 cc of 3% H_2O_2 (purchased from local pharmacies) was slowly injected through the tubing (outside of the PMT box) to insure fresh reactant for each trial, the tip was placed in the middle of the tissue dish containing the fresh hypochlorite over the center of the aperture of the PMT (beneath the plate). The box containing the PMT and the ring of eight solenoids was then covered with several layers of black heavy cloth. The background photon emissions for this procedure have been remarkably reliable and stable over the last two years except during the days that precede major global seismic events. The second dish, also containing 6 cc of hypochlorite, was placed in the second circular array of 8 solenoids that was housed 10 m away in an industrial acoustic chamber that was also a Faraday environment in another room.

4.2.2 Magnetic Field Exposures

Both arrays of 8 solenoids in the different rooms were connected to custom constructed (U.S. Patent 6,312,376 B1: Nov. 6, 2001; Canadian Patent No: 2214296) units that controlled the sequential activation of each of the solenoids. The control units

were connected to the same IBM 286 computer that contained the custom-constructed software for generating the magnetic fields. The shapes and intensities of the magnetic fields were completed by transforming a column of numbers each between 0 and 256 to between -5 and +5 V (127=0 V) through a digital to analogue converter. The duration each number (or voltage) that was activated was programmable and in these experiments was 1 msec. The duration was selected on the bases of theoretical assumptions [Persinger & Koren, 2007].

On the bases of their effectiveness to produce biological responses in human volunteers [Persinger, 2003], rats [Martin et al, 2004], and cell cultures [Buckner, 2011] two "physiologically patterned" magnetic fields were employed. Their shapes are shown in **Figure 2**. The first frequency modulated pattern was considered decreasing while the second pattern was considered increasing. The numbers of points (numbers between 0 and 256) that composed each pattern was 859 and 230, respectively.

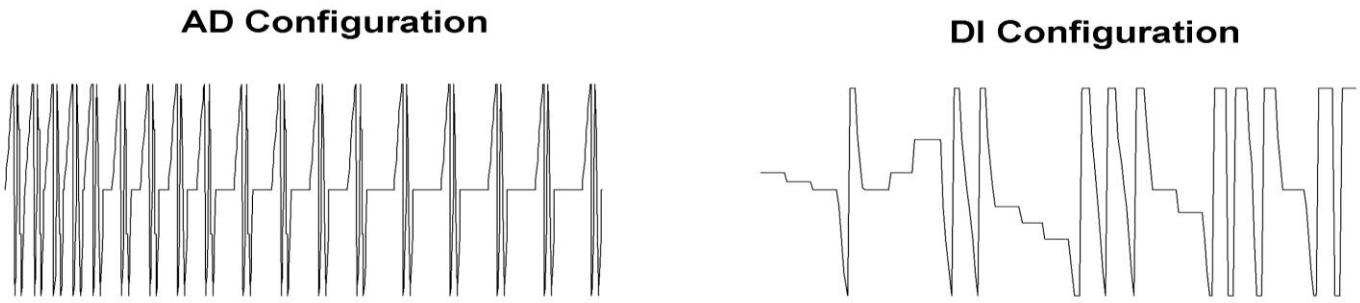

Figure 2. The decreasing frequency or "phase velocity" (left) and increasing frequency or "phase velocity" wave forms that were generated continuously during the accelerating or decelerating angular velocities required to produce the nonlocal+local "double photon duration" effect.

These patterns were continuously presented but were also rotated to each of the 8 solenoids in a counterclockwise (from the top) direction. Each solenoid was separated by 45 deg around a circumference of ~60 cm. The software was constructed to generate two parameters: 1) initial duration of the magnetic field generation at the "first" solenoid in the circle, and, 2) the rate of change of the duration. For the increasing angular velocity (acceleration) of 20+2 ms, this meant that the duration of the magnetic field at the first solenoid was 20 ms, and then decreased to 18, 16, 14, 12, 10, 8, and 6 ms to each of the successive solenoids before increasing to 20 ms continually.

For the decreasing angular velocity (deceleration) of 20-2 ms, this meant that the duration of the field at the first solenoid was 20 ms which then increased with each successive solenoid to 22, 24, 26, 28, 30, 32, and 34 ms. The time required to deliver the patterned magnetic field to each solenoid (the port time) was about 200 μs. The strength of the magnetic field within the center of the array of solenoids where the dishes containing the sodium hypochlorite were placed averaged 1 μT (10 mG) as measured by an AC milligauss meter. Each solenoid was a pair of reed switches [Richards et al, 1996] contained within a plastic cylinder (film canisters) that were connected to its own custom constructed commutator and both units were controlled by the same computer at a central location.

4.2.3 Experimental Protocol and Nomenclature

The complex magnetic field configurations simultaneously generated in both arrays of solenoids involved two major components. We employed the terminology from Tu and his colleagues [2005] who described that one of the implications of the photon displaying a nonzero mass would be to produce a difference between group velocity and phase velocity. We did not assume that our utilization of these terms were identities with their inferences but instead served as convenient metaphors for the application of our procedures to future theoretical pursuits.

The first component of the magnetic field configuration was the changing angular velocity of the circular rotating magnetic field which we considered analogous to the "group velocity." The second was the changing frequency modulation of the patterned magnetic field which we considered analogous to the "phase modulation". We had found by trial and error in the previous cell-based experiments [Dotta et al, 2011] that to obtain the excess correlation between enhanced photon emission from cells in the dark and intervals when the other cells in another room were receiving light flashes both dishes must be first exposed for about 5 minutes to an accelerating group velocity (20+2) containing a decreasing (**Figure 2a**) phase modulation (AD) followed by a comparable time of exposure to a decelerating group velocity (20-2 ms) carrying an

increasing (Figure 2b) phase modulation (DI). This ADDI sequence was defined as our *standard protocol*.

The protocol involved the following sequences. Once each dish in the two rooms was centered in its array of solenoids (about 5 to 10 min after removal of reactants from the stock solutions), 40 repetitions of the AD configuration (about 30 s) were presented to each array of solenoids to verify the presence of the magnetic fields in both locations. This was completed by listening to the sound from a commercial audioamplifier connected to a telephone solenoid sensor. The sound pattern also allowed verification of the fidelity of the temporal pattern. After about 2 min, the two experimenters synchronized their cell phone stop watches to the nearest 0.1 s and then the DA configuration was again activated.

For the next 6 min during odd minutes (1, 3, and 5) the experimenter in the PMT room injected 0.1 cc of hydrogen peroxide through the tubing. During even minutes (2, 4, and 6) both experimenters in the separate rooms injected 0.1 cc of hydrogen peroxide into their respective dishes simultaneously. At the end of 6 min, the AD field was stopped and the DI field was activated from the computer, which required about 50 s, and occurred continuously for the next 12 min. Starting at 9 min single quantities of 0.1 cc of hydrogen peroxide were injected during the odd minutes (9, 11, 13, 15) and the simultaneous "double" quantities at the nonlocal and local dishes were injected during even minutes (10, 12, 14, 16,

18 min). Each injection by both experiments required ~2 s and was always verified independently by stopwatches. As indicated the increased duration of photon emission occurred *only* during this second component and during the local+nonlocal paired injections (**Figure 3**). Subsequent manipulations of the parameters were then dependent upon the results of each triplet of experiments.

4.2.4 Data Analysis

The primary measure for the photon emission was the duration of the spike (Figure 1). Each raw data file comprising the 3 samples per sec were observed visually. The number of serial samples (~333 ms/sample) from the time the PMT values deviated by 10 units above the background baseline and then return to below this criterion was converted to seconds. These values were strongly correlated with the calculated area under the curve of the spike (see Figure 4). Because of the convenience of employing the spike duration and the robustness of the visual display, this measure was selected for analyses.

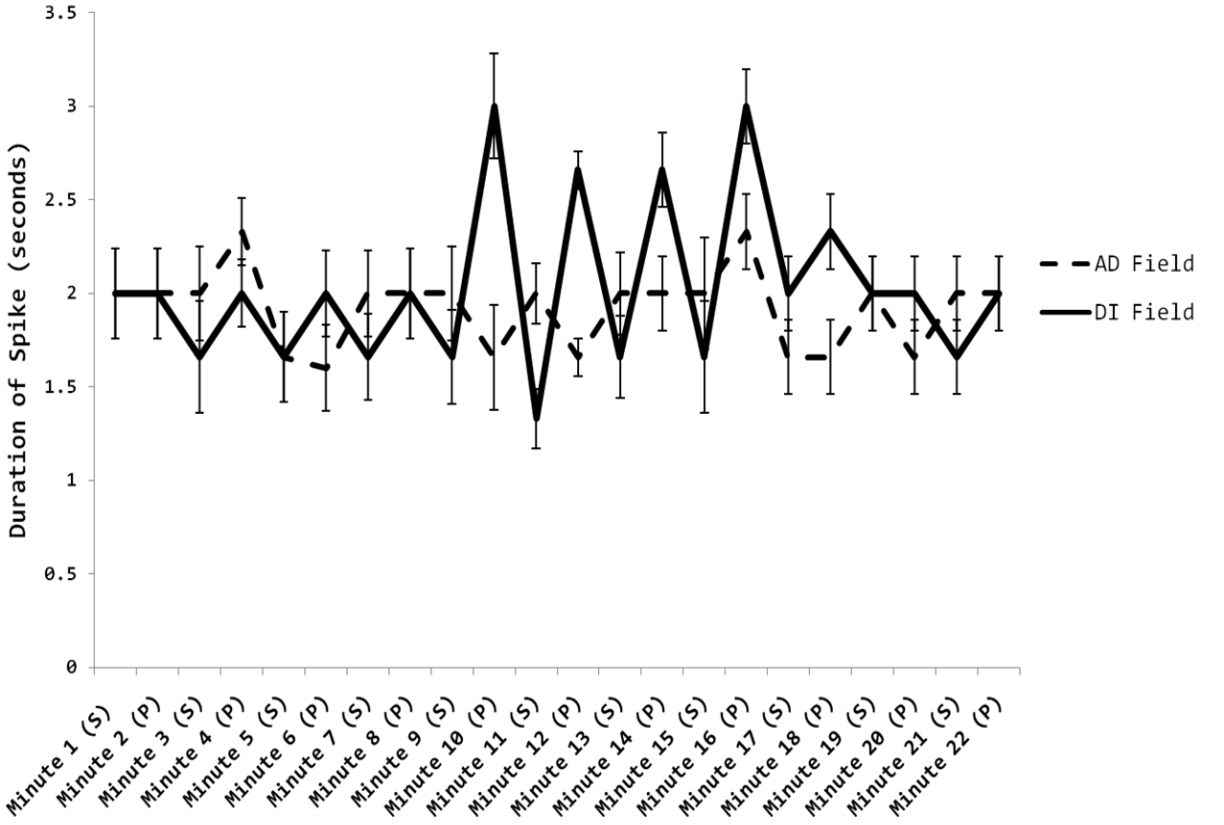

Figure 3. Absolute duration for the photon spikes during our standard protocol for single (local) and double (nonlocal+loal) simultaneous injections once per minute (odd numbers, local injections; even numbers, nonlocal+local injections) while both plates were exposed to only the DI phase (control=the dashed line) or the AD component for 6 min followed by the AI component for 9 to 22 min.

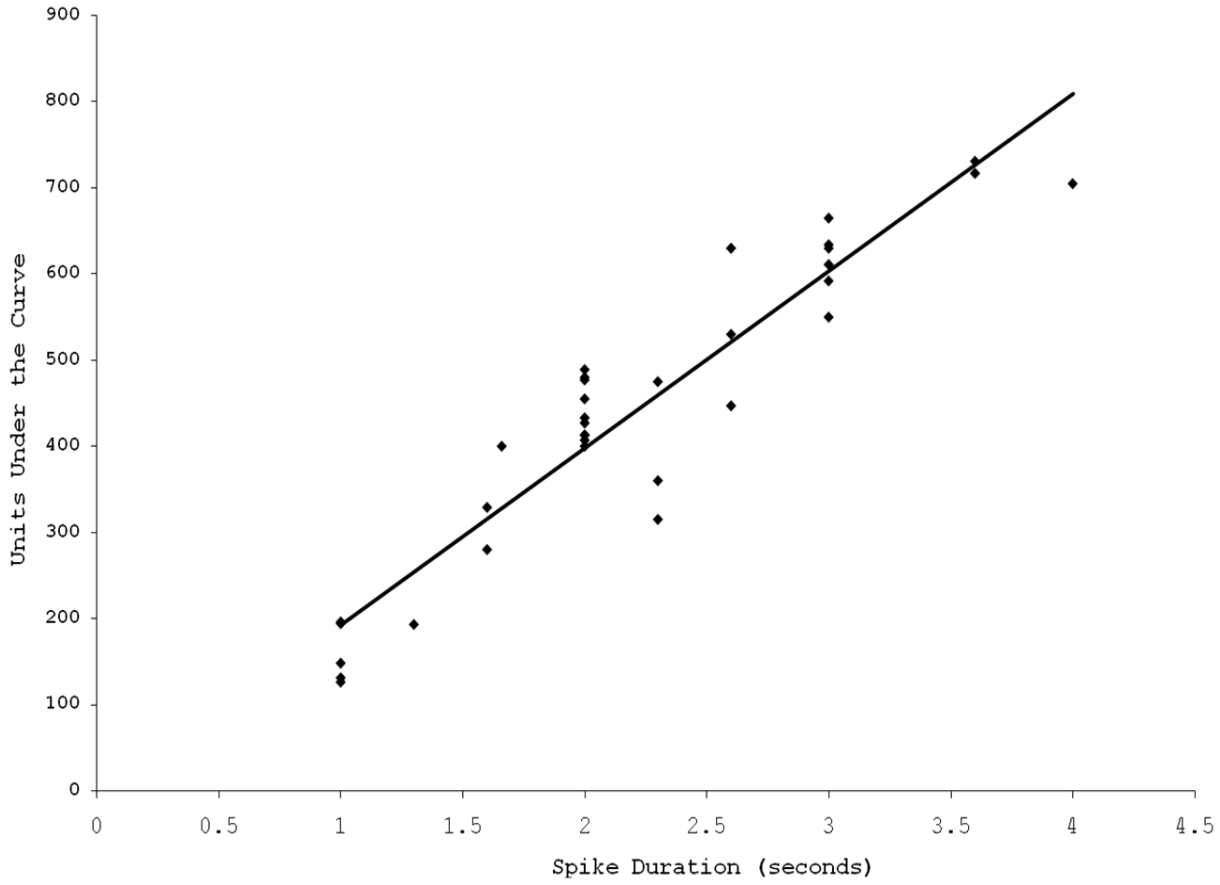

Figure 4. Correlation between the photon spike duration (in sec) and the total number of PMT units under the curve of the spike for events randomly selected from several initial experiments.

The means and standard deviations for the 3 local and local+nonlocal injections during the AD field exposures and the 5 local and local+nonlocal injections during the DI field exposures were obtained. Two way analyses of variance for these values (AD:local, AD: nonlocal+local, DI:local, DI:nonlocal+local) were completed for each experiment. One way analyses of variance were also conducted when appropriate. Effect sizes, the amount of variance explained, were calculated in order to estimate the magnitude of the effect. Spectral analyses employed classic methods. All data were analyzed by PC SPSS 16.

4.3 Results and Systematic Manipulations of Parameters

4.3.1 Reliability and Validity of Effect

The means and standard deviations for the durations of the photon emission for the local (single) injections and nonlocal+local paired injections for the AD and DI components for a total of 15 experiments on different days distributed over a three month period are shown in Figure 5. Analysis of variance demonstrated a statistically significant difference [$F(1,71)=59.81$, $p < .001$] that explained (Ω^2 estimates) about 50% of the variance of the dependent variable. The effects were so large and qualitatively conspicuous that statistical analyses were note required to discern them but were included as a formality.

Because the duration of the photon emission when both experimenters each injected 0.1 cc of hydrogen peroxide simultaneously (nonlocal+local paired injections) were only about 0.65 to 0.69 wider than a single local injection, twice (0.2 cc) the usual amounts of hydrogen peroxide were serially injected once per min into the dish above the PMT. As can be seen in Figure 6, the photon duration of the 0.2 cc single local injection did not differ significantly from the nonlocal+local paired injection trials when the two experimenters each injected 0.1 cc simultaneously into the dish over the PMT and into the dish in another room that shared the same magnetic field configuration. We inferred that equivalent quanta of photon emission from the single 0.2 cc injection in the dish over the PMT and the two 0.1 cc injections in separate dishes indicated that the latter was equivalent to 0.2 cc injected locally.

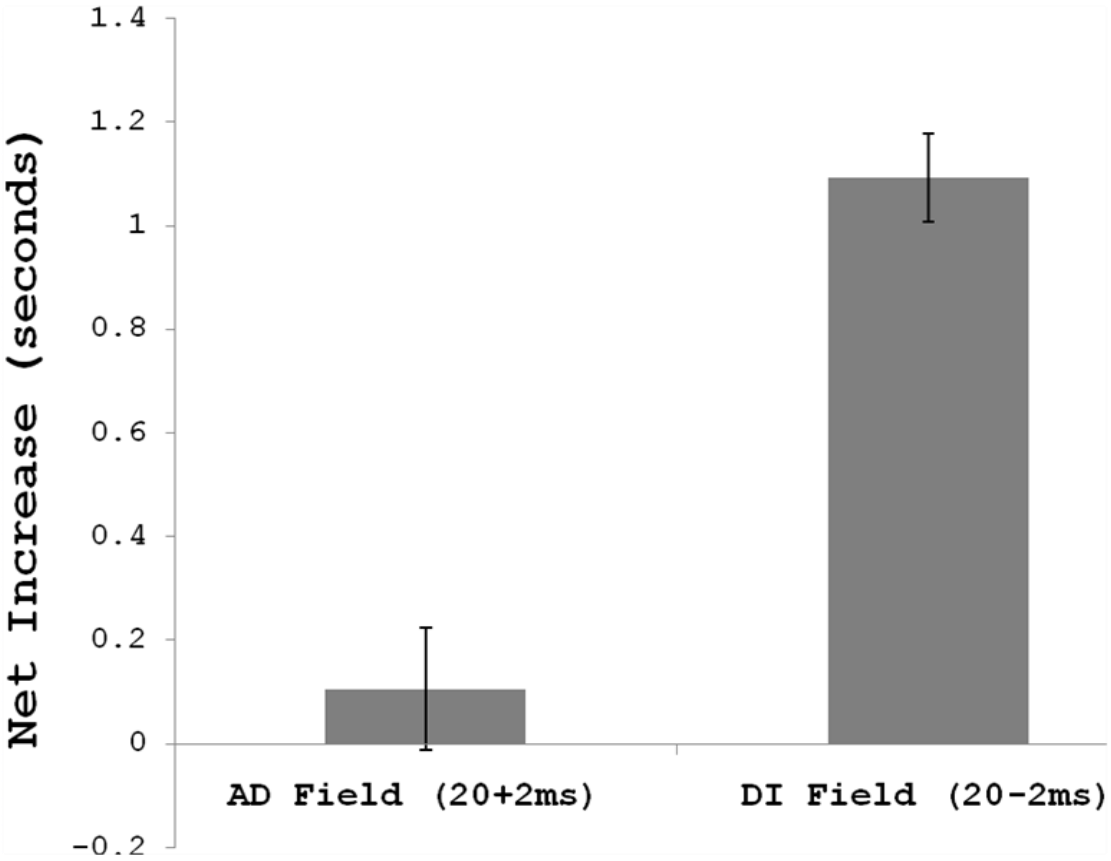

Figure 5. Means and standard deviations for the net increase in duration of the photon spike during the simultaneous nonlocal+local injections of 0.1 cc of hydrogen peroxide compared to the previous single 0.1 cc (local) injection during the presentation of the AD (accelerating angular velocity, decreasing phase velocity) and DI (decelerating angular velocity, increasing phase phase velocity) periods for 15 experiments.

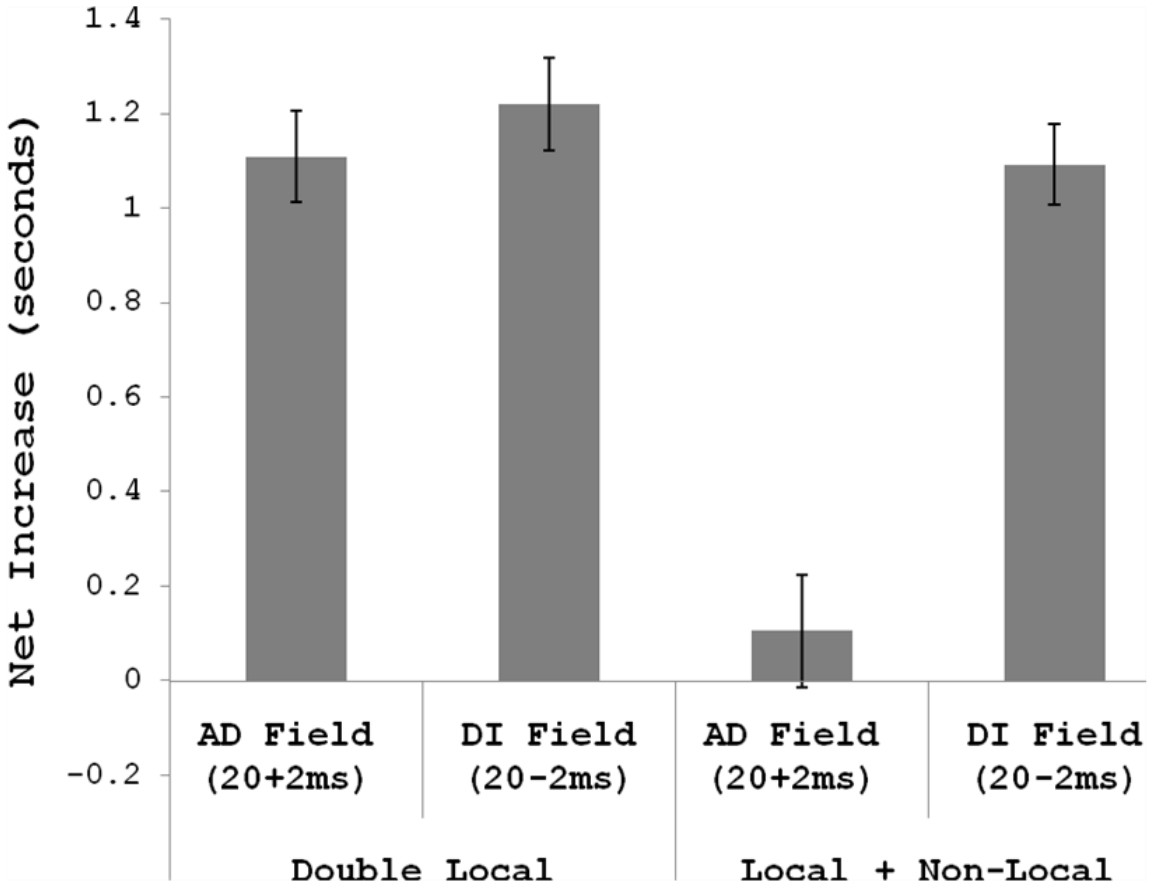

Figure 6. Mean and standard deviations for the net increase of the width of photon spike when 0.2 cc (double the standard amount) was injected locally (into the plate over the PMT) during the AD and DI durations.

4.3.2 Verifying Optimal Magnetic Field Temporal Sequence and Configuration

We then investigated if the continuous application for 20 min of *only* either the AD field or the DI field would produce "double" photon duration that we obtained during the nonlocal+local paired injections. There was no significant widening of the photon spike between the nonlocal+local and local injections during the 9 to 18 min period, the interval where the effect was reliably produced using the standard protocol. Presentations of the DI field first for 6 min and *then* the AD field afterwards (reversed sequence) for 9 to 18 min also did not evoke the effect. Because these results suggested that a DI configuration must *follow* an AD configuration, we first applied the typical AD field for 6 min and then applied the DI field as usual except that the same patterned ("phase-modulated") field was the *reversed* temporal order of the 859 points of the decreasing frequency or "phase" modulation field. In other words, the frequency or "phase" was now increasing (the reversed direction for the pattern in Figure 2a). As can be seen in Figure 7 the significant increases in the durations of photon spikes, the nonlocal+local paired injection effect, were again displayed. These results suggested that the requirement for the AD-DI sequence as an operational process rather than dependent upon a specific wave form.

4.3.3 Manipulating the Acceleration and Phase Modulation Components

To discern if the AD-DI configuration was essential, the accelerating group velocity was presented with the increasing phase modulation (AI) and the decelerating group velocity was presented with the decreasing phase modulation (DD). This was the opposite of our standard protocol where the accelerating packet was associated with a decelerating phase (AD) and the decelerating packet was associated with an increasing phase (DI). There was no statistically significant evidence of the local+nonlocal effect regardless of the presentation order AI-DD or DD-AI.

To test the importance of the "phase-modulation" within the group velocity the same accelerating field (20+2 ms) contained a synchronous, sine-wave 7 Hz pattern (no frequency or phase modulation) and the decelerating field (20-2 ms) also contained the synchronous (sine wave) 7 Hz pattern. The pattern was generated by converting the appropriate row of numbers that produced the 7 Hz sequence to voltages by the same software and hardware as the "phase modulated" patterns. Again, there was no evidence of significant widening of the photon emission duration during the nonlocal+local double injection. In all of the above experiments the average durations of photon spikes during the single (local) injections in the dish over the PMT did not differ from any of the other single (local) injections. The mean and SD of 40 randomly selected values from our records for single injections was 1.92 sec

and 0.29 sec (coefficient of variation=15%), respectively, which reiterates the precision of the duration of the photon emission and rate of injection of reactant.

To verify that the change in velocity of the rotating magnetic field was important for the 20+2 ms (AD) and 20-2 ms (DI) group acceleration, the standard protocol was applied using 20+0 ms for both the AD and DI components. This meant that, with the exception of the "acceleration" of moving in a circle, the "velocity" of the changing magnetic field (duration of activation of each successive solenoid) was constant. There was no significant widening of the duration of the spike during the local+nonlocal paired injections.

To insure that the acceleration component was important but was not unique to the 20+2 ms and 20-2 ms parameters, the standard protocol was applied using 100+10 ms during the DA component and 100-10 ms during the DI component, or, 30+3 ms during the DA component and 30-3 ms during the DI component. The phase directions remained the same. For the first parameter, for the 100 ms base duration, this meant that the duration of the field at each successive solenoid along the 8 circularly arranged solenoids changed from 100 ms to 30 ms during one rotation and from 100 ms to 170 ms during one rotation, respectively. The widening effect during the local+nonlocal paired injections was clearly observed for both the 30±3 ms and 100±10 ms configurations; the latter is shown in Figure 8.

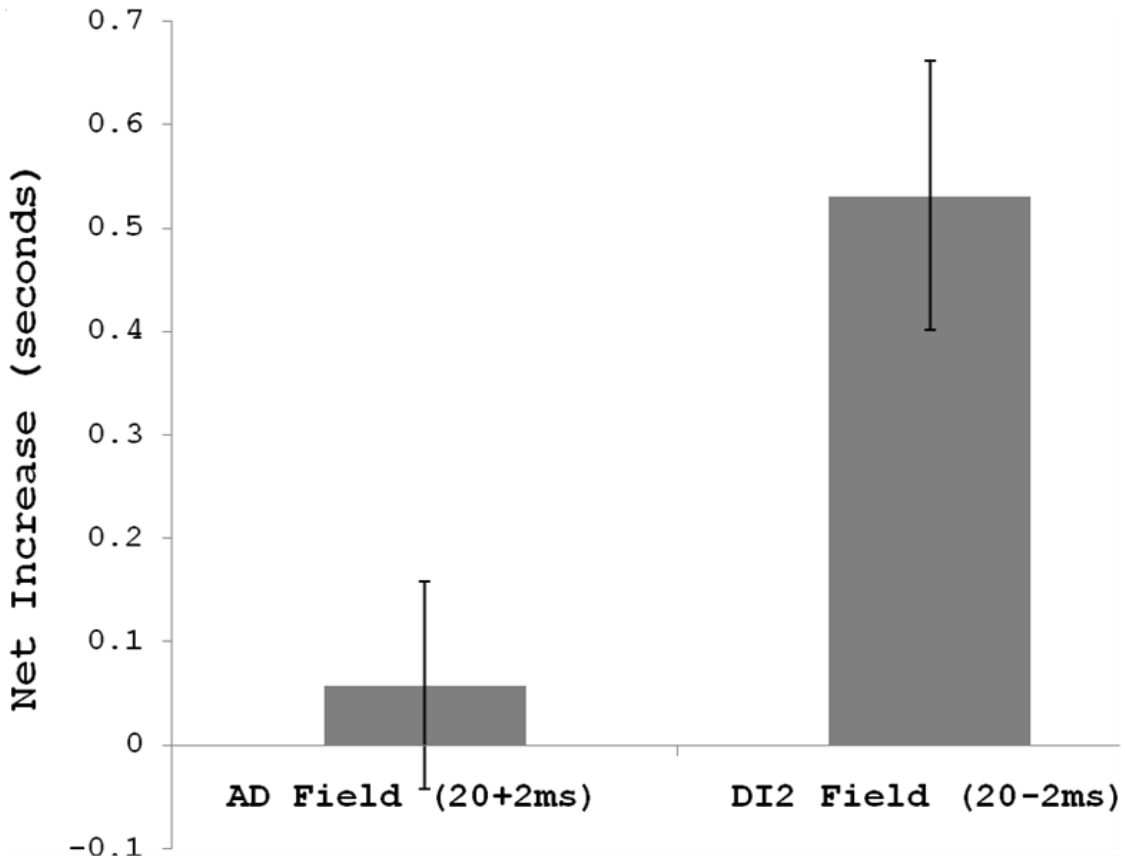

Figure 7. Means and standard deviations for the net increase in the durations of the photon spike when the decreasing frequency or "phase velocity" pattern generated during the accelerating angular velocity condition was reversed (DI2) so it was displaying an increased frequency or "phase velocity" during the decelerating angular velocity condition.

These result reaffirmed the observation that the sequence of an accelerating field embedded with a decreasing phase modulation followed by a decelerating field embedded with an increasing phase modulation was essential for the phenomenon.

4.3.4 Determining the Temporal Window of the Effect

In our standard protocol in which we first observed the local+nonlocal paired injection effect the AD component was presented for 6 min while the DI component was presented for 18 min. To isolate the temporal duration of this "window" for the "doubling" of photon emission, the duration of the first standard component, AD, was varied in a randomized order over several days to be: 0.5, 1, 2, 3, 4, 6, 8, 9, 10, 12 and 16 min before the standard AI field was initiated. The sequence of single and double injections followed the same procedure as usual: single injections 1, 3, 5, 9, 11, 13, 15, and 17 min after the beginning of the experiment and nonlocal+local paired injections 2, 4, 6, 10, 12, 14, 16, and 18 min after the beginning of the experiment. The emergence of the local+nonlocal paired injection effect was measured by averaging the duration of those photon spikes and subtracting the values from the previous spike durations of the local injections. The results are shown in Figure 9. A statistically significant increase (divide the SD by the number of trial, i.e, 12) in the spike duration during of the DI field when

the nonlocal+local injections occurred was evident if only 1 min of the AD field was first presented. The optimal duration of the AD pre-exposure before the AI field was presented was between 3 and 6 min. However if the AD field was presented for more than 8 min, the effect did not emerge even if the DI field was applied for an additional 16 min.

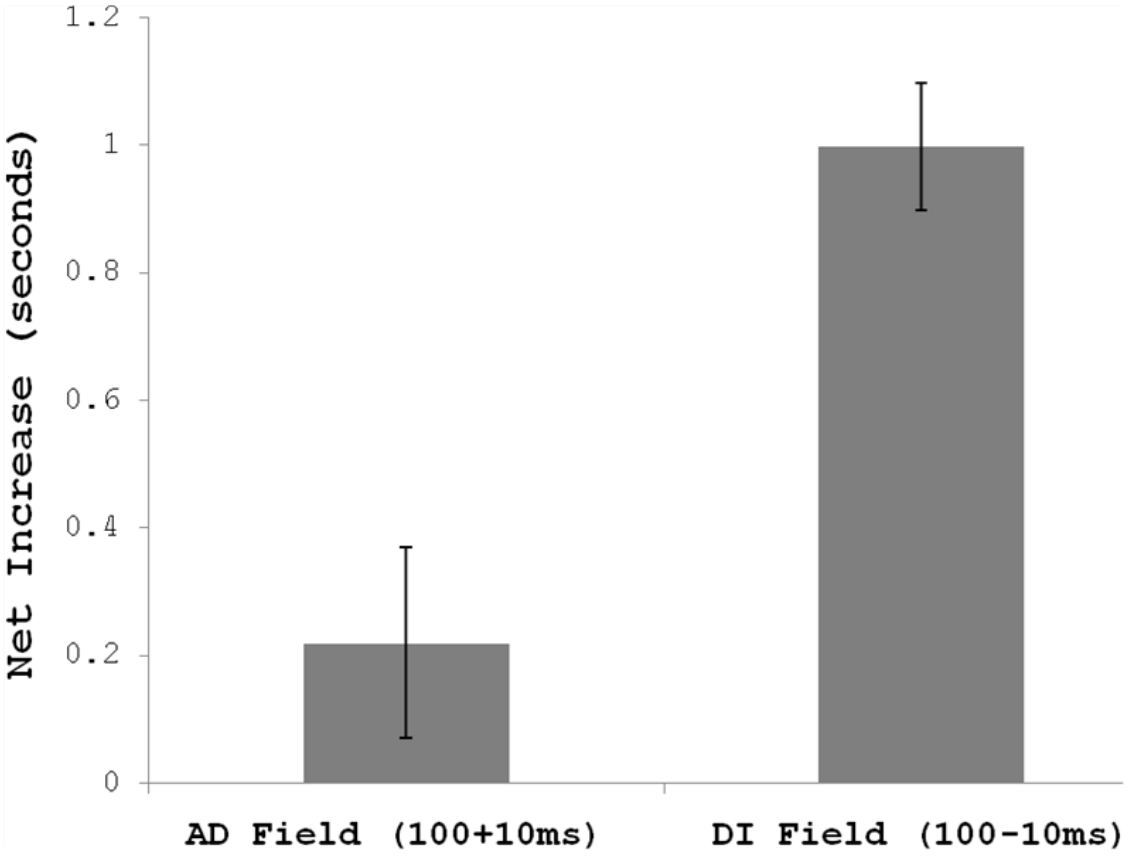

Figure 8. Means and standard deviations for the net increase in the duration of the photon spike when the same decreasing and increasing frequency or "phase velocity" fields were employed and the accelerating and decelerating angular velocity durations where 100+10 ms and 100-10 ms instead of the standard 20+2 ms and 20-2 ms.

4.4 Discussion

The macroscopic demonstration of "excess correlation" between spatial loci from which photons are emitted would have potentially paradigm-shifting implications for our interpretations of interactions between chemical reactions within and without the living cell. The results suggest that under special conditions two loci separated by significant distances would become "the same space". Living cells and organisms emit photons in the order of 10^6 photons/m^2·s [Popp et al, 1988]. Hippocampal slices emit photons with power densities of about 10^{-12} W/m^2 that are phase-locked to theta activity [Isojima et al, 1995]. Theta activity (4 to 7 Hz), upon which 40 Hz ripples are carried, is the intrinsic dominant frequency band for this neuroanatomical structure that is central to memory consolidation for the mammalian brain, that is, the representation of spatial experience.

Human beings instructed to engage in imagery while sitting in the dark also display reliable increases of comparable densities in photon emissions that are strongly correlated with the quantitative electroencephalographic activity [Vogel & Suessmuth, 1988]. The imagery-coupled increases in photon emission from the right side of the head are about a factor of 2 (doubling) within the order of 10^{-11} W/m^2 or the equivalent energy associated with about 10^7 cortical neurons if each generated 10 action potentials per second with ~2 x 10^{-20} J per action potential. During the last ten years several

experiments [Persinger et al, 2008] in our laboratory have shown that the conditions that contribute to entanglement between two brains, a history of shared spatial proximity, is associated with coherent experiences and cognitive processes if both participants shared the same circularly rotating magnetic fields with the changing angular velocities employed in the present experiment. However the complexity of these biological systems has made pursuit of the mechanism difficult.

In the present study a discrete chemical reaction that produces a reliable, measured amount of photon emissions displayed an even more robust effect that did not require complex statistical analyses to be discerned. When two spatially separate volumes of liquid hypochlorite shared the same configuration of angularly accelerating magnetic fields simultaneous injection of 0.1 cc of hydrogen peroxide into each volume by two experimenters (nonlocal+local) produced a widening of the photon duration in the volume over the PMT that was equivalent to injecting twice the amount (0.2 cc) only into this volume in that location.

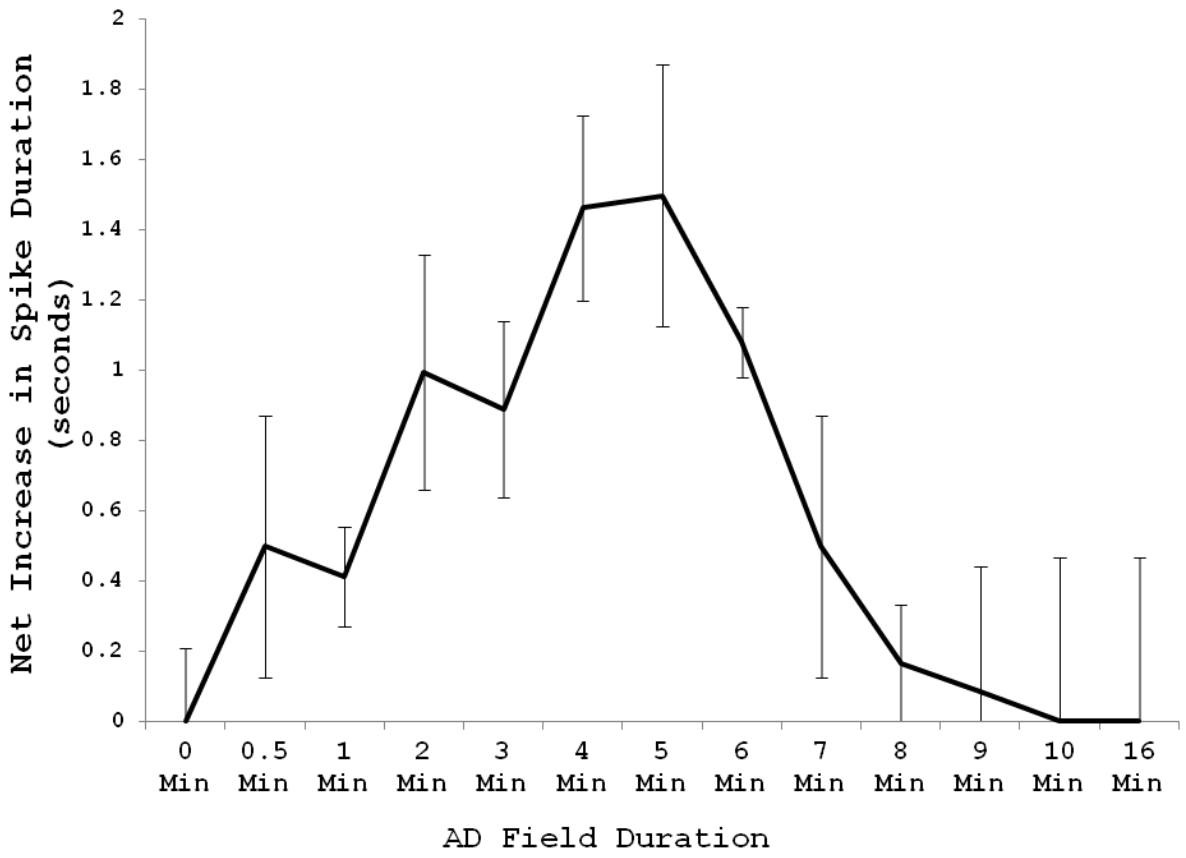

Figure 9. Means and standard deviations of the net increase in duration of the photon spike during the usual DI phase during nonlocal+local injections as a function of the initial duration of the first AD phase (the duration "0" means the DI phase was presented from the beginning).

4.4.1 The Precision of Temporal Configurations

The results of approximately 45 different experiments over several months demonstrated this "entanglement": two separate loci behaved as a single space for the duration of about eight (8) minutes under optimal conditions. This first required the application of an accelerating group velocity within which the phase modulation was decreasing followed by a second application of a decelerating group velocity within which the phase modulation was increasing. The "double photon" effect from nonlocal+local injections was evident with only 1 min of exposure to the first application but was maximal between 3 and 6 min of exposure before the second application was presented.

The data clearly indicated that a change in angular velocity (acceleration) was required; constant velocity magnetic fields did not produced the effect. In addition, the phase modulation of the group velocity must be changing (in the opposite direction to the group velocity) as well; a fixed frequency "phase" did not produce the effect. That this combination of temporal processes was essential rather than the precise 20 msec base rate of the magnetic field for the first solenoid was shown by the production of the effect if the base rate was shifted to 100 ms but the vectorial configuration of the group and phase velocities remained the same.

We selected the nomenclature of Tu et al [2005] so that potentially convenient applications might be applied to potential

mechanisms. One of the implications of a photon mass being non-zero is the resulting frequency dependence of the velocity of electromagnetic waves propagating in free space. Although the magnetic fields in our study were *not* propagating but were time-coupled, spatially rotating, time-varying fields, the application may be relevant for conditions of non-locality and entanglement. The superposition principle of entanglement can be satisfied if classical phases of interfering electromagnetic waves, such as optical holograms, occur [Ahn et al, 2000].

4.4.2 Potential Origins for the "Temporal Dilatation"

The challenge is to discern the mechanism that would accommodate the approximately 8 min duration of entanglement (or the effective transposition of two loci), as inferred by the "doubling" of the photon spike duration during simultaneous nonlocal+local stimulation. In addition to the obvious similarity between the time required for light to travel between the earth and the sun in comparison with the presumed instantaneous effect of gravitational waves [Klocchek et al, 1995], there are avenues of investigation for which experiments can be designed to systematically manipulate critical variables. For example, with a nonzero photon mass, the dispersion elicits a frequency dependence whereby the group velocity and the phase velocity differ as we simulated in our experiments. A dispersion of velocity of a photon

with a nonzero mass allows a potential condition for space-time dilation or contraction.

The direct experimental measurements of the dispersion of light within the 10^8 Hz to 10^{15} Hz range, the increment associated with visible light, showed a relative difference in velocity of $\Delta c/c < 10^{-7}$ [Tu et al, 2005]. Using the classic Lorentz contraction of:

$$t_{\Delta} = 1/\sqrt{[1-(v^2/c^2)]}$$

the above difference would be equivalent to about 500 s or 8 minutes. This "window" is within the range of the doubling of the photon effect measured repeatedly in this study.

If we assume there is some scale invariance operating within the phenomenon then the duration of our inference of entanglement, about 8 minutes, should be proportional to the maintenance of the 0.5 msec (5×10^{-4} s) spin state observed [Julsgaard et al, 2001] for two volumes of caesium gas each contain 10^{12} molecules. The number of molecules in the quantum of H_2O_2 we injected would be 0.1 cc (10^{-4} L) x 3 x 10^{-2} (3%) in water (55 M/L) times 6.023×10^{23} molecules/M or ~10^{20} molecules. When the quantum efficiency and the results of photon scatter are accommodated, the numbers of

molecules could be ~10^{18}. The proportional entanglement would be in the order of 500 s which is within the range of our observations.

From a third perspective with direct connections to causal quantum gravity [Ambjorn et al, 2004], the phenomenon observed may be explored as events within quantum gravity Hilbert space and a possible extended particle analogous to a soliton. El Naschie [2004] mathematically reproduced the result of this assumption and deduced that the mass of the fundamental exotic transfinite particle would be ~1.8 MeV or ~3 x 10^{-13} J in a standardized setting. This may be important because the quantum of photon energy associated with the 0.1 cc injections was within this order of magnitude (10^{-12} to 10^{-11} J). Although often considered exotic, gravitational instantons are related to tunneling events where there is a sudden appearance of a microscopic window in space-time.

4.5 Conclusion

The results presented in this manuscript are the most reliable and internally consistent demonstrations of a possible macroscopic example of non-locality and entanglement that we have encountered in the laboratory. Unlike the cell studies where concurrence of photon emissions between two loci could not be controlled easily, the photon emissions from H_2O_2 and NaClO between two sites could be synchronized. The experimental examination of the maximum distance

between the two plates sharing the appropriate magnetic configurations that exhibit the phenomenon is the next logical step.

4.6 References

Ahn, J., Weinacht, T. C. and Bucksbaum, P. N. (2000) Information storage and retrieval through quantum phase. *Science*, **287**, 463-465.

Ambjorn, J., Jurkiewicz, J., and Loll, R. (2004). Emergence of a 4D world from causal quantum gravity. *Physics Review Letters*, **93**, 13101(10-4.

Arnesen, M. C., Bose, S. and Vedral, V. (2001) Natural thermal and magnetic entanglement in the 1D Heisenberg model. *Physical Review Letters*, **87**, 017901-1/017901-4.

Buckner, C. A. Effects of electromagnetic fields on biological processes are spatial and temporal-dependent (2011). Ph.D. Thesis, Laurentian University.

Dotta, B. T., Mulligan, B. P., Hunter, M. D. and Persinger, M. A. (2009) Evidence of macroscopic quantum entanglement during double quantitative electroencephalographic (QEEG) measurements of friends vs strangers. *NeuroQuantology*, **7**, 548-551.

Dotta, B. T., Buckner, C. A., Lafrenie, R. M. and Persinger, M. A. (2011) Photon emissions from human brain and cell culture exposed to distally rotating magnetic fields shared by separate light-stimulated brains and cells. *Brain Research*, **388**, 77-88.

Dotta, B. T., Buckner, C. A, Cameron, D., Lafrenie, R. F. and Persinger, M. A. (2011) Biophoton emission from cell cultures:

biochemical evidence of the plasma membrane as the primary source. *General Physiology and Biophysics*, 30, 301-309.

El Naschie, M. S. (2004) Gravitational instanton in Hilbert space and the mass of high energy elementary particles. *Chaos, Solitons & Fractals*, **20**, 917-923

Isojima, Y., Isohima, T., Nagai, K, Kikuchi, K. and Nakagawa, H. (1995) Ultraweak biochemiluminesence detected from rat hippocampal slices. *NeuroReports*, **6**, 658-660.

Julsgaard, B., Kozhekin, A. and Polzik, E. S. (2001) Experimental long-lived entanglement of two macroscopic objects. *Nature*, **413**, 400-403.

Kahn, A. U. and Kasha, M. (1994) Singlet molecular oxygen evolution upon simple acidification of aqueous hypochlorite: application to studies on the deleterious health effects of chlorinated drinking water. *Proceedings of the National Academy of Sciences*, **91**, 12362-12364.

Klocchek, N.V., Palamarchuk, L. E. and Nikonova, M. V. (1995). Preliminary results of investigations into the effect of cosmophysical radiation of a non-electromagnetic nature on physical and biological systems. *Biophysics,* **40**, 883-891.

Martin, L. J., Koren, S. A. and Persinger, M. a. (2004) Thermal analgesic effects from weak, complex magnetic fields and

pharmacological interactions. *Pharmacology, Biochemistry and Behavior*, **78**, 217-227.

Persinger, M. A. (2003) Neurobehavioral effects of brief exposures to weak intensity, complex magnetic fields within experimental and clinical settings. In M. J. McLean, S. Engstrom and R. R. Holocomb (eds) *Magnetotherapy: potential therapeutic benefits and adverse effects*. N.Y.: TFG Press, pp. 89-118.

Persinger, M. A. and Koren, S. A. (2007) A theory of neurophysics and quantum neuroscience: implications for brain function and the limits of consciousness. *International Journal of Neuroscience*, **117**, 157-175.

Persinger, M. A., Tsang, E. W., Booth, J. N. and Koren, S. A. (2008) Enhanced power within a predicted narrow band of theta activity during stimulation of another by cirumcerebral weak magnetic fields after weekly spatial proximity: evidence of macroscopic quantum entanglement? *NeuroQuantology*, **6**, 7-21.

Persinger, M. A. and Lavallee, C. F. (2010) Theoretical and experimental evidence of macroscopic entanglement between human brain activity and photon emissions: implications for quantum consciousness and future applications. *Journal of Consciousness and Research*, **1**, 785-807.

Persinger, M. A., Saroka, K. S., Lavallee, C. F., Booth, J.M., Hunter, M.D., Mulligan, B. P., Koren, S. A., Wu-H.P. and Gang, N.

(2010) Correlated cerebral events between physically and sensor isolated pairs of subjects exposed to yoked circumcerebral magnetic fields. *Neuroscience Letters*, **486**, 231-234.

Popp, F.-A., Li, K. H., Mei, W. P., Galle, M., and Neurorh, R. (1988) Physical aspects of biophotons. *Experientia*, **44**, 576-585.

Richards, P. M., Persinger, M. A. and Koren, S. A. (1996) Modification of semantic memory in normal subjects by application across the temporal lobes of a weak (1 microTesla) magnetic field structure that promotes long-term potentiation in hippocampal slices. *Electro-and Magnetobiology*, **15**, 141-148.

Stapp, H. (2009) Nonlocality. In D. Greenberger, K. Hentschel, & F. Weinert (Eds). *Compendium of Quantum Physics.* Springer: N.Y., pp. 404-410.

Tillbury, R. N. and Quickenden, T. I. (1988) Spectral and time dependence studies of the ultraweak bioluminescence emitted by bacterium *Escherichia coli*. *Photochemistry and Photobiology B*, **47**, 145-150.

Tu, L-C., Luo, J. and Gillies, G. T. (2005) The mass of the photon. *Reports on Progress in Physics*, **68**, 77-130.

Vogel, R. and Suessmuth, R. (1988) Interaction of bacterial cells with weak light emission from culture media. *Bioelectrochemistry and Bioenergetics*, **45**, 93-101.

5 Discussion

When Schrodinger asked the question "What is Life?" he was referring to the atomic and quantum bases to the complexity of biochemical pathways that contribute to the integrity of the cell and its aggregates over time. The precision available by knowing the directionality and co-directionality of the multiple signalling pathways between the cell membrane through the cytoplasm into the nucleus and the subsequent responses that maintain the structure and dynamics of the cell has allowed the biomolecular sciences to answer some of the most enigmatic and critical questions that have dominated cell biology for at least a century.

The experiments in this dissertation were designed to compliment and to extend the information obtained from classical biomolecular science which relies upon matter and its interaction to the domains of energy and light. If patterns of weak light are the actual "keys" by which the complex machinery of the cell are activated, then the quantification of the frequencies of light associated with specific molecular reactions and their interactions with the weak applied magnetic fields could allow greater control of both normal and aberrant activity.

One metaphor is that the emission of light as a source of intercell communication would be analogous to the ignition of an automobile. Although knowing the innumerable parts, dynamics,

components and even their composition is essential to build a car and to ensure its optimal operation, the ignition determine if the automobile will have the potential to move or to not move. The metaphor applied here is that light emissions are the "key" to the ignition. It could be easier to turn the key or not to initiate or stop a complex process that once begins would require a myriad of interventions to stop. Each of the three separate experiments that contributed to this interpretation will be discussed as well as their general significance, limitations, and potential future research.

5.1 Cosic's RRM for Shifting Wavelengths in UPE from Dying Cells

All living systems emit photons in the range of 100 – 1000 photons$\cdot cm^{-2} \cdot s^{-1}$ [Popp, 1979]. The interactive relationships between metabolic pathways and wavelength specific UPE are still being investigated. In this experiment the unique emission patterns were noted for 7 different wavelengths. The most conspicuous shifts were observed at the 370 nm and 950 nm wavelength.

To discern if we could exacerbate or diminish emission characteristics for specific wavelengths only, Cosic's Resonant Recognition Model for Macromolecules [Cosic, 1994] was used to determine which group of proteins that could be inhibited or facilitated should be selected for each filter. Specific activators and inhibitors for specific wavelengths based upon the Cosic model

elicited either enhancement or diminishment of photons in a predictable manner. Inhibitors or activators predicted for other wavelengths, even within 10 nm, were less or not effective.

Perhaps the most interesting result was the untreated effects of wavelengths 370 nm and 950 nm. These two wavelengths had very similar UPE patterns, in fact if the IR (950 nm) wavelength was shifted by 3 hours there was a correlation of 0.85 between wavelengths 950 nm and 370 nm. Interestingly, the Cosic Model predicted 950 nm wavelength to be associated with signalling molecules within the cell as well as cell proliferation and the 370 nm wavelength to be related to macromolecules associated with cell growth and structure.

The latency of 3 hours is within range of cell signalling and transcription of proteins [Gossen et al, 1994; Bensaude, 2011]. It is important to note that the IR spectrum (signalling) displayed increases in UPE followed by UPE increases in the UV spectrum (cell structure). This relationship between IR and UV may be interpreted as addition support for the critical role of very small quantities of photons as the initiators of numerous molecular processes involved with cell proliferation, repair, and adaptation.

5.2 UPE from Stimulated Melanoma Cells Coupled to Lateral Diffusion

Initial studies [Dotta et al, 2011] revealed that cell cultures emit photons continuously upon removal from an incubator for a period of about 12 – 24 hours. The energy associated with this emission regardless of condition was 10^{-20} $J \cdot s^{-1} \cdot cell^{-1}$. This most recent study demonstrated that the numbers of photons from cooling cells can be modified by applying specific intensities of temporally patterned magnetic fields. Assuming lateral diffusion of lipids within membranes are macroscopic metaphors of the angular magnetic moment of the Bohr magneton then the photon emission observed matches the calculation for the applied ~1 μT magnetic fields.

A range of magnetic field intensities were applied to cooling cell cultures and a dose-dependent relationship between photon emission and intensity was observed. We hypothesize that this UPE dose-dependency is a function of lateral diffusion with the membrane. The movements of components of the cell membrane (lipids and proteins) through this three-dimensional shell may be analogous to moving charge-currents. They might be considered a field of point current charges.

The physical properties would be similar to (but reflective of the more complex macroscopic level) an electron moving around a proton in the hydrogen atom. There may be a type of "cellular" magnetic moment that, when stimulated by intensity-tuned magnetic

fields, results in photon emissions whose peak frequencies reflect predicted energies for fundamental orbital/spin properties of the electron and atomic aggregates with large principal quantum numbers. The resulting "membrane magnetic moment" when exposed to the appropriate intensity from an applied magnetic field would be associated with an energy that was discerned by measurement of photons.

In addition, the energy equivalent of 10^{-20} $J \cdot s^{-1}$ is within the order of magnitude of, and convergent with, the coefficients for the energy over distance for the forces between K+ charges that maintain the plasma membrane potential [Persinger, 2010] and the energy associated with the sequestering the dynamic components of many agonists to receptors. The dose dependency associated with the applied magnetic field strength illustrates further validly to the hypothesis as the effect was most robust at 0.9 μT and dissipated as the applied intensity deviated from this value. The results strongly suggest the membrane is capable of EMF detection that resulted in UPE from the cells. There were convergences in mathematical and experimental results that add to the legitimacy of this hypothesis.

5.3 Doubling of UPE from Reactions Sharing EMF Configurations

The "doubling" of the duration of photon emissions during simultaneous injections of the same amount of peroxide into a local

dish (above a PMT) and a dish 10 m away in a closed chamber is the most consistent example of a macroscopic excess correlation we have produced in our laboratory. To produce this reliable effect an applied highly specialized and configured magnetic field was the only required variable. With other studies of non-locality involving human or cellular subjects, variables like proximity, a priori interaction, and the state of the cells could have confounded the amount of UPE and size of the effect [Dotta et al, 2011b; Dotta et al, 2009]. The simple reaction of H_2O_2 and NaClO producing a macroscopic demonstration of "excess correlation" between spatially separated spaces has potentially paradigm-shifting implications for our interpretations of interactions between chemical reactions within and outside the living cell.

For example, hippocampal slices emit photons with power densities of 10^{-12} $W \cdot m^{-2}$ that are tied to theta activity [Popp et al, 1988; Isojima et al, 1995]. Theta activity is the dominant frequency band for the hippocampus that is central in memory consolidation and spatial representation. During theta activity synchronous photon emission would be produced from synchronous firing of neurons. This firing is coupled with membrane depolarization that is caused by the movement of charges.

These charges in a circular shaped cell could act as our applied rotating applied magnetic field. The patterns of applied magnetic fields that were effective in producing these "entanglement like" effects are not uncommon in nature. Very

similar patterns occur frequently within the interface between the earth's surface and the ionosphere that is the source of the Schumann resonance. Given the power densities of 10^{-11} $W \cdot m^{-2}$ assuming 10^{-20} J per action potential [Persinger, 2010] an equivalent energy of 10^{8} neurons are associated with this hippocampal theta activity.

With 10^{8} neurons producing photon emission for a minimum of 20 minutes and the potential for rotational diffusion with the membrane only two potentially synchronous neurons out of 100 million would be needed to produce this macroscopic entanglement effect. Recent experiments have shown that only one neuron is required to alter the state of the entire cerebral cortices and to determine the direction of an overt response.

5.4 Limitations

The main measure throughout this dissertation was light emission from cell cultures as recorded by two types of photomultiplier tubes (SENS-TECH DM0090C and Pacific Photometric Instruments, model 15, with photomultiplier tube housing for a RCA electron tube (BCA IP21)). While this gave a dynamic view of potential ongoing cellular processes, a more comprehensive assessment of cellular activity may be required to further validate the hypotheses within this dissertation. Biomolecular tools like Western Blot analysis may be relevant to determine how much protein is responsible for a given amount of light emission. The more measures used to demonstrate the link between electromagnetic energy and

protein activity, the better understood the relationship between the two become.

In addition, all measurements from cell cultures were taken at room temperature and not physiological temperature (~20° C vs. 37° C). This was done to stress the cells and produce the most robust photon emission possible. However, emission spectra under proper temperatures could be different. But given previously published photon emission data from other groups (Popp, 1979a; Cifra et al., 2011) it remains likely that any changes are subtle and the stressed environment generally increases overall emission. Despite this, it would be prudent to test cells under physiological conditions (in an incubator) and observe changes at this temperature.

Furthermore, the release of photons from a biological system is spherical in nature. While our single or double PMT measurements produced reliable emission intensities from these two planes, a more comprehensive representation (spherical) of overall emission intensity may be revealing. In addition to this, under normal conditions cells develop three dimensionally. However, cultured B16-BL6 cells can only grow on a horizontal plane (monolayer). This could eliminate any potential electromagnetic influence neighbouring cells directly above or below a given cell may have. Accommodating for the third plane of space may be useful in understanding any communication properties between cells by electromagnetic energy.

5.5 Future Research

This dissertation looked to augment the existing hypotheses of how electromagnetic energy can potentially influence cells. But more research is still needed to create a definitive hypothesis on how cellular processes and electromagnetic energy interact. Because ultraweak photon emission is a relatively new area of research the future is laden with potential research projects and implications. Some of the most obvious directions of future research are measuring emission at physiological temperature, light stimulation of cells, using different biomolecular techniques, and understanding how the electromagnetic spectrum contributes to cell communication and development as a whole.

First, the starting point for future research should focus on photon emissions from cells at physiological temperature. Thus far it has been difficult for the scientific community to measure cells at 37° C. This is due to the fact that incubators do not provide significant light shielding, so an adequate darkened environment becomes difficult to attain. In addition, the equipment used for measuring photons is typically not suited for such high and humid temperatures. These problems must be solved before any measurement at physiological temperature can be taken. Once these problems are solved, this research could provide a greater overall indication of the level of electromagnetic radiation that is occurring at the level of the cell. Understanding UPE from cells under physiological conditions could provide a framework for the pattern and intensity of

electromagnetic radiation from different cell lines, developmental stages, and disease states.

Second, the effect of light stimulation on cells has yet to be fully explored. Light irradiation of tissue, or "light therapy", has the potential for significant clinical applications. As mentioned, Choi and colleagues [2012] demonstrated increased neurite growth following the application of 710 nm light. This was an exciting result as this light application alleviated some of the cellular deficits associated with an ischemic event. These results demonstrate reliable positive effects when cells are stimulated with the properly patterned, wavelength, and intensity light. In addition to this, there have been publications observing magnetic field effects at the level of the ion channel (Pall, 2013), but more research observing the effects of light irradiation on cultured cells and whole organisms need to be published. As a starting point, it would be sensible to pattern light application after previously measured light emission from other cells.

This dissertation demonstrated the effects of applied electromagnetic fields on cells. But perhaps the application of light can produce the same effects. Because the application of light at a specific intensity can produce emission, and stimulate growth, an electromagnetic communication hypothesis begins to take shape. Perhaps light, or electromagnetic energy in general, can be viewed as the "code" by which all cells operate.

As mentioned previously, it would be prudent to use other tools of measurement to solidify these results. Specifically, systematically demonstrating increases or decreases in different cellular proteins and how it relates to increases or decreases in photon emission. For example, selecting a single protein (Protein Kinase A (PKA)) and then manipulating the amount of PKA within a cell culture and taking both photon emission and protein measures. From this it could be possible to quantify the amount of protein required to measure light from the cell.

These potential avenues of research would further illuminate the relationship between electromagnetic radiation and biological systems. If electromagnetic energy is coupled to multiple components of cellular activity (as the dissertation has shown) then these avenues should provide additional information on cellular processes. This potential research could have large implications in the clinical and scientific community.

5.6 Integration and General Significance

The detection and generation of electromagnetic energy has been a central component of this thesis. A plethora of examples of how this detection and generation can take place in the cell has been described in the prior experiments and also in the literature [Cifra et al, 2011; Popp, 1979]. The experiments described demonstrate how closely UPE is associated with cellular functions and how applied EMF can produce emission (and potentially vice

versa). From the results it may be deduced that cellular detection and generation of electromagnetic energy are coupled to one another.

We have demonstrated that appropriately applied EMF produce photon emissions. Other researchers have established that irradiance of applied light can induce cell proliferation and mobility in planaria [Wu & Persinger, 2011]. Intuitively these results suggest that biological systems are constantly adapting to electromagnetic energy possibly through energy transfer. This simple relationship of electromagnetic energy being transferred to another form of energy still reiterates a matter and energy duality concept within cell systems [Persinger, 2010].

The Cosic model has quintessentially demonstrated this potential relationship between the functional properties of macromolecules specific wavelengths. Cosic's model predicts an optimal wavelengths of light from a representation of the distribution of free electron energy along a protein may contain the code by which complex molecular structure and electromagnetic frequency can be equated. If each macromolecule has a unique corresponding optimal wavelength associated with it, all that is required for interaction with specific proteins is a fine tuning of applied electromagnetic energy.

The capacity to quantitatively predict the type of biomolecule associated with specific wavelengths of photons during the different stages of cellular demise has implications for

intervention. That application of a predicted intensity of a magnetic field can interact with the "membrane magnetic moment" to release photons may help explain why certain magnetic fields can be carcinogenic while others inhibit or eliminate this possibility. If photons are the carriers of intercellular information that determines the machinery of the cell then their entanglement or display of non-locality predicts different models for both the dissemination of cellular aberrance as well as the stimuli that produce spontaneous mutations.

5.7 References

Bensaude, O. (2011). Inhibiting eukaryotic transcription, Transcription. 2(3); 103-108

Cifra, M., Fields, J.Z., Farhadi, A. (2011) Electromagnetic cellular interactions. Prog. Biophys. Mol. Biol. **105**, 223-246.

Cosic, I. (1994) Macromolecular bioactivity: is it resonant interaction between macromolecules? Theory and application, IEEE Trans. BioMed. Engineer. 41, 1101-1114.

Choi, D-H., Lee, K-H, Kim, J-H, Moon Young, K., Lim, J-H. (2012) Effect of 710 nm visible light irradiation on neurite outgrowth in primary rat cortical neurons following ischemic insult. Biochem. Biophys. Res. Commun. 422, 272-279.

Dotta, B. T., Mulligan, B. P., Hunter, M. D. and Persinger, M. A. (2009) Evidence of macroscopic quantum entanglement during double quantitative electroencephalographic (QEEG) measurements of friends vs strangers. *NeuroQuantology*, 7, 548-551.

Dotta, B. T., Buckner, C. A., Cameron, D., Lafrenie, R. M., Persinger, M. A. (2011) Biophoton emissions from cell cultures: biochemical evidence for the plasma membrane as the primary source, Gen. Physiol. Biophys. 30, 301-309.

Dotta, B. T., Buckner, C. A., Lafrenie, R. M., Persinger, M. A. (2011) Photon emissions from human brain and cell culture exposed

to distally rotating magnetic fields shared by separate light-stimulated brains and cells. Brain Res. 388, 77-88.

Gossen, M., Binin, A. L., Freundlieb, S., Bujard, H. (1994) Inducible gene expression systems for higher eukaryotic cells, Curr Opin Biotecnol. 5(5), 516-520.

Isojima,Y., Isoshima, T., Nagai, K., Kikuchi, K., Nakagawa, H. (1995) Ultraweak biochemiluminesence detected from rat hippocampal slices. NeuroReports, 6, 658-660.

Pall, M. L. (2013) Electromagnetic fields act via activation of voltage-gated calcium channels to produce beneficial or adverse effects. J Cell Mol Med. doi: 10.1111/jcmm.12088.

Persinger, M.A. (2010) 10^{-20} Joules as a neuromolecular quantum in medicinal chemistry: an alternative approach to myriad molecular pathways. Cur. Med. Chem. 17, 3094-3098.

Popp, F.-A. (1979a) Photon storage in biological systems, In F. A. Popp, G. Becker, H. L. Konig, W. Pescha (eds), Electromagnetic bioinformation. Munich: Urban and Schwarzenberg: 123-149.

Popp, F.-A. (1979b) Electromagnetic bioinformation. New York: Urban and Schwarzberg. pp. 123-149.

Popp, F-A. (1988). Biophoton emission, Experientia 44 543-630.

Popp, F.-A., Li, K.H., Mei, W.P., Gale, M., Neurohr, R. (1988) Physical aspects of biophotons. Experientia 44, 576-585.

Wu, H-P., Persinger, M.A. (2011) Increased mobility and stem-cell proliferation rate in Dugesia tigrina induced by 880nm light emitting diode. J Photochem. Photobiol. B., 102(2), 156-160.